NATURAL CONVECTION FROM AN INCLINED FLAT PLATE

A thesis submitted to the University of Nottingham

for the degree of

Doctor of Philosophy

by

Ian Paul Warneford, B.Sc. (Eng.)

May 1975

PAGE
NUMBERS
CUT OFF
IN
ORIGINAL

CONTAINS PULLOUTS

VOLUME CONTAINS CLEAR OVERLAYS

OVERLAYS SCANNED SEPERATELY AND OVER THE RELEVANT PAGE.

ABSTRACT

This thesis describes an experimental and theoretical study of natural convection heat transfer from a downward-facing constant-heat-flux inclined flat plate in water.

The theoretical investigation, which comprised an analysis of the integrated boundary layer equations for steady two-dimensional laminar and turbulent flows, produced analytical solutions for a heated plate inclined at any angle of inclination.

Experiments, using two rigs, investigated heat transfer in the laminar, transition and turbulent regimes. The major outcome is a correlation for the local Nusselt Number over a range of modified Rayleigh Number from 10^6 to 10^{15}. In addition, boundary layer temperature and velocity profiles were measured using traversing probes and the flow outside the boundary layer was investigated using flow visualization techniques.

LIST OF CONTENTS

LIST OF FIGURES

LIST OF PLATES

LIST OF TABLES

NOMENCLATURE

b	overheat ratio
$C_{1..10}$	constants
C_p	specific heat at constant pressure (J/ kg K)
d	diameter of hot-fibre probe (m)
e	output voltage from anemometer (v)
g	acceleration due to gravity (m/s^2)
$\underline{g}$	gravity vector (m/s^2)
Gr_x	local Grashof Number
Gr_x^*	modified local Grashof Number
Gr_L^*	Grashof Number
Gr_d	Grashof Number based on diameter
h	heat transfer coefficient (W/m^2K)
$K_{1..8}$	experimental constants
k	thermal conductivity (W/mK)
l	half width of plate (m)
L	characteristic length (m)
Nu_x	local Nusselt Number
Nu_L	Nusselt Number
Nu_{CALC}	calculated local Nusselt Number
Nu_{EXP}	experimental local Nusselt Number
n	number of experimental points
Pr	Prandtl Number
$p(x)$	polynomial in minimisation routine
p	hydrostatic pressure (N/m^2)
p'	piezometric pressure (N/m^2)
$\dot{q}''$	heat flux density (W/m^2)
$\dot{q}'''$	source strength (W/m^3)

R_F	active sensor resistance (Ω)
$R_{F,L}$	leads resistance of probe (Ω)
R_T	resistance of temperature-compensating coil (Ω)
$R_{L,T}$	leads resistance of coil (Ω)
R_s	series resistance (Ω)
R_p	parallel resistance (Ω)
R_c	total resistance of compensating unit (Ω)
Ra_x	local Rayleigh Number
Ra_x^*	local modified Rayleigh Number
Re_d	Reynolds Number based on diameter
Sh_x	local Sherwood Number
Sc	Schmidt Number
SD	standard deviation
S	residual in minimising routine
T	temperature (K)
T'	fluctuating component of temperature (K)
t	time (s)
u	velocity component in x direction (m/s)
u_1	characteristic velocity (m/s)
u_1^*	dimensionless characteristic velocity $u_1 L/\nu$
u_2	characteristic velocity (m/s)
v	velocity component in y direction (m/s)
$\underline{v}$	velocity vector (m/s)
w	velocity component in z direction (m/s)
w_n	weighting factor
X	x/L
x	streamwise co-ordinate (m)
Y	y/L
y	transverse co-ordinate (m)

z	transverse co-ordinate parallel to plate (m)
α	thermal diffusivity $k/\rho Cp$
α_{F_o}	temperature coefficient of sensor at T_o (Ω/m)
α_{L,F_o}	" " " sensor leads at T_o (Ω/m)
α_{T_o}	" " " coil at T_o (Ω/m)
α_{L,T_o}	" " " coil leads at T_o (Ω/m)
β	volumetric thermal expansion coefficient (1/K)
ΔT	$T_w - T_\infty$ (K)
δ	boundary layer thickness (m)
δ_h	thermal displacement thickness (m)
δ^*	δ/L
ϵ	$\frac{y}{x}\sqrt{\frac{Gr_x \sin \phi}{5}} \cot \phi$
η	$\frac{y}{x}\left[\frac{Gr_x^* Pr \cos \phi}{5}\right]^{\frac{1}{5}}$
λ	bulk viscosity (kg/(ms))
μ	dynamic viscosity (kg/(ms))
ν	kinematic viscosity (m^2/s)
ρ	density (kg/m^3)
τ	shear stress (N/m^2)
Φ	dissipation function
ϕ	angle of inclination, positive for an upward-facing plate, negative for a downward-facing plate
χ	geometry function for a horizontal plate

Subscripts

w	conditions at the wall
∞	conditions far away from the plate
o	evaluate at 0^oC

ACKNOWLEDGMENTS

The author wishes to express his sincere thanks to Dr. D. E. Fussey who supervised this project, to Professor A. G. Smith for provision of research facilities in the Department of Mechanical Engineering, University of Nottingham, and for his help during the absence of Dr. Fussey in Australia, and to Messrs. D. Lampard, N. Sheriff (U.K.A.E.A.) and N. W. Davies (U.K.A.E.A.) for their many valuable comments. Thanks are also due to Mr. V. Hawley and the technicians of L4 Laboratory for the construction of the experimental rigs and to Mrs. D. Boardman for typing the final manuscript. The project was funded by the Science Research Council to whom the author expresses his thanks. Finally I should like to thank my parents for their encouragement during the progress of this work.

CHAPTER 1

INTRODUCTION

During the design of a nuclear reactor, a detailed safety assessment is carried out which considers the effects on the reactor of a number of faults. Methods are provided for dealing with any dangerous situations, usually by avoiding the possible accident or containing its consequences. In the fast reactor, one of the most unlikely accidents is the loss of coolant from a single fuel sub-assembly.

Local blockages in the sub-assemblies due to coolant debris are important for fast reactor safety because they are difficult to detect and they could initiate a whole core incident. Gregory and Lord (1974) have shown that at least 12% of the available flow area must be blocked before local boiling of the sodium could be initiated, implying that blockages due to coolant debris are not an important hazard. They suggested that a major failure of either the fuel or structure of the sub-assembly would be necessary to cause a serious problem. Farmer (1970) has pointed out the possibility of a failure in one sub-assembly propagating to other sub-assemblies which could then lead to the melt-out of the core or some part of the core. In order to prevent molten debris damaging the reactor vessel, Hunt and Moore (1970) have suggested the use of a core catcher placed beneath the core to catch the debris. The function of the core catcher would be to initially catch the debris and then cool it to prevent boiling and dispersal of the material.

They suggested that the most likely type of core catcher would be a shallow V section channel which would be cooled by natural convection from its lower face into the main bulk of the

sodium. Their analysis of the heat transfer from the core catcher, discussed in detail later, showed that the temperature difference between the core catcher and the liquid sodium would be 87°C for a V section channel inclined at 15° to the horizontal.

As the above figure was based on unreasonable extrapolation of the available heat transfer data, the investigation reported in this thesis was aimed at providing data relevant to the design of such a core catcher. In a large number of liquid sodium heat transfer experiments, preliminary information is obtained using water models where flow visualization may also be undertaken. From these results, a feel is obtained as to which parameters are important and this may lead to modifications to any proposed liquid sodium experiment. Naturally, the results of these experiments will not be quantitatively applicable to liquid metals due to their high molecular conduction (low Prandtl Number).

To ease manufacture of the experimental rig, it was decided to consider only one side of the core catcher. The experimental situation which models the problem is that of a downward-facing inclined flat plate in water, the plate having a uniform heat output as suggested by Hunt and Moore (1970). It was hoped that this would give a reasonable representation of the practical situation.

The objectives of the investigation are summarised as follows:

1. To determine experimentally the relationship between the local heat transfer coefficient and the Grashof Number in the laminar and turbulent regions as the angle of inclination of the plate varies from the vertical to the horizontal facing down.

2. To determine experimentally, profiles of mean velocity and temperature in the laminar and turbulent boundary layers over a range of values of Grashof Number and plate angle of inclination.

3. To investigate the characteristics of the flow by means of flow visualization techniques.

4. To obtain a theoretical solution for the laminar and turbulent boundary layers using integral momentum techniques.

At the beginning of the project it was decided to modify and rebuild an experimental rig constructed by Taft (1971) for laminar flow measurements. Once this was commissioned and producing results, the detailed design and construction of a larger rig was undertaken. The presentation of the work is as follows:

Chapter 2 reviews the previous work on inclined plate natural convection heat transfer and reveals a lack of both experimental and theoretical data on turbulent flow and constant-heat-flux surfaces. The difficulties of computing turbulent flows on a vertical isothermal flat plate have been revealed by Smith (1972) who concluded that:

> "... theoretical work should not be attempted until further understanding of the physics governing turbulence is secured."

This difficulty is not present for laminar flows where finite difference solutions have solved the vertical plate solution accurately. This lack of knowledge was the other reason for this project being formulated.

Chapter 3 presents a theoretical description of both the laminar and turbulent boundary layers using the integral momentum method. Assumed velocity and temperature profiles in the boundary layer are used to obtain solutions to the equations.

Chapter 4 deals with the method of measurement in natural convection flows. The decisions leading to the selection and design of the thermocouple probe and a hot-fibre anemometer are given and details of the calibration of the anemometer are discussed.

Chapter 5 presents a detailed description of the two experimental rigs together with a discussion on the type of instrumentation used.

Chapters 6 and 7 describe the experimental procedure and results obtained from the small and large rigs respectively. The results from the two rigs are then discussed jointly in Chapter 8 and compared with the theoretical predictions of Chapter 3.

Chapter 9 summarises the conclusions of this programme of work and Chapter 10 suggests areas of work where further research is necessary.

CHAPTER 2

PREVIOUS WORK ON HEAT TRANSFER BY NATURAL CONVECTION FROM INCLINED FLAT PLATES

2.1 INTRODUCTION

The study of natural convection adjacent to inclined surfaces has received comparatively little attention compared with the classical study of heat transfer from a vertical plate. The earliest investigator to study this problem was Schmidt (1932) who obtained a fine collection of schlieren photographs of natural convection flows above and below an inclined surface.

Before continuing further with the inclined plate, a brief description of the development of the flow adjacent to a vertical plate will be given. There are several excellent review articles dealing with this situation by Ede (1956, 1967), Ostrach (1964) and Gebhart (1973a, 1973b).

Figure 2.1, taken from Godaux and Gebhart (1974), shows the development of the boundary layer in water. Initially a laminar boundary layer develops along the plate and after some distance downstream small disturbances enter the laminar flow from the surrounding medium and become two-dimensional. These are convected downstream and amplified over a narrow band of frequencies. The second stage of breakdown is when the secondary mean flow longitudinal vortices occur. This seems to be the main cause of the laminar flow breakdown.

The beginning of turbulence is first shown by the change in the velocity field which alters the mean temperature profile further downstream. Moving downstream the mixing becomes very intense to produce fully developed turbulent flow.

In order to present an effective summary of the available literature, the remainder of this chapter is divided into a

discussion of the laminar, transition and turbulent regions of an inclined flat plate. Table 2.1 gives a brief résumé.

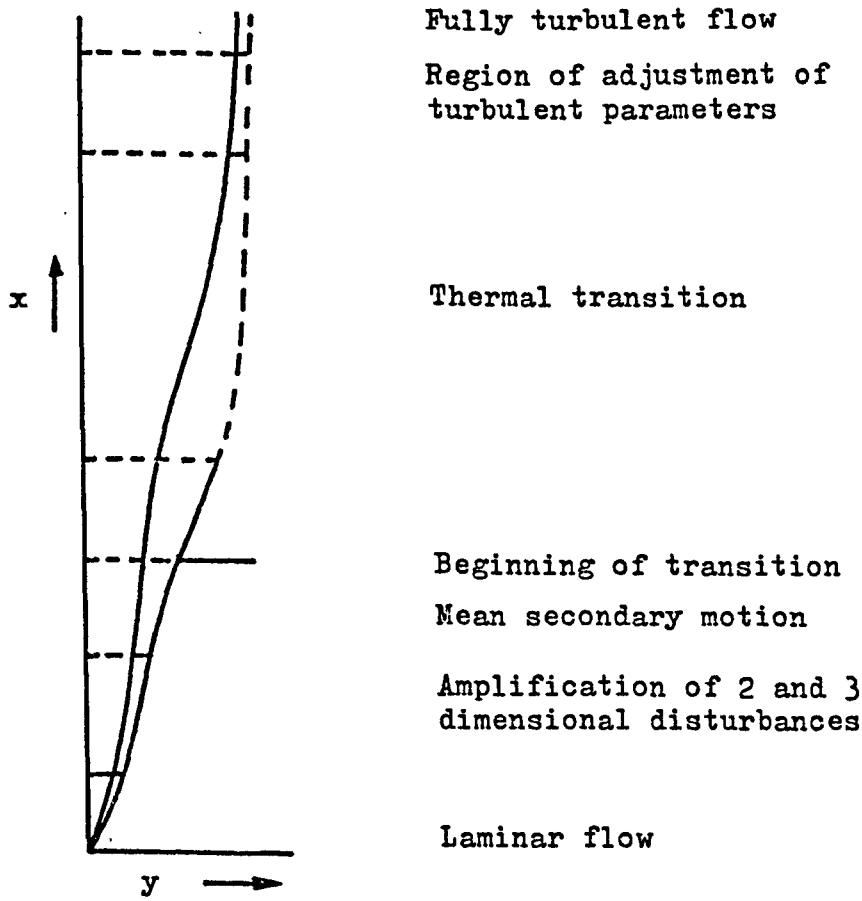

FIGURE 2.1 MECHANISMS OF TRANSITION IN WATER

2.2 LAMINAR FLOW

Tautz (1943) showed that the heat transfer coefficient on an inclined plate in air was independent of angle up to 45° from the vertical and between 45° and 90° decreased linearly with angle. Since then, several papers have shown theoretically that by neglecting the pressure gradient in the direction normal to the plate, the heat transfer correlation could be expressed as

$$Nu_x \propto (Gr_x \cos\phi \; Pr)^{\frac{1}{4}}$$

INVESTIGATOR	TREATMENT		FLUID	PLATE CONDITIONS			ORIENTATION OF PLATE		TYPE OF FLOW			EXPERIMENTAL OBSERVATIONS				
	Experimental	Theoretical		Isothermal	Constant $\dot{q}''$	Other	Upward facing	Downward facing	Laminar	Transition	Turbulent	Plate Surface Temperature	Lateral Temp. Profile	Lateral Velocity Profile	Flow Visualisation	Mass Transfer
Schmidt (1932)	/		air		Not known		/	/	/							
Tautz (1943)	/		air		Not known		Not known		/			/				
Schuh (1948)		/	any	/			/	/	/							
Rich (1953)	/	/	air		/		/		/			/	/			
Merk and Prins (1954)		/	any	/			/	/	/							
Inger (1955)	/	/	air		/		/	/	/			/	/			
Levy (1955)		/	any	/			/		/		/					
Plapp (1957)		/	any		Any		/	/		/						
Enikeev (1958)	/		air		/		/	/	/			/				
Tritton (1963a)	/		air	/			/				/	/	/	/		
Tritton (1963b)	/		air	/			/			/				/		
Michiyoshi (1964)		/	any	/			/	/	/							
Lock, Gort and Pond (1967)	/		air	/			/	/		/						
Kierkus (1968)	/	/	air	/			/	/	/			/	/	/		
Vliet (1969)	/		water and air		/		/		/	/	/	/				
Kung and Oetting (1969)	/		air		/			/	/			/	/			
Sparrow and Husar (1969)	/		water	/			/			/						
Hassan and Mohamed (1970)	/		air	/			/	/	/			/				
Lloyd and Sparrow (1970)	/		water	/			/	/		/						
Fujii and Imura (1972)	/		water			/	/	/	/			/				
Lee and Lock (1972)		/		/			/	/		/						
Lloyd, Sparrow and Eckert (1972a, b)	/		electrolyte Sc = 2000			uniform concentration	/		/	/	/					/
Pera and Gebhart (1973a)	/	/	air	/	/		/		/							
Pera and Gebhart (1973b)	/	/	air	/	/		/			/	/	/				
Haaland and Sparrow (1973a)		/	Pr = .7,2,6.7	/			/			/						
Haaland and Sparrow (1973b)		/	Pr = 6.7				/			/						
Iyer and Kelly (1974)		/		/			/			/						
Kahawita & Meroney (1974)		/		/			/			/						

TABLE 2.1 SUMMARY OF AVAILABLE LITERATURE

where ϕ is the angle of inclination measured from the vertical, i.e. using the value of the gravitational force parallel to the plate surface. This correlation implies that the heat transfer coefficient is the same for both upward-and downward-facing plates.

Levy (1955) solved the integral form of the boundary layer equations for an upward-facing isothermal plate. His method of solution was to first solve the equations by neglecting the pressure in the direction normal to the plate. From this first approximation, the neglected term was evaluated and a second approximation was obtained. The second approximation was

$$Nu_x = 0.427\ (Gr_x Pr \cos\phi)^{\frac{1}{4}} \quad \frac{1 - \frac{1}{5}\tan\phi\ (\frac{480}{Gr_x Pr})^{\frac{1}{4}}}{[1 - \frac{1}{6}\tan\phi\ (\frac{480}{Gr_x Pr})^{\frac{1}{4}}]}^{\frac{1}{2}}$$

Michiyoshi (1964) solved the governing equations by assuming that the plate could be represented by a thin ellipse. His analysis showed that the average heat transfer coefficient of the lower surface was larger than the upper surface and both coefficients increased as the angle approached the vertical.

Both Kierkus (1968) and Pera and Gebhart (1973a) presented perturbation analyses for two-dimensional laminar natural convection about an inclined plate using the classical boundary layer solution as the zero order approximation. Kierkus (1968) covered a range of angles from $-60^\circ \geq \phi \leq 60^\circ$ and found agreement between the theory and his experiments. Pera and Gebhart (1973a) considered the range of angles $90^\circ \geq \phi \geq 82^\circ$ and obtained some agreement between their theory and experiments.

In both analyses, it was shown that perturbation analysis had only a slight effect on the temperature distribution but a large effect on the velocity profile.

Experimental studies of laminar natural convection have been more numerous than the theoretical studies. Rich (1953) used an approximately constant-heat-flux narrow plate and an inferior quality interferometer to determine the temperatures. The boundary layer temperature profiles were lower than predicted by theory while the heat transfer coefficients were in good agreement with the vertical plate theory provided the gravity component parallel to the surface was used.

Using a similar experimental arrangement to that used by Rich (1953), Inger (1955) obtained heat transfer coefficients from a constant-heat-flux inclined plate from the horizontal facing down, through the vertical to the horizontal facing up. His data did not agree with the simple inclined plate theory, the heat transfer coefficient increasing after 30° and -60° from the vertical. This peculiar behaviour may be attributed to the narrowness of his plate (3 in. wide x 12 in. long).

Enikeev (1958) confirmed the analytical prediction for a downward-facing plate but when the plate faced upwards he found the heat transfer coefficient increased to a maximum at 60° and then began decreasing.

Yung and Oetting (1969) used an unusual method of correlating their results for an approximately constant-heat-flux downward-facing plate in air. Instead of using the gravitational component parallel to the plate surface, they used the ordinary gravitational component and correlated their results to the vertical plate theory using the correlation factor $(1 + \cos \phi)$ suggested by Yung (1965).

All the previous analyses have compared their data with isothermal surfaces, even though their heated plates were nearly

constant-heat-flux. Using the integral solutions for laminar natural convection by Squire (1938) and Sparrow (1955) for isothermal and constant-heat-flux plates respectively, the heat transfer correlations obtained for a Prandtl Number of 0.7 (air) are

$$Nu_x = 0.411\ (Gr_x Pr)^{\frac{1}{4}} \qquad \text{isothermal}$$

$$Nu_x = 0.451\ (Gr_x Pr)^{\frac{1}{4}} \qquad \text{constant-heat-flux}$$

There is a difference of approximately 9% between the two boundary conditions indicating that in the majority of the previous papers the heat transfer coefficient had been underestimated.

The first paper dealing specifically with a constant-heat-flux surface was presented by Vliet (1969). The heated plate used a 0.002 in. stainless steel foil as the heating element. Covering a range of angles from the vertical to 30° from the horizontal facing up he obtained the correlation

$$Nu_x = 0.6\ (Gr_x^* Pr \cos \phi)^{\frac{1}{5}}$$

which compared well with theory.

Covering the full range of angles from the horizontal facing upwards, through the vertical to the horizontal facing downwards position Hassan and Mohamed (1970) obtained heat transfer correlations for an isothermal inclined plate. The data were correlated using g cos ϕ with a maximum deviation of less than $\pm$ 10% for a range of angles of $-75° \geq \phi \leq 60°$.

Experiments on natural convection mass transfer adjacent to vertical and upward-facing plates were performed by Lloyd, Sparrow and Eckert (1972a,b). The local laminar mass transfer coefficient agreed very well with the analytical prediction.

Fujii and Imura (1972) extended the measurements down to 5° from the horizontal for a downward-facing plate and their results

universally accepted. Vliet (1969) using a constant-heat-flux plate took the beginning of transition as the point at which the temperature of the heated plate began to decrease. Others have used the fluctuations of velocity or temperature in the boundary layer as an indication of instability. Godaux and Gebhart (1974) suggested that the amount of energy entering the boundary layer gave a good indication of the point of transition.

Numerous papers dealing with transition on inclined surfaces are available, the majority dealing with the upward-facing plate. Tritton (1963b) was the first to experimentally show that the flow on the underside of a heated plate is more stable than that above the plate. Using a schlieren system in air, Lock, Gort and Pond (1967) showed that the disturbances adjacent to a heated plate were wavelike, the frequency and wavelength of these disturbances being little affected by inclination.

Using an electrochemical technique developed by Baker (1966), Sparrow and Husar (1969) found longitudinal vortices. Lloyd and Sparrow (1970) studied this problem further using the same techniques. For an upward-facing plate, their results showed that between 0° and 14° from the vertical, waves were the mode of instability. For inclinations greater than 17° the instability was characterised by longitudinal vortices. Between 14° and 17° the two modes co-existed. Pera and Gebhart (1973b) have questioned Baker's technique of flow visualization, pointing out that gas bubbles produced in the method could have generated additional fluid circulations.

The transition data obtained by Vliet (1969) for an upward-facing inclined plate were two orders of magnitude greater than that for an isothermal plate. This difference may be due to the

differing boundary conditions or the heat capacity of the plate.

The mass transfer technique of Lloyd, Sparrow and Eckert (1972a,b) gave transition criteria much higher than other investigators. They attributed the discrepancy to the large difference between their Schmidt Numbers and the Prandtl Numbers used in heat transfer experiments and also to the lack of disturbances in the flow.

Pera and Gebhart (1973b) using an upward-facing plate in air, obtained values of transition near the horizontal. Their work also included details of the separation of the flow.

The theoretical aspects of the instability of natural convection flow on a vertical plate are now very well understood. Two-dimensional linear instability theory correctly predicts the characteristics and disturbance amplification for instability. Gebhart (1973a,b) has recently reviewed what is known about such effects. Plapp (1957) was the first to derive the instability equations for natural convection from a flat plate but it is only recently that attempts have been made to solve them.

Lee and Lock (1972) presented an analysis but the terms involving the non-parallel effects of the mean flow were neglected. Haaland and Sparrow (1973a) showed that this assumption led to significant errors and they took into account the streamwise variation of the basic flow and temperature fields. This moved the neutral stability curves to higher Grashof and wave numbers. In a later paper (1973b) they showed that the curves are displaced towards lower Grashof Numbers as one goes from a downward-facing plate to an upward-facing plate. The range of unstable wave numbers is greater for upward-facing plates than downward-facing plates.

Using the parallel flow model Iyer and Kelly (1974) showed theoretically the change in instability from waves to longitudinal vortices for an upward-facing plate. To correlate the theory with the experimental results it was necessary to calculate the total amplification of each disturbance from the theoretically predicted point of onset of instability to the point of observation of instability. Similar conclusions were obtained by Kahawita and Meroney (1974) using linear perturbation theory.

Pera and Gebhart (1973b) have studied theoretically the flow adjacent to horizontal and nearly horizontal upward-facing plates. They correctly predicted the trend of the stability limits but their results were not in as good agreement as the work on the vertical plate.

Finally, it has been shown by Gebhart (1969) that a direct comparison between experiments involving natural disturbances and linear stability theory should not be made. Natural disturbances involve disturbances of many frequencies and amplitudes whereas the theory only considers a single frequency and, to be able to detect instability, the disturbances will have to be amplified before instruments will detect them.

2.4 TURBULENCE

Very little information is available in the literature for turbulent natural convection from inclined surfaces. Levy (1955) modified the equations of motion set out by Eckert and Jackson (1955) using the gravitational component parallel to the plate surface. For an isothermal plate he obtained the equation

$$Nu_x = 0.0295\ Pr^{\frac{7}{15}}\ (1 + 0.494\ Pr^{\frac{2}{3}})^{-\frac{2}{5}}\ \ (Gr_x \cos\phi)^{\frac{2}{5}}$$

for angles near the vertical.

Tritton (1963a) studied turbulent natural convection above a heated isothermal plate inclined at 10° to the horizontal. He obtained temperature and velocity profiles but no indication of the range of Grashof Numbers is given.

The work of Vliet (1969) was the first extensive study of turbulent natural convection above a constant-heat-flux plate. He obtained the heat transfer correlation

$$Nu_x = 0.30\ (Gr_x^* Pr)^{0.24}$$

for $0^\circ \leq \phi \leq 60^\circ$. It should be noted that he found that the inclination made no effect on the heat transfer, i.e. he used the ordinary gravity component rather than the component parallel to the plate as suggested by Levy (1955). Also, from this equation it will be seen that the heat transfer coefficient decreased with distance up the plate. Vliet found that the index of the Grashof Number varied from 0.22 for the vertical plate to 0.24 for the horizontal plate, the best fit data giving an index of 0.24.

Using a mass transfer technique, Lloyd, Sparrow and Eckert (1972a) obtained local turbulent natural convection mass transfer coefficients for an upward-facing plate. They presented their results as

$$Sh_x = \text{constant}\ (Gr_x\ Sc)^{\frac{1}{3}}$$

where Sh_x and Sc are the local Sherwood Number and Schmidt Number. Their results covered a range of angles from 0° to 45°. The constant was found to be a function of the angle of inclination. The use of the gravitational component parallel to the plate surface did not correlate the data and it would appear that

$$\text{constant} \propto \phi$$

The differences between the results of Vliet (1969) and Lloyd,

Sparrow and Eckert (1972a) are not understood. The plate boundary conditions were not identical, Vliet (1969) using a constant-heat-flux plate and Lloyd, Sparrow and Eckert (1972a) the equivalent of an isothermal plate. Also the Schmidt Numbers of the mass transfer experiments were 500 times the Prandtl Numbers used in the water tests.

From this brief review, it will be seen that there are still a large number of gaps in our knowledge of inclined plate natural convection, particularly from constant-heat-flux surfaces. No accurate laminar boundary layer temperature or velocity profiles have been obtained, even for the vertical constant-heat-flux plate. Transition data are only available for an upward-facing plate and no data are available on turbulent natural convection. It was therefore the aim of this project to attempt to fill some of the gaps in our knowledge.

CHAPTER 3

THEORETICAL CONSIDERATIONS

3.1 THE GOVERNING EQUATIONS

The mathematical difficulties involved in the exact solution of the momentum and energy equations are numerous even for very special cases. In this chapter the integral-momentum techniques of von Kārmān (1921) and Pohlhausen(1921) are used to solve the boundary layer form of the equations.

The continuity, momentum and energy equations governing the non-steady flow of a compressible fluid are given below:

$$\frac{D\rho}{Dt} + \rho \operatorname{div} \underline{v} = 0 \qquad \ldots (3.1)$$

$$\rho \frac{D\underline{v}}{Dt} = \rho \underline{g} - \nabla p + \mu \nabla^2 \underline{v} + \tfrac{1}{3}\mu \nabla (\nabla \cdot \underline{v}) \qquad \ldots (3.2)$$

$$\rho C_p \frac{DT}{Dt} = \nabla k \nabla T + \beta T \, Dp/Dt + \dot{q}''' + \Phi \qquad \ldots (3.3)$$

where Φ is the dissipation function given by

$$\Phi = (\lambda - \tfrac{2}{3}\mu)\left(\frac{\partial u}{\partial x} + \frac{\partial v}{\partial y} + \frac{\partial w}{\partial z}\right)^2 + 2\mu\left[\left(\frac{\partial u}{\partial x}\right)^2 + \left(\frac{\partial v}{\partial y}\right)^2 + \left(\frac{\partial w}{\partial z}\right)^2\right]$$
$$+ \mu\left[\left(\frac{\partial v}{\partial x} + \frac{\partial u}{\partial y}\right)^2 + \left(\frac{\partial w}{\partial y} + \frac{\partial v}{\partial z}\right)^2 + \left(\frac{\partial u}{\partial z} + \frac{\partial w}{\partial x}\right)^2\right]$$

In this chapter we will only consider natural convection flows due to temperature-caused density changes. Equations (3.1), (3.2) and (3.3) show the complexity and coupling inherent in natural convection problems. The motion results because of local density changes caused by changes in temperature, hence equations (3.1) and (3.2) are coupled to equation (3.3). It is convenient to replace p by $p' = p + \rho_\infty g\underline{x}$, the piezometric pressure, which has the property that it is constant in the external fluid and varies in the boundary layer only. When this is done equation (3.2) becomes

$$\frac{\rho Dv}{Dt} = (\rho_\infty - \rho)\underline{g} - \nabla p' + \mu\nabla^2\underline{v} + \tfrac{1}{3}\mu\nabla(\nabla \cdot \underline{v})$$

The system of co-ordinates is shown in Figure 3.1. The origin is taken at the bottom of the heated plate with the body force acting downwards. It is customary to take the angle, ϕ, as being positive when the heated surface is facing upwards and negative when the heated surface is facing downwards.

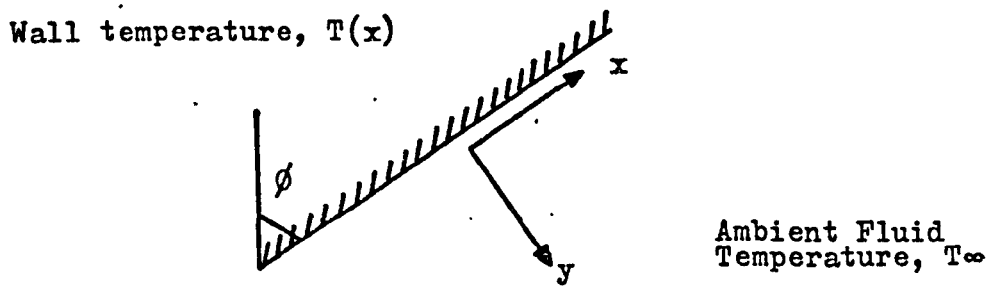

FIGURE 3.1 CO-ORDINATE SYSTEM

To reduce the complexity of the problem, the following assumptions are made:

1. The flow is steady, two-dimensional and incompressible.
2. The heat source, $\dot{q}'''$, is zero.
3. The physical properties remain constant except for the density and changes of density are only allowed to influence the mathematical model by the production of the buoyancy force.
4. The dissipation function, Φ, is negligible as shown by Gebhart (1962).
5. The buoyancy force may be written using the Boussinesq approximation as:

$$\underline{g}(\rho_\infty - \rho) = \underline{g}\rho\beta(T - T_\infty)$$

(see Gebhart (1973a) for a more detailed discussion of the approximations involved.)

The system of equations now reduces to:

$$\frac{\partial u}{\partial x} + \frac{\partial v}{\partial y} = 0$$

$$u\frac{\partial u}{\partial x} + v\frac{\partial u}{\partial y} = -\frac{1}{\rho}\frac{\partial p'}{\partial x} + g\beta(T - T\infty)\cos\phi + \nu\left(\frac{\partial^2 u}{\partial x^2} + \frac{\partial^2 u}{\partial y^2}\right)$$

$$u\frac{\partial v}{\partial x} + v\frac{\partial v}{\partial y} = -\frac{1}{\rho}\frac{\partial p'}{\partial y} + g\beta(T - T\infty)\sin\phi + \nu\left(\frac{\partial^2 v}{\partial x^2} + \frac{\partial^2 v}{\partial y^2}\right)$$

$$u\frac{\partial T}{\partial x} + v\frac{\partial T}{\partial y} = \frac{k}{\rho Cp}\left(\frac{\partial^2 T}{\partial x^2} + \frac{\partial^2 T}{\partial y^2}\right)$$

The boundary conditions associated with the above set of equations are:

$$y = 0,\ u = 0,\ v = 0,\ \frac{\partial T}{\partial y} = -\frac{q''}{k}$$

$$y \to \infty,\ u \to 0,\ v \to 0,\ T \to T\infty$$

The measurements of Schmidt and Beckmann (1930) in a flow around a heated vertical plate showed that the boundary layer was thin compared with the height of the plate. Hence, the equations may be further simplified using Prandtl's boundary layer theory by assuming

$$\frac{\partial^2}{\partial y^2} >> \frac{\partial^2}{\partial x^2}$$

The equations now reduce to:

$$\frac{\partial u}{\partial x} + \frac{\partial v}{\partial y} = 0 \qquad \ldots\ldots(3.4)$$

$$u\frac{\partial u}{\partial x} + v\frac{\partial u}{\partial y} = -\frac{1}{\rho}\frac{\partial p}{\partial x} + g\beta\,(T - T\infty)\cos\phi + \nu\frac{\partial^2 u}{\partial y^2} \qquad \ldots\ (3.5)$$

$$0 = -\frac{1}{\rho}\frac{\partial p}{\partial y} + g\beta\,(T - T\infty)\sin\phi \qquad \ldots\ (3.6)$$

$$u\frac{\partial T}{\partial x} + v\frac{\partial T}{\partial y} = \alpha\frac{\partial^2 T}{\partial y^2} \qquad \ldots\ (3.7)$$

where $\alpha = k/\rho Cp$

The pressure terms in equations (3.5) and (3.6) are eliminated by differentiating equation (3.6) with respect to x and then integrating with respect to y. The result is

agreed with theory. For angles between -85° and -90° from the vertical, the data wereplotted using the ordinary gravitational component giving $Nu_x \propto Gr_x^{\frac{1}{5}}$. For an upward-facing plate covering a range of angles from 0° to 85° their data again followed the analytical prediction but the scatter was much worse than for the downward-facing plate.

2.3 INSTABILITY AND TRANSITION

There are two common causes of instability, viz thermal and hydrodynamic. Thermal instability occurs when a heavier fluid overlies a lighter fluid causing a tendency to motion. This is the case for an upward-facing heated flat plate. Hydrodynamic instability is caused by the forces acting on the fluid amplifying the everpresent disturbances in the flow and producing a breakdown of the laminar flow. For an upward-facing inclined flat plate the tendency is to thermal instability, whereas when the plate is facing downwards there is a tendency to stabilize the flow.

The experimental determination of transition from laminar to turbulent flow on a vertical plate has received a considerable amount of effort but there is still poor agreement on the results. This is perhaps because no accepted standard has been used to determine the start and finish of transition.

A commonly used procedure is to calculate the beginning and end of transition from the $Nu_x - Ra_x$ relationship, there usually being a noticeable change in the relationship. This procedure is not foolproof. Fujii, Takeuchi, Fujii, Suzaki, and Uehara (1970) found that in fluids with large Prandtl Numbers there was no noticeable change. Kato, Nishiwaki and Hirata (1968) suggested the ratio of the shear velocity to the buoyancy velocity should be a good guide to instability but this method has not been

$$-\frac{\partial p}{\partial x} = \rho g\beta \sin\phi \int_y^\infty \frac{\partial}{\partial x}(T - T_\infty)\, dy$$

Substituting this result into equation (3.5) gives

$$u\frac{\partial u}{\partial x} + v\frac{\partial u}{\partial y} = g\beta (T-T_\infty)\cos\phi + \frac{\partial}{\partial x}\int_y^\infty g\beta(T-T_\infty)\sin\phi dy + \nu \frac{\partial^2 u}{\partial y^2} \qquad \ldots (3.8)$$

For fluids with a Prandtl Number near unity (strictly Pr = 1) it may be assumed that the hydrodynamic and thermal boundary layers have the same thickness. Integrating equations (3.8) and (3.7) on this assumption with respect to y from y = 0 to y = δ and eliminating v by using equation (3.4) we obtain

$$\frac{d}{dx}\int_o^\delta u^2 dy = \int_o^\delta g\beta\,(T - T_\infty)\cos\phi\, dy + \int_o^\delta \frac{d}{dx}\int_y^\delta g\beta\,(T - T_\infty)\sin\phi\, dy dy - \nu\frac{du}{dy}\Big|_o \qquad \ldots (3.9)$$

and

$$\frac{d}{dx}\int_o^\delta u(T - T_\infty)\, dy = \alpha \int_o^\delta \frac{d^2}{dy^2}(T - T_\infty)\, dy \qquad \ldots (3.10)$$

Equations (3.9) and (3.10) are the integrated boundary layer equations for an inclined flat plate with the new boundary conditions

$$y = 0,\ u = v = 0,\ \frac{dT}{dy} = \frac{-q''}{k}$$

$$y = \delta,\ u = 0,\ T = T_\infty$$

3.2 STEADY LAMINAR BOUNDARY LAYER FLOW

To evaluate the integrals in the momentum and heat balance equations, the velocity and temperature distributions in the boundary layer are written as polynomials in y whose coefficients are functions of x. Experimental evidence has shown that the velocity profile may be represented by a cubic polynomial

$$u = u_1 \frac{y}{\delta}\left(1 - \frac{y}{\delta}\right)^2 \qquad \ldots (3.11)$$

where u_1, is a characteristic velocity. The polynomial satisfies the boundary conditions

$y = 0,\ u = 0$

$y = \delta,\ u = 0$ and $\frac{du}{dy} = 0$ (smooth fit condition)

but gives a maximum velocity too far from the wall and of too great a magnitude (8% high).

The temperature profile may be approximated by the parabola

$$T - T_\infty = \frac{\dot{q}''\delta}{2k}\left(1 - \frac{y}{\delta}\right)^2 \qquad \ldots (3.12)$$

which satisfies the boundary conditions

$y = 0,\ \frac{dT}{dy} = \frac{-\dot{q}''}{k}$

$y = \delta,\ T = T_\infty$ and $\frac{dT}{dy} = 0$ (smooth fit condition)

The polynomials for the velocity and temperature distribution are substituted into equations (3.9) and (3.10) and after integration the boundary layer equations assume the following forms

$$\frac{d}{dx}\left(\frac{u_1^2\delta}{105}\right) = \frac{\dot{q}''\beta g\cos\phi}{6k}\delta^2 + \frac{\dot{q}''\beta g\sin\phi}{8k}\delta^2\frac{d\delta}{dx} - \frac{\nu u_1}{\delta} \qquad \ldots (3.13)$$

$$\frac{d}{dx}\left(\frac{u_1\delta^2}{60}\right) = \alpha \qquad \ldots (3.14)$$

These equations will first be solved for the special cases of the vertical and horizontal plate and approximately for the inclined plate.

3.2.1 Laminar Natural Convection from a Vertical Plate

Equations (3.13) and (3.14) were first solved by Siegel (1954) and Sparrow (1955) for a constant-heat-flux vertical plate ($\phi = 0^\circ$) following the method of Squire (1938). The variables are separated by means of the substitution

$$u_1 = C_1 x^{C_2}$$

$$\delta = C_3 x^{C_4}$$

Introducing these into equations (3.13) and (3.14) gives

$$\frac{C_1^2 C_3\,(2C_2+C_4)}{105} \times^{2C_2+C_4-1} = \frac{\dot{q}''\beta g}{6k} C_3^2 \times^{2C_4} - \nu \frac{C_1}{C_3} \times^{C_2-C_4}$$

$$\frac{C_1 C_3^2\,(2C_4+C_2)}{60} \times^{2C_4+C_2-1} = \alpha$$

For the equations to be valid at any position on the plate, the exponents must have the same values in both equations. The constraint is satisfied for $C_2 = 3/5$ and $C_4 = 1/5$ and the following solution is obtained

$$u_1 = \frac{60}{360^{2/5}}\,\alpha\, Pr^{2/5}\,(0.8 + Pr)^{-2/5}\,\left(\frac{\dot{q}''\beta g}{k\nu^2}\right)^{2/5} x^{3/5} \qquad \ldots (3.15)$$

$$\delta = 360^{1/5}\, Pr^{-2/5}\,(0.8 + Pr)^{1/5}\,\left(\frac{\dot{q}''\beta g}{k\nu^2}\right)^{-1/5} x^{1/5} \qquad \ldots (3.16)$$

or in the more usual form

$$Nu_x = 0.616\, Pr^{2/5}\,(0.8+Pr)^{-1/5}\, Gr_x^{*\,1/5} \qquad \ldots (3.17)$$

3.2.2 Laminar Natural Convection from a Horizontal Plate

For the horizontal plate, $\cos \phi = 0$. Equations (3.13) and (3.14) are solved by separating the variables using the same substitutions as in Section 3.2.1 giving

$$\delta = 3.36\, Pr^{-\frac{1}{3}}\,\left(\frac{4}{7} + Pr\right)^{1/6}\,\left(\frac{\dot{q}''\beta g}{k\nu^2}\right)^{-1/6} x^{\frac{1}{3}}\,(\sin\phi)^{-1/6}$$

and

$$u_1 = 5.313\,\alpha\, Pr^{\frac{2}{3}}\,\left(\frac{4}{7} + Pr\right)^{-\frac{1}{3}}\,\left(\frac{\dot{q}''\beta g}{k\nu^2}\right)^{\frac{1}{3}} x^{\frac{1}{3}}\,(\sin\phi)^{\frac{1}{3}}$$

or in the more usual form

$$Nu_x = 0.595\, Pr^{\frac{1}{3}}\,\left(\frac{4}{7} + Pr\right)^{-1/6}\, Gr_x^{*\,1/6}\,(\sin\phi)^{1/6} \qquad \ldots (3.18)$$

The $\sin\phi$ term has been retained in equation (3.18) to describe the orientation of the plate. For the horizontal plate facing upwards ($\sin\phi = +1$) the boundary layer starts at the plate edge and moves inwards whereas for a horizontal plate facing downwards ($\sin\phi = -1$) the boundary layer thickness is a maximum at the centre of the plate and decreases with the flow moving towards

the plate edges. As this solution assumed that the boundary layer originated at the plate edges and grew inwards, equation (3.18) is only valid for an upward-facing horizontal plate.

3.2.3 Approximate solution for an inclined flat plate

From equation (3.13) it may be shown that the buoyancy forces in the x and y directions are the same order of magnitude for angles of inclination greater than $|75^{\circ}|$ from the vertical. Substitution of $u_1 = C_1 x^{C_2}$ and $\delta = C_3 x^{C_4}$ into equations (3.13) and (3.14) yields

$$\frac{C_1^2 C_3 (2C_2+C_4)}{105} x^{2C_2+C_4-1} = \frac{\hat{q}'' \beta g \cos\phi C_3 x^{2C_4}}{6k} + \frac{\hat{q}'' \beta g \sin\phi C_3^3 C_4 x^{3C_4-1}}{8k} - \frac{\nu C_1}{C_3} x^{C_2-C_4} \quad \ldots (3.19)$$

$$\frac{C_1 C_3^2 (2C_4+C_2)}{60} x^{2C_4+C_2-1} = \alpha \quad \ldots (3.20)$$

The differing values of C_2 and C_4 obtained in the two limiting cases (vertical plate and horizontal plate) indicate the impossibility of obtaining a general solution for all angles of inclination (at least while retaining $u_1 = C_1 x^{C_2}$ and $\delta = C_3 x^{C_4}$).

To overcome this problem, the equations have been solved by three approximate methods:

a. Ignoring the $\sin\phi$ term in equation (3.19)

b. Calculating the $\sin\phi$ term in equation (3.19) using a horizontal plate solution

c. Calculating the $\sin\phi$ term in equation (3.13) from solution a.

By ignoring the $\sin\phi$ term in equation (3.19), i.e. the pressure gradient across the boundary layer, equations (3.19) and (3.20) may be solved in a similar manner to the vertical plate

solution giving

$$Nu_x = 0.616\ Pr^{2/5}\ (0.8 + Pr)^{-1/5}\ (Gr_x^* \cos \phi)^{1/5} \qquad \ldots (3.21)$$

This solution was first obtained by Schuh (1948).

The second method of solution is to assume that the constants C_2 and C_4 derived from the vertical plate solution hold over most angles of inclination. These values are substituted in the first, second and fourth terms of equation (3.19) and equation (3.20). The value of the constant C_4 in the sin ϕ term is taken from the horizontal plate solution ($C_4 = \frac{1}{3}$). Solving equations (3.19) and (3.20) for C_3 gives

$$C_3^5 = 360\ Pr^{-2}\left[0.8 + Pr - \frac{q''\beta g \sin\phi}{1440\ k\nu^2}\ Pr^2\ C_3^6\right]\left(\frac{q''\beta g\cos\phi}{k\nu^2}\right)^{-1} \qquad \ldots (3.22)$$

In Section 3.2.2 it was shown that the horizontal plate solution was only valid for an upward-facing plate. Experiments have shown (see, for example, Birkebak and Abdulkadir (1970)) that data for both the upward- and downward-facing horizontal plates may be represented by

$$Nu_x = C_5\ (Gr_x^*\ Pr)^{1/6}$$

for a constant-heat-flux plate. The constant C_5 is a function of Prandtl Number. Knowing that $Nu_x = 2x/\delta$ and $\delta = C_5 x^{1/6}$ then

$$C_3^6 = \frac{k\nu^2}{g\beta q''}\ \frac{1}{Pr}\ \frac{2^6}{C_5^6}$$

and on substitution this gives

$$\delta = 360^{1/5}\ Pr^{-2/5}\left[0.8+Pr - \frac{0.444}{C_5^6}\ Pr\sin\phi\right]^{1/5}\left(\frac{q''\beta g\cos\phi}{k\nu^2}\right)^{-1/5} x^{1/5}$$

and

$$u_1 = \frac{60}{360^{2/5}}\ \alpha\ Pr^{2/5}\left[0.8+Pr - \frac{0.444}{C_5^6}\ Pr\sin\phi\right]^{-2/5}\left(\frac{q''\beta g\cos\phi}{k\nu^2}\right) x^{3/5}$$

or in the more usual form

$$Nu_x = 0.616\ Pr^{2/5}\left[0.8+Pr - \frac{0.444}{C_5^6}\ Pr\sin\phi\right]^{-\frac{1}{6}}(Gr_x^*\cos\phi)^{1/5} \qquad \ldots (3.23)$$

The final method of solution is to evaluate $\frac{d\delta}{dx}$ in the third term of equation (3.13) from the approximate inclined plate solution (equation (3.21)) for δ, i.e.

$$\frac{d\delta}{dx} = \frac{360^{1/5}}{5}\ Pr^{-2/5}\ (0.8+Pr)^{1/5}\ \left(\frac{\dot{q}''\beta g\cos\phi}{k\nu^2}\right)^{-1/5}\ x^{-4/5}$$

$$= \frac{360^{1/5}}{5}\ Pr^{-2/5}\ (0.8+Pr)^{1/5}\ (Gr_x^*\cos\phi)^{-1/5} \qquad \ldots (3.24)$$

The solution proceeds in the same manner as before giving

$$Nu_x = 0.616\ Pr^{2/5}(0.8+Pr)^{-1/5}(1+0.487\ f\ (Pr,Gr_x^*,\phi)\ \tan\phi)^{1/5}(Gr_x^*\cos\phi)^{1/5} \qquad \ldots (3.25)$$

where

$$f\ (Pr,Gr_x^*,\phi) = Pr^{-2/5}(0.8 + Pr)^{1/5}\ (Gr_x^*\cos\phi)^{-1/5}$$

A comparison of the three approximate solutions for a downward-facing plate is shown in Figure 3.2. The results were calculated for Pr = 5 (water) and $Gr_x^* = 10^{10}$. The constant C_5 in equation (3.23) was obtained from the results of Fujii, Honda and Morioka (1973) for a downward-facing horizontal plate. Their results gave $C_5 = 0.57$ for Pr = 5. From this figure it may be seen that equations (3.21) and (3.25) only begin to deviate from each other for angles of inclination less than -75°, whereas equation (3.23) is up to 14% lower. The large difference in equation (3.23) is due to an overcorrection from the sin ϕ term in equation (3.19).

3.2.4 Numerical solution for an upward-facing inclined flat plate

A numerical solution of equations (3.13) and (3.14) was obtained using the subroutine D02ABF from the University of Nottingham N.A.G. Library Routines (1974). The subroutine

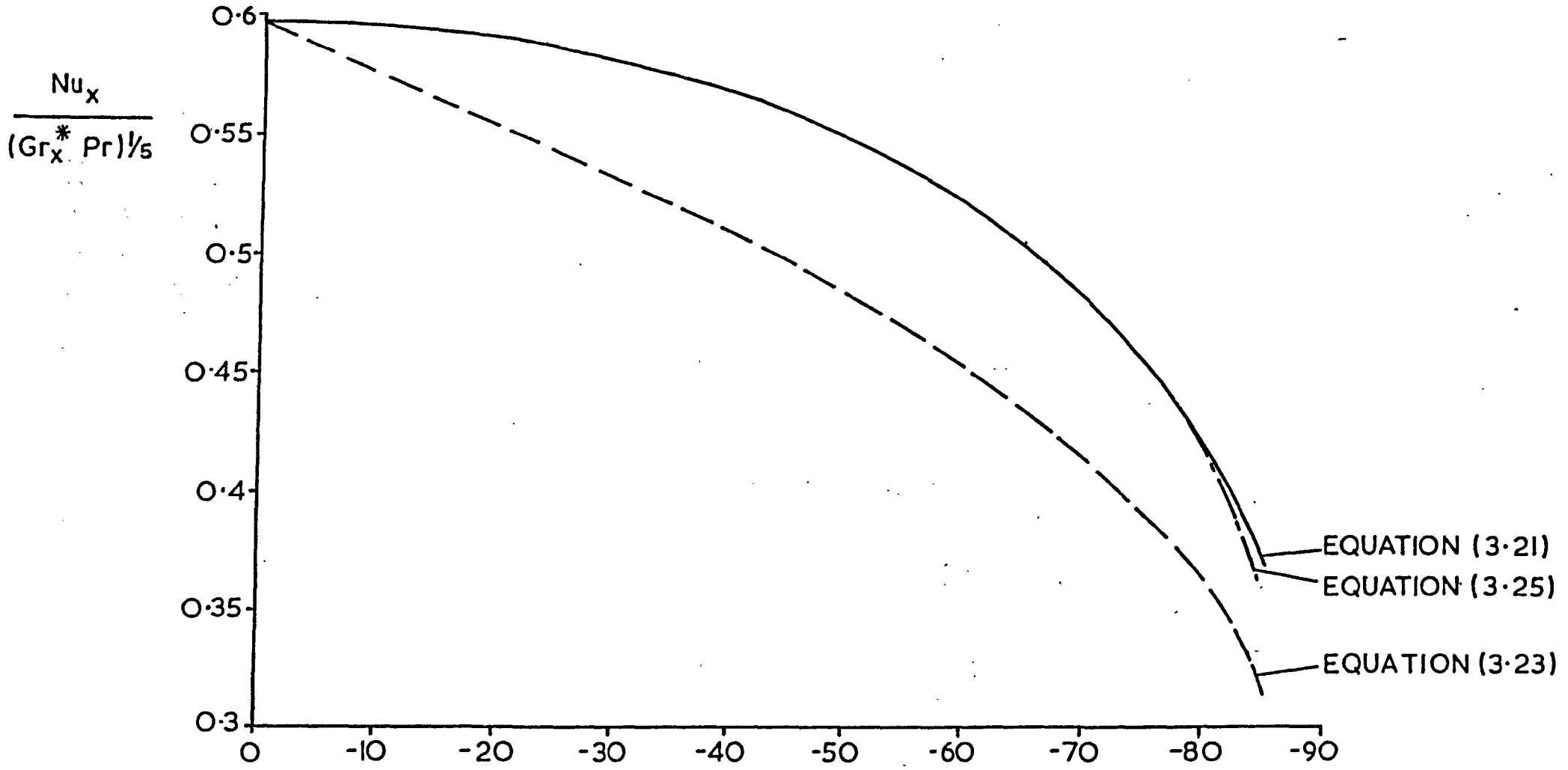

FIGURE 3·2

GRAPH OF $Nu_x / (Gr_x^* Pr)^{1/5}$ AGAINST ANGLE OF INCLINATION FOR $Pr = 5$ AND $Gr_x^* = 10^{10}$

advanced the solution of a system of ordinary differential equations using a number of steps of Merson's form of the Runge-Kutta method (see Mayers (1962)).

Equations (3.13) and (3.14) were made non-dimensional using the substitution

$$Y = \frac{y}{L}\ ,\ X = \frac{x}{L}\ ,\ \delta^* = \frac{\delta}{L}\ ,\ u_1^* = \frac{u_1 L}{\nu}$$

and after rearrangement we obtained two ordinary differential equations

$$\frac{du_1^*}{dX} = \frac{1}{\delta^{*2}}\left[\frac{60}{Pr} - 2u_1^*\,\delta^*\,\frac{d\delta^*}{dX}\right]$$

$$\frac{d\delta^*}{dX} = \frac{\frac{24}{21}\frac{u_1^*}{\delta^* Pr} - \frac{Gr_L^*\cos\phi\,\delta^{*2}}{6} + \frac{u_1^*}{\delta^*}}{\frac{Gr_L^*\sin\phi\,\delta^{*2}}{8} + \frac{3u_1^{*2}}{105}}$$

with the boundary conditions

$$X = 0,\ u_1^* = 0,\ \delta^* = 0$$

At $X = 0$, $\frac{d\delta^*}{dX}$ and $\frac{du_1^*}{dX} \to \infty$ hence the solution was started at a finite value of X, the values of $\frac{d\delta^*}{dX}$ and $\frac{du_1^*}{dX}$ being obtained from equation (3.24) and its equivalent for u_1. When

$$x = L,\ X = 1,\ Gr_L^* = Gr_x^* \text{ and } Nu_x = 2/\delta^*$$

The subroutine obtained an estimate of the local truncation error at each step, and varied the step length automatically to keep this estimate below a given error band. When the programme was run with negative angles of inclination (downward-facing plate) the step length became too small and the subroutine terminated the programme. It was felt that this was due to the singularity at the plate leading edge and it was not possible to overcome the problem.

These equations were solved for $\phi = 0^\circ$ to $\phi = 90^\circ$ over a range of Prandtl and Grashof Numbers. The data were then correlated

in the form

$$Nu_x = C_7 \, (Gr_x^* \, Pr)^{C_8}$$

Table 3.1 gives values of C_7 and C_8 for Pr = 0.1, 1 and 10 for various values of angle of inclination. Figure 3.3 shows the variation of C_7 and C_8 with angle of inclination for Pr = 1. C_8 remains almost constant up to $\phi = 60^\circ$ after which it slowly decreases until 80° when there is a sharp fall in value. Table 3.1 shows that C_8 also varies with Prandtl Number. The constant C_7 decreases until $\phi = 86^\circ$ when it sharply increases. Fujii and Imura found experimentally that over the range $86.8^\circ < \phi \leq 90^\circ$, the data were best correlated using

$$Nu_x \propto Ra_x^{*1/6}$$

From their graphs, it is not possible to ascertain whether there is a gradual change of C_8 from 0.2 to 0.167.

To compare the analytical and numerical solutions, Figure (3.4) shows the variation of Nusselt Number against angle of inclination at $Gr_x^* = 10^{10}$ and Pr = 5. This graph shows that the heat transfer coefficient is slightly larger than that predicted by equations (3.21) and (3.25) for ϕ greater than 80°.

3.3 STEADY TURBULENT BOUNDARY LAYER FLOW

When the flow mechanism is turbulent, equations (3.9) and (3.10) are valid if the terms

$$\nu \left.\frac{du}{dy}\right|_o \qquad\qquad \alpha \int_o^\delta \frac{d^2}{dy^2} (T - T_\infty) dy$$

are replaced by

$$\left[\frac{1}{\rho} \frac{dr}{dy}\right]_o^\delta \qquad \text{and} \qquad \left[\frac{1}{\rho C_p} \dot{q}''\right]_o^\delta$$

Angle of Inclination	Pr = 0.1		Pr = 1.0		Pr = 10	
	C_7	C_8	C_7	C_8	C_7	C_8
0	0.397	0.200015	0.548	0.200020	0.607	0.200000
20	0.396	0.199678	0.544	0.199793	0.600	0.200000
40	0.386	0.199057	0.525	0.199687	0.578	0.199850
60	0.366	0.197860	0.487	0.199270	0.534	0.199650
80	0.349	0.192912	0.423	0.196883	0.449	0.198450
82	0.340	0.191365	0.415	0.195990	0.436	0.198017
84	0.342	0.189195	0.409	0.194650	0.422	0.197200
86	0.348	0.185902	0.406	0.192157	0.410	0.195610
88	0.367	0.179993	0.420	0.186647	0.410	0.191360
89	0.389	0.175012	0.449	0.180748	0.433	0.185663
89.5	0.407	0.171378	0.483	0.175395	0.472	0.179603
90	0.434	0.166635	0.552	0.166677	0.590	0.166680

TABLE 3.1

NUMERICAL VALUES OF C_7 AND C_8 IN THE EQUATION $Nu_x = C_7 \, Ra_x^{*C_8}$

FOR AN UPWARD-FACING PLATE

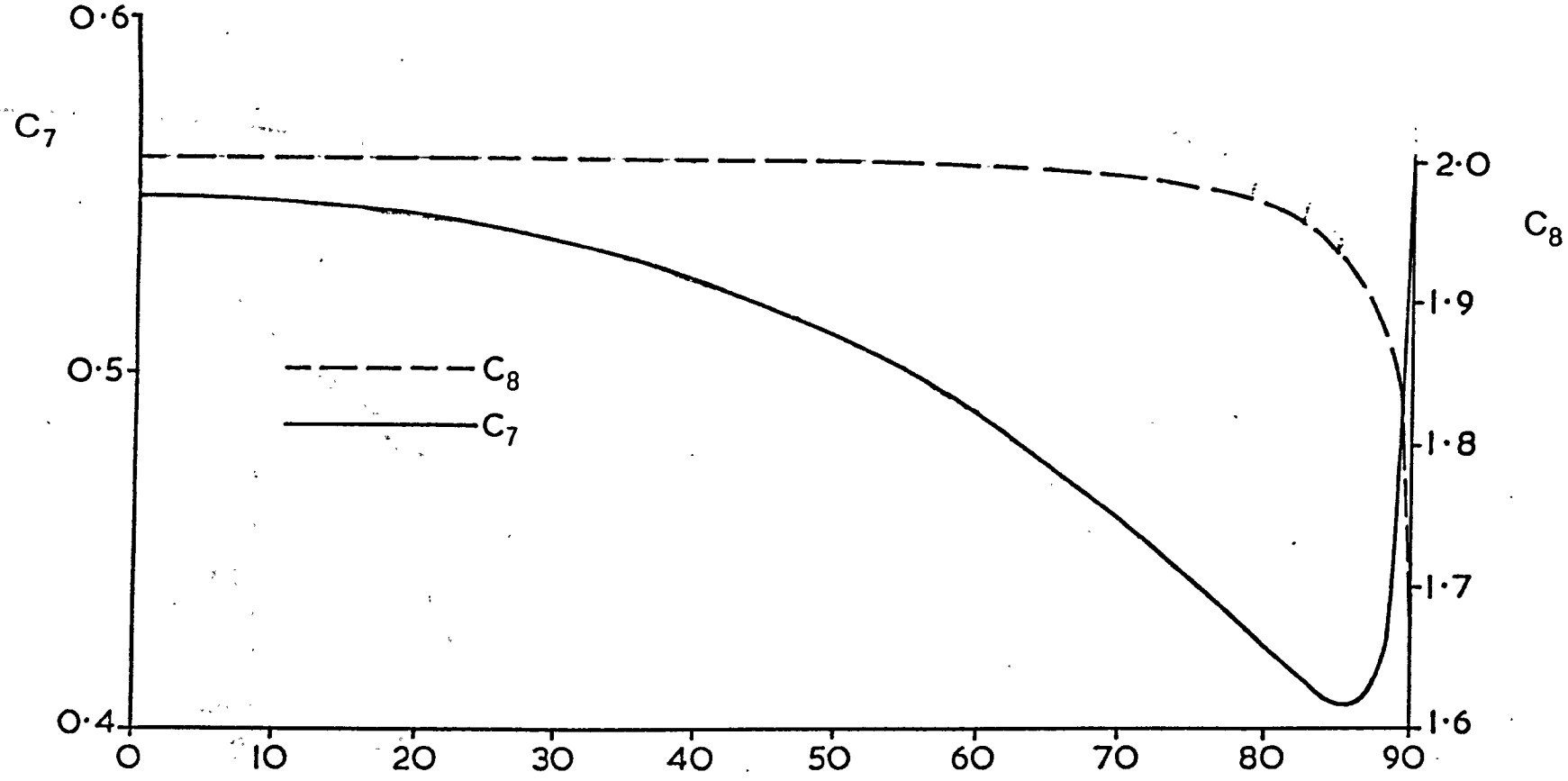

FIGURE 3·3

GRAPH OF C7 AND C8 IN THE EQUATION $Nu_x = C_7 Ra_x^{*C_8}$ AGAINST ANGLE OF INCLINATION FOR Pr = 1 FOR AN UPWARD FACING PLATE

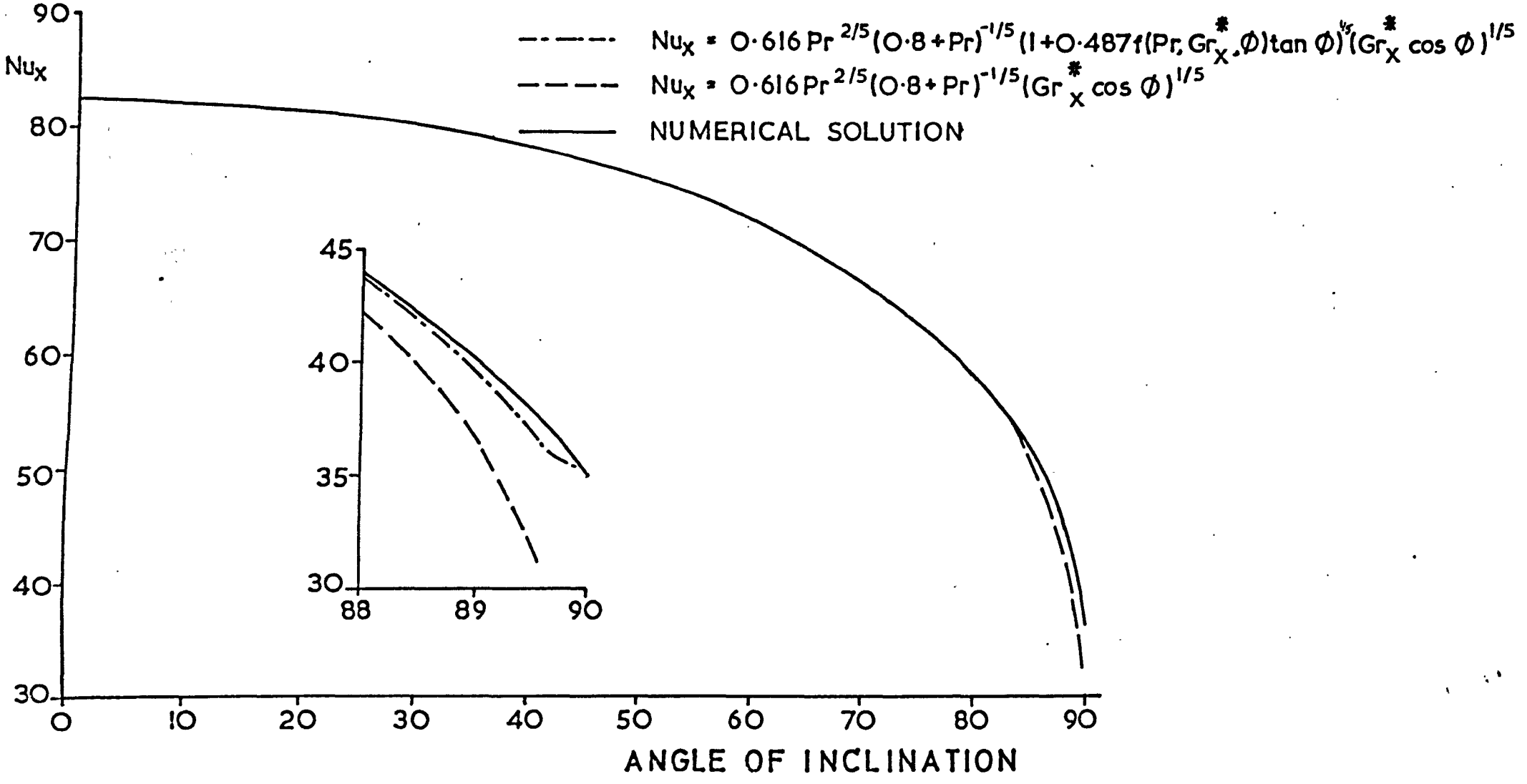

FIGURE 3·4

GRAPH OF NUSSELT NUMBER AGAINST ANGLE OF INCLINATION FOR AN UPWARD FACING PLATE.

The integrated boundary layer equations now become

$$\frac{d}{dx}\int_o^\delta u^2 dy = \int_o^\delta g\beta(T-T_\infty)\cos\phi\, dy + \int_o^\delta \frac{d}{dx}\int_y^\delta g\beta(T-T_\infty)\sin\phi\, dy\, dy - \frac{\tau_w}{\rho} \quad \ldots (3.26)$$

$$\frac{d}{dx}\int_o^\delta u(T-T_\infty)dy = \frac{1}{\rho Cp}\, q'' \quad \ldots (3.27)$$

Equations (3.26) and (3.27) have been solved by Eckert and Jackson (1955) for an isothermal vertical flat plate. They chose the following velocity and temperature profiles to represent the flow

$$u = u_2 \left(\frac{y}{\delta}\right)^{1/7}\left(1-\frac{y}{\delta}\right)^4$$

$$T - T_\infty = (T_w - T_\infty)\left[1-\left(\frac{y}{\delta}\right)^{1/7}\right]$$

but because the shear stress τ_w, and the heat transfer rate, q'', cannot be calculated from these profiles (as the laminar sub-layer has not been taken into account), they used the following expressions from forced convection work

$$\tau_w = 0.0225\, \rho u_2^2 \left(\frac{u_2\delta}{\nu}\right)^{-\frac{1}{4}}$$

$$q'' = 0.0225\, u_2 \rho Cp\, (T_w - T_\infty)\, Pr^{-\frac{2}{3}} \left(\frac{u_2\delta}{\nu}\right)^{-\frac{1}{4}}$$

On substitution into equations (3.26) and (3.27) and neglecting the sin ϕ term, the equations become

$$0.0523\, \frac{d}{dx}(u_2^2\, \delta) - 0.125\, g\beta\,(T_w-T_\infty)\, \delta \cos\phi - 0.0225\, u_2^2 \left(\frac{u_2\delta}{\nu}\right)^{-\frac{1}{4}} \quad \ldots (3.28)$$

$$q'' = 0.0366\, \rho Cp\, \frac{d}{dx}(\delta u_2 [T_w - T_\infty]) \quad \ldots (3.29)$$

These equations were solved by Siegel (1954) for a constant-heat-flux vertical plate ($\cos\phi = 1$) by replacing $(T_w - T_\infty)$ by

$$\frac{q''}{0.0225 \rho Cp u_2 \left(\frac{u_2\delta}{\nu}\right)^{-\frac{1}{4}} Pr^{-\frac{2}{3}}}$$

Equations (3.28) and (3.29) now become

$$0.0523 \frac{d}{dx}(u_2^2\delta) = \frac{5.56 g\beta\delta \dot{q}'' \cos\phi}{\rho C p u_2 \left(\frac{u_2\delta}{\nu}\right)^{-\frac{1}{4}} Pr^{-\frac{2}{3}}} - 0.0225\, u_2^2 \left(\frac{u_2\delta}{\nu}\right)^{-\frac{1}{4}} \quad \ldots (3.30)$$

$$0.615\, Pr^{-\frac{2}{3}} \nu^{\frac{1}{4}} = \frac{d}{dx}\left[\delta(u_2\delta)^{\frac{1}{4}}\right] \quad \ldots (3.31)$$

Equations (3.30) and (3.31) may be solved by using the substitution $u_2 = C_9 x^{C10}$ and $\delta = C_{11} x^{C12}$ giving

$$Nu_x = 0.0804\, Pr^{\frac{1}{3}} (1 + 0.444\, Pr^{\frac{2}{3}})^{-2/7} (Gr_x^* \cos\phi)^{2/7} \quad \ldots (3.32)$$

Equation (3.32) implies that, in turbulent flow, the effect of inclination is more important than in laminar flow

i.e. $Nu_x \propto (Gr_x^* \cos\phi)^{0.2}$ laminar flow

$Nu_x \propto (Gr_x^* \cos\phi)^{0.286}$ turbulent flow

This is contrary to the results of Vliet who found that over the range $\phi = 0^\circ$ to 60°, his data were best correlated by using the ordinary gravity component and not that parallel to the plate. The results of Lloyd, Sparrow and Eckert for turbulent natural convection mass transfer from an upward-facing inclined plate show that the constant $= Sh_x/(Gr_x Sc \cos\phi)^{\frac{1}{3}}$ varies appreciably over the range of angles $\phi = 0^\circ$ to 45°, the constant increasing as ϕ increases. The results of Lloyd, Sparrow and Eckert were for Schmidt numbers 500 times larger than the Prandtl numbers used by Vliet which might explain the discrepancy.

CHAPTER 4

METHODS OF MEASUREMENT OF TEMPERATURE AND VELOCITY

Due to the non-isothermal conditions in natural convection heat transfer experiments, the measurement of velocity can be difficult. The low velocities make calibration of anemometers difficult. In the turbulent region, the fluctuating temperature field produces difficulties in interpreting the non-linear anemometer signals and the low frequency of turbulence necessitates long integration times. In this chapter, details of the temperature and velocity sensors are described together with the calibration of the velocity sensor.

4.1 MEASUREMENT OF TEMPERATURE

As we were only interested in measuring mean temperature profiles, the frequency response of the sensor was not important. The requirements for the sensor were that it must be robust, have a stable calibration and be cheap. It should preferably have a linear response and require little instrumentation. A suitable sensor which filled these requirements was a copper-constantan thermocouple.

In the design of the thermocouple, the main consideration was to minimise the effect of conduction along its leads. To overcome this problem, a length of thermocouple wire was placed after the hot junction parallel to the test surface as shown in Figure 4.1.

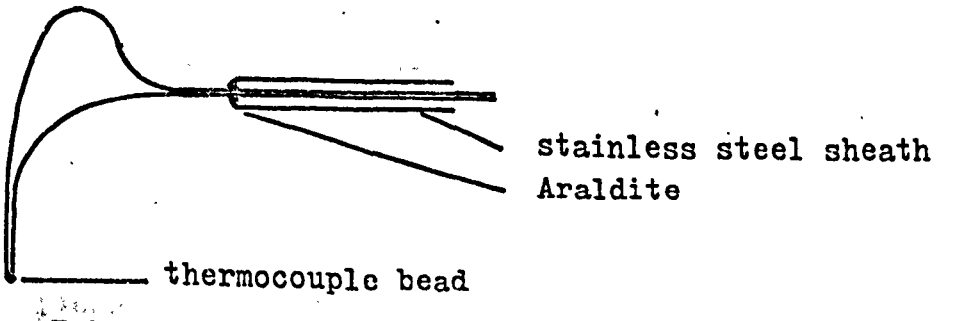

FIGURE 4.1 THE TEMPERATURE PROBE

4.2 MEASUREMENT OF VELOCITY

4.2.1 Survey of Velocity Sensors

In natural convection flows, a velocity sensor must be able to measure very low velocities, of less than 60 mm/sec in water. In the turbulent region, where the velocity fluctuations are of the order of $\pm$ 10% of the mean velocity, it is necessary to average the velocity for up to one minute or longer. There are various methods available for the measurement of low velocities and these will be discussed in turn. The various methods are listed below:

1. pressure difference with a pitot-static tube
2. hot-wire anemometry
3. quartz fibre anemometry
4. optical techniques

Using a pitot-static tube, it will be necessary to measure a pressure difference from 0 to 10^{-4} mm H_2O. This may be achieved by weighing the pressure as described by Head (1972). A top-loading balance is used as a micromanometer. A sketch of the arrangement is shown in Figure 4.2.

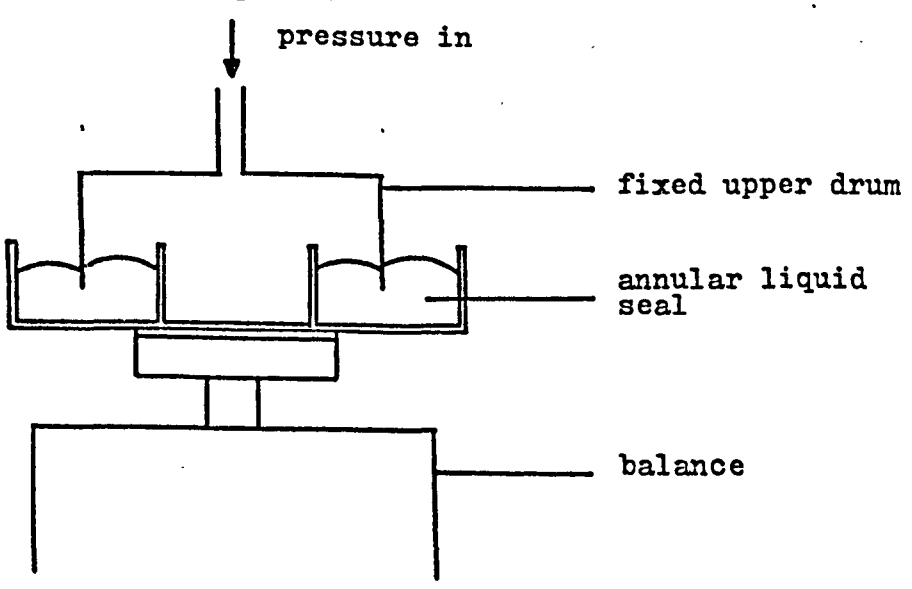

FIGURE 4.2 SKETCH OF MICROMANOMETER

By a suitable choice of drum and balance, the sensitivity of the arrangement may be increased. However, excessive lag might become a problem, and continuous evaporation of the liquid forming the seal might create difficulties.

The principle of hot-wire anemometry* is that the velocity of a fluid flowing past a thin electrically heated wire can be related to the heat transfer from the wire. The sensitive element of the anemometer is a thin wire suspended between two supports or a thin metal film deposited on a quartz support. In conducting liquids, fibre or film probes with a thin quartz coating are used instead of wire probes. The anemometer may be used in either a constant-current mode or in a constant-temperature mode. In the former, the resistance of the wire allows the heat transfer, and so the velocity, to be calculated. The most frequently used method is the constant-temperature mode where the resistance of the wire is kept constant by controlling the voltage across it. This mode has greater ease of operation.

As the heat transfer from the sensor is proportional to the temperature difference between the fluid and sensor, a change in fluid temperature will cause a change in bridge voltage. For natural convection flows, the probe will have to be calibrated for both changes in velocity and temperature.

Doubt has been cast on the use of a hot-wire anemometer in turbulent natural convection flows by Kutateladze, Kirdyashkin and Ivakin (1972), suggesting that the velocities are too low and the turbulence too high. Nevertheless, Cheesewright (1968),

---

* The term hot-wire includes hot-fibre and hot-film probes unless otherwise stated.

Vliet and Liu (1969) and Dring and Gebhart (1969) have successfully used hot-wires.

A quartz-fibre anemometer measures the velocity by the deflection of a fine quartz fibre cantilever. This system has been described by Tritton (1963c) who obtained mean and fluctuating components of velocity in a turbulent natural convection flow. The main disadvantage of this system is that it is very labour intensive.

Various optical techniques have been developed which depend on measuring the velocity of a tracer particle in the flow, usually by photography. Eichhorn (1961) used a colloidal suspension of finely divided particles of elemental tellurium produced by an electrolytic reaction. The dye has a very low settling rate and a low rate of diffusion. The method has been successfully used by Birkebak and Abdulkadir (1970) for natural convection from a downward facing horizontal plate. Brodowicz and Kierkus (1965) used dust particles and flash photography to obtain velocity profiles in air. Gaster (1964) used a similar procedure by introducing small neutral density particles into the flow and measuring their velocity from the frequency of reflected light passing through a diffraction grating. The final method to be discussed used a flash pyrolysis method described by Popovich and Hummel (1967). A dilute solution of 2 - (2,4 - dinitro-benzyl) - pyridine in 95% alcohol is employed. When a high intensity light beam is exposed to the solution, a blue tracer line is produced which may be recorded photographically.

Of the various options described, a hot-fibre anemometer was chosen as the most suitable system to use. The pitot-static tube was rejected because of its excessive lag. The quartz fibre was

rejected because of the difficulty of viewing the fibre when the plate was inclined and it being very labour intensive in turbulent flows. The problems envisaged with the optical techniques concerned the determination of the distance of the tracer from the wall and the effects of reflection and refraction through the tank windows. Also, this method would not have been suitable for turbulent flows.

Since the decision to use a hot-fibre anemometer was made, laser anemometry has emerged as a leader in velocity measurements. The laser beam is scattered by particles suspended in the flow and the scattered light may be interpreted by optoelectric means to give the velocity. A recent report by Morrison and Tran (1974) has shown that the laser doppler anemometer may be used to measure velocities down to 0.25 mm/sec with a typical error of $\pm \frac{1}{2}\%$. The system is attractive as its response is insensitive to temperature. However, at the time of decision on a choice of velocity measuring technique, laser anemometry was still in its infancy and we envisaged a lengthy development programme to implement it in the large water volumes to be used in this project.

4.2.2 Hot-fibre Anemometry

A typical fibre probe (DISA 55F06) consists of a nickel film deposited on a 70 μm diameter quartz film. The sensitive film length is 1.25 mm giving a length to diameter ratio of 18. The probe is gold plated at the ends and the nickel film is protected by a quartz coating approximately 2 μm in thickness. The main reason for choosing a quartz coated probe was to electrically insulate the probe from the electrical potential gradient in the water tank. The Reynolds Number (based on

diameter) for this probe in a flow of 60 mm/sec is 6.

The heat transfer from the film is by radiation, buoyant convection, conduction along the film to its end supports and forced convection by the fluid flow. For a typical probe, radiation loss is only 0.1% of the electrical input to the probe. From the work of Collis and Williams (1959) for forced convection past thin wires, buoyant convection may be neglected provided

$$Re_d > 2 \sqrt[3]{Gr_d}$$

For a probe with an overheat ratio of 1.1 we find $Gr_d = 0.08$ giving

$$2 \sqrt[3]{Gr_d} = 0.86$$

As the Reynolds Number is of the same order of magnitude as $2 \sqrt[3]{Gr_d}$ the probe will be working in a mixed convection region where neither forced nor natural convection forces are dominant.

4.3 CALIBRATION OF THE HOT-FIBRE PROBE

4.3.1 Survey of Calibration Procedures

It is usual to calibrate a probe against another standard, for example, a pitot tube or a flow meter. For natural convection flows, these methods become inaccurate and do not usually include the calibration of the probe for the effects of temperature. For these types of flows it is also advisable to calibrate the probe in a flow field similar to that in which it is going to be used.

The calibration of the probe for the effect of temperature may be approached in several ways. Cheesewright (1968) calibrated a hot-wire anemometer in the laminar natural convection boundary layer on a vertical isothermal flat plate assuming that the boundary layer conformed to the theoretical solution. This

method has the disadvantage that only a limited number of conditions of velocity and temperature are encountered and it does assume that the experimental rig conforms to the theoretical boundary layer solution. It has the advantage that the probe is calibrated in a flow field similar to that in which it is to be used. Using a linearized hot-film anemometer, Vliet and Liu (1969) calibrated the probe over the temperature range 21° - 45°C at 5° intervals using a temperature regulated heated vessel.

Hollasch and Gebhart (1972) calibrated for the effects of temperature by varying the overheat ratio of the hot-wire at a single reference temperature. They then derived an analytical relationship relating the anemometer output with a variable overheat resistance to anemometer output with fluid temperature variations.

The final method of accounting for temperature effects is to use a temperature-compensated probe, which ensures that the overheat ratio always remains constant. Two types of compensating element were available, a tungsten wire coil sensor or another identical hot-fibre sensor acting as a resistance thermometer. The tungsten temperature-compensating element has a slow response time and is only applicable to the compensation of changes in mean temperature, whereas the dual sensor option has a much higher frequency response to temperature fluctuations.

Of the various options discussed, a temperature-compensated hot-fibre probe using a tungsten wire coil was chosen as this simplified the velocity calibration procedure. The reason for choosing this option as opposed to the dual sensor option was economic, the latter option requiring a considerable outlay in

a new anemometer system.

Returning to the problem of velocity calibration, there are two basic methods of calibration at low velocities. The first method consists of holding the fluid stationary and moving the probe through it. The disadvantage of this method is mechanical vibration of the probe which obscures the output. The second method, developed by Dring and Gebhart (1969), is to hold the probe stationary and move the fluid which is contained in a vessel. The advantage of this is that vibrations are reduced because of the relatively large mass of the fluid. Its disadvantage, for the present application, is that there is a difficulty in orientating the probe in a manner similar to that in the actual experiment as the angle of inclination of the heated plate is changed. The first method was therefore chosen.

4.3.2 The Velocity Calibration Rig

The calibration equipment is shown schematically in Figure 4.3 and a photograph of the equipment is shown in Plate 4.1.

The equipment was designed to simulate, as closely as possible, the actual experimental situation. The probe was driven through a large tank of de-aerated and de-ionized water (230 ℓ capacity) by a thin stainless steel rod which was connected via a carriage to a screwed rod. The screwed rod was driven via a flexible drive and reduction gears by a variable speed $\frac{1}{2}$ h.p. D.C. motor. The probe could be traversed through the water at any angle from the vertical to the horizontal as it was thought that there might have been a slight difference in the calibration curves for differing angles. A counter-weight was suspended from the carriage to reduce the vibrations of the probe.

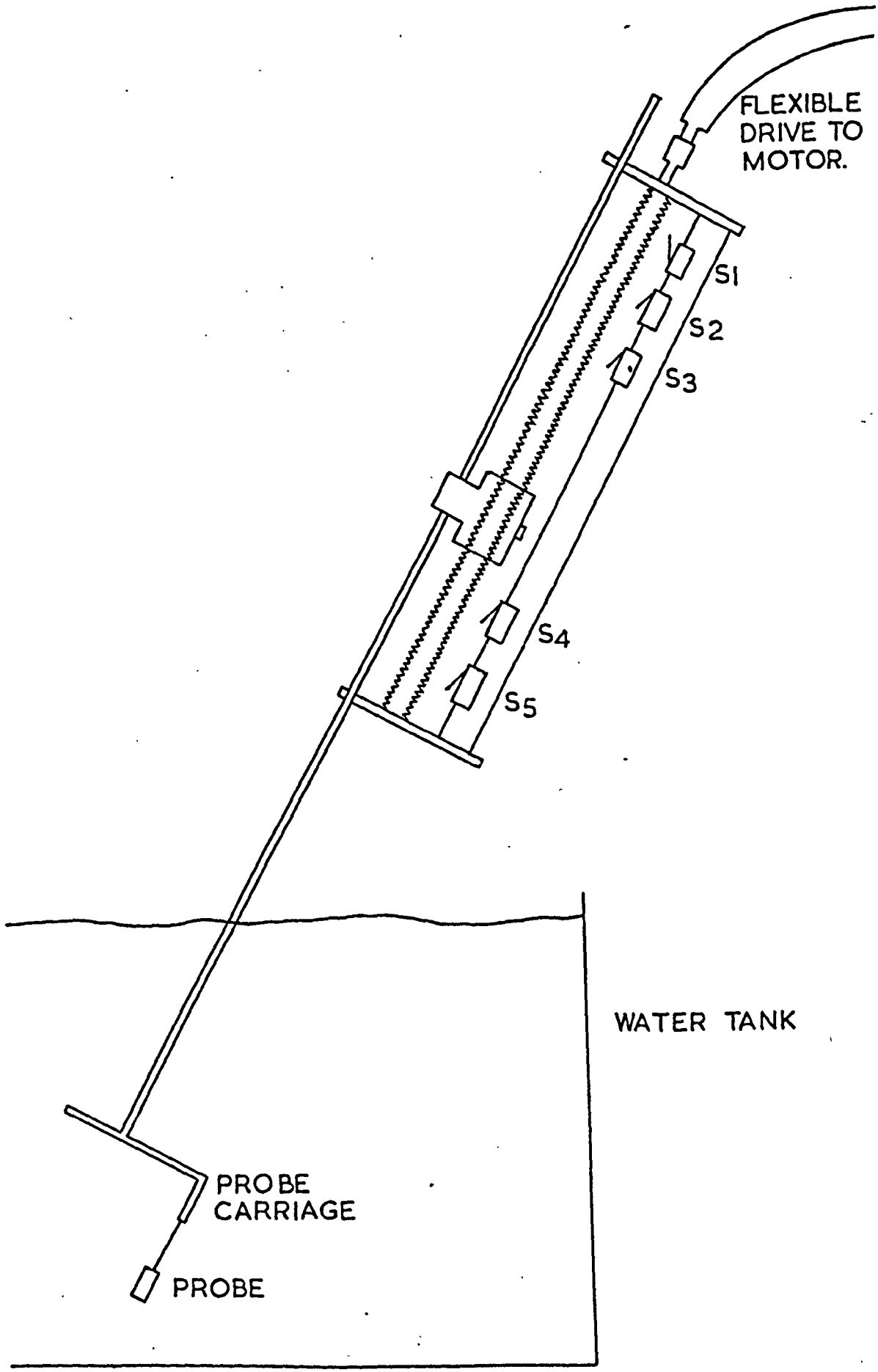

FIGURE 4·3
SKETCH OF VELOCITY CALIBRATION RIG.

PLATE 4·1

PROBE CALIBRATION RIG

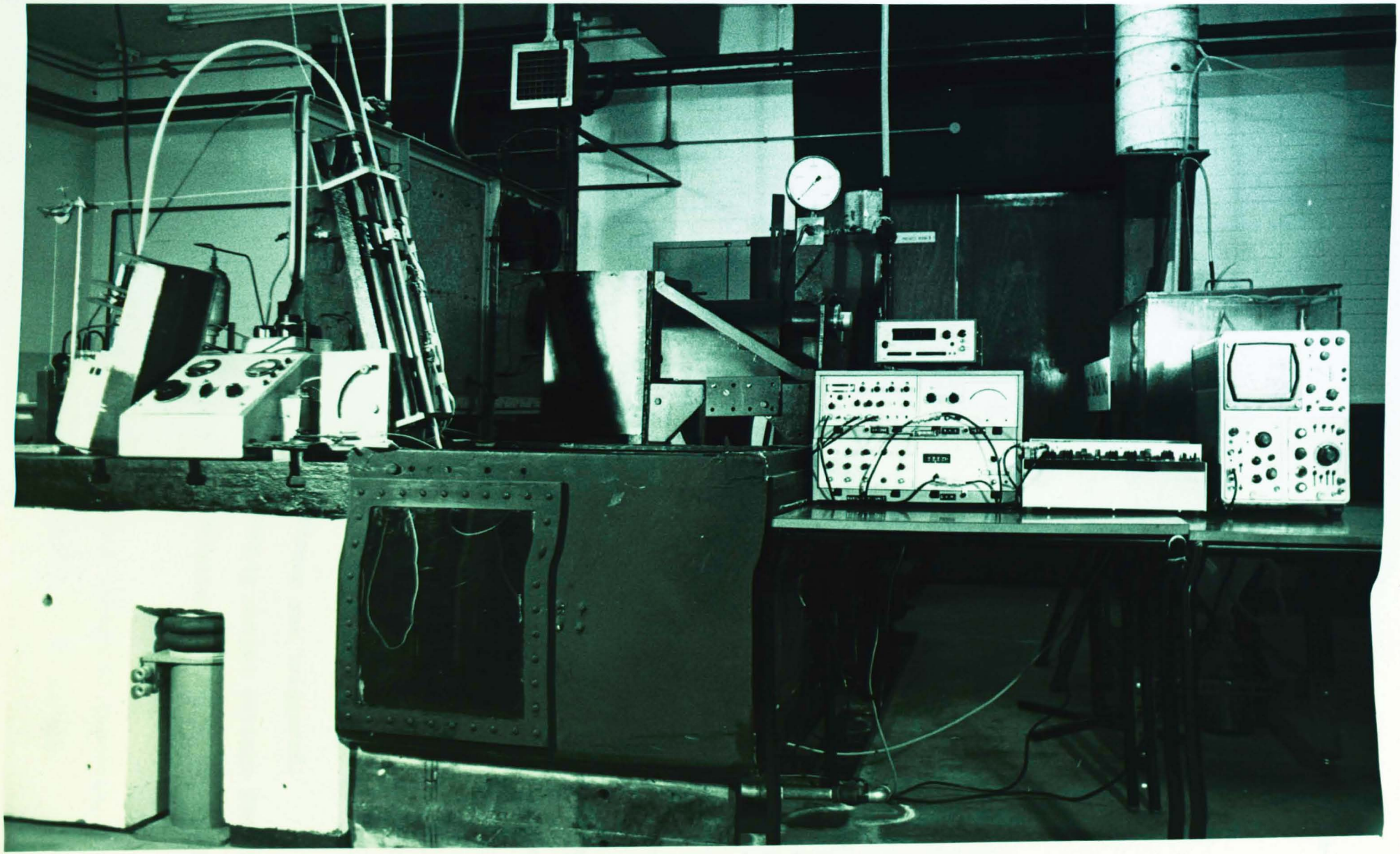

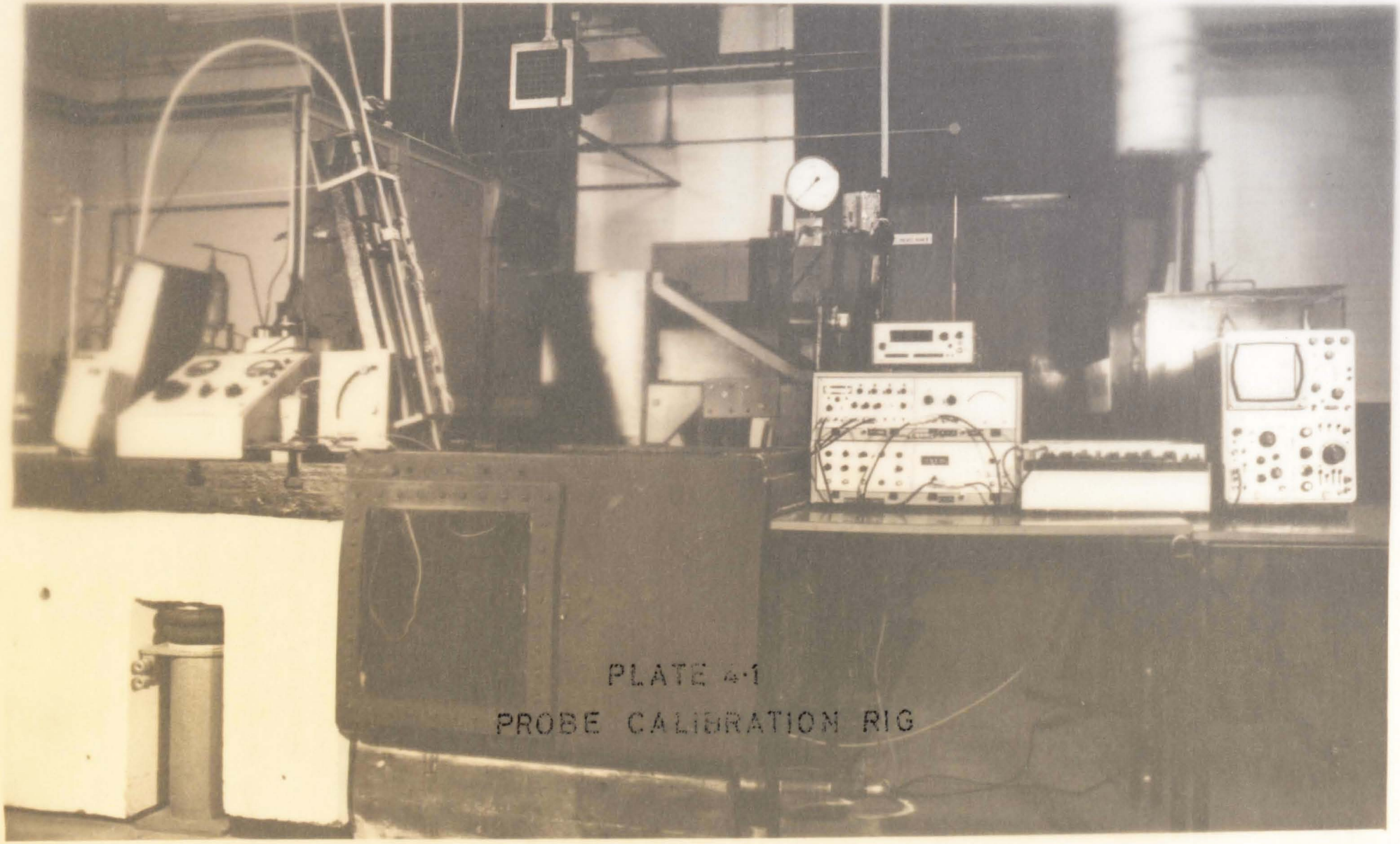

PLATE 4·1
PROBE CALIBRATION RIG

A pair of microswitches (S_1 and S_5) were used to stop the probe at the ends of its travel. A Venner Digital Counter Model 7737 was used to time the travel of the probe between microswitches S_3 and S_4 which had previously been set at a known distance apart.

The temperature-compensating element, together with a matching network, was connected to a DISA 55D01 anemometer together with the hot-fibre probe (55F06). The output from the anemometer was recorded on a Bryan's/Southern Instruments XY/t plotter and a DISA Digital Voltmeter. The system is shown in Figure 4.4. The XY/t plotter was automatically started by microswitch S_2. Details of the matching network are given in Appendix A.

4.3.3 Experimental Procedure

The following procedure was used to calibrate the fibre probe. The angle of traverse was first set and the probe was then moved to its starting position. The water in the tank was allowed to settle until the output voltage from the anemometer was steady. The XY/t plotter and Venner Timer were re-set. The motor was then switched on to give the desired velocity.

The probe moved a short distance before the XY/t plotter was triggered to allow the flow field around the probe to stabilize. A short time later the timer was triggered.

It was found that the zero velocity output voltage from the anemometer was very sensitive to vibration and could vary by up to 6%.

The probe was calibrated at three angles of traverse, 0°, 60° and 81°, the velocity ranging from 0 to 80 mm/sec.

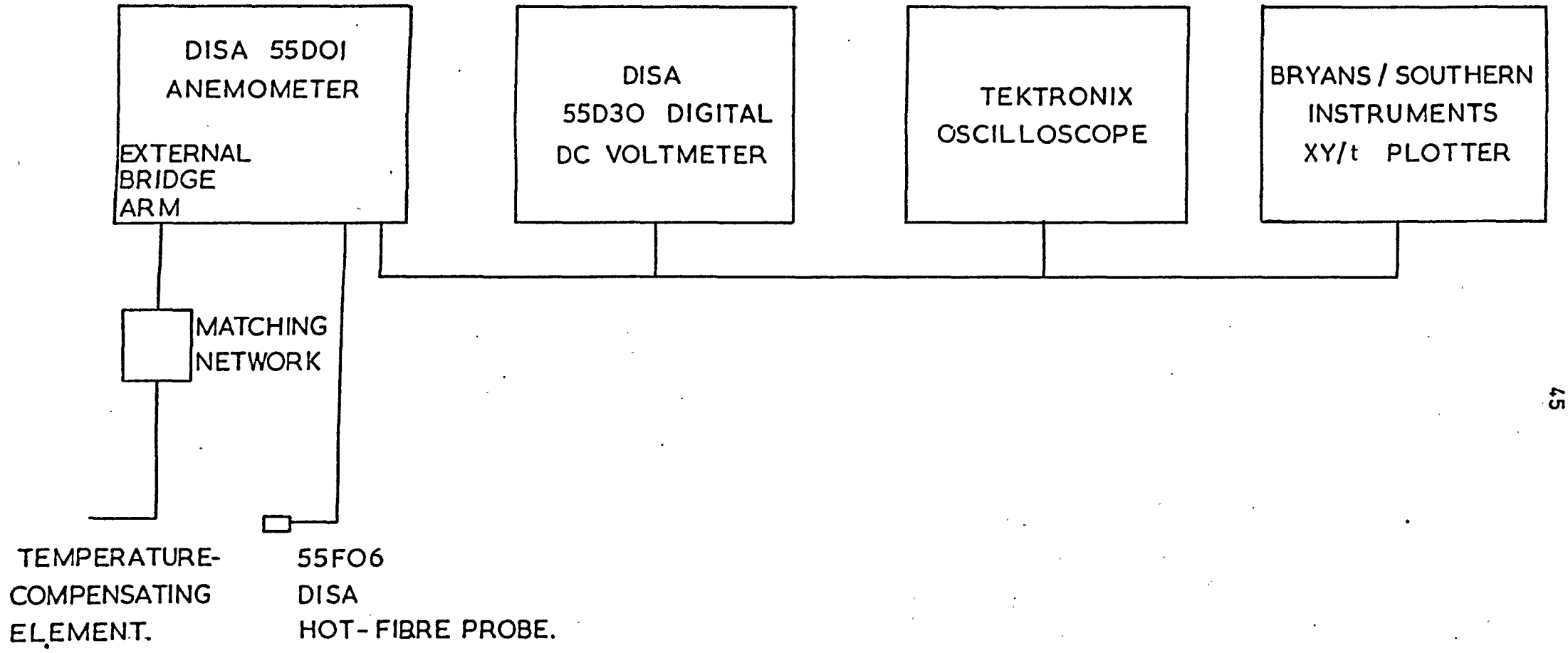

FIGURE 4·4

VELOCITY CALIBRATION SYSTEM

4.3.4 Presentation of Calibration Data

Various universal correlations have been suggested for correlating the heat transfer from hot-wires. In situations where the buoyancy force may be neglected, the universal correlations like King's Law or the 0.45 law give a useful guide to the best way of plotting the results (see Bradshaw (1971)). When buoyancy forces are important these forms of correlation do not hold. The data were therefore plotted as a graph of anemometer output voltage against velocity and a best fit curve was fitted (see Figure 4.5). The best fit curve is given in equation (4.1)

$$u\ (\text{mm/sec}) = 653.37 - 383.67e + 82.76e^2 - 7.84e^3 + 0.28e^4 \quad \ldots (4.1)$$

where e is the output voltage from the anemometer.

This was used to calculate the velocities from the anemometer output voltage.

Within the scatter of the data, there is no noticeable difference between the calibration points for each angle of traverse for velocities less than 30 mm/sec. Above this value, there was some divergence of the data for differing angles but as no velocity profiles were obtained above this value, equation (4.1) was assumed to be only a fit for velocities less than 30 mm/sec.

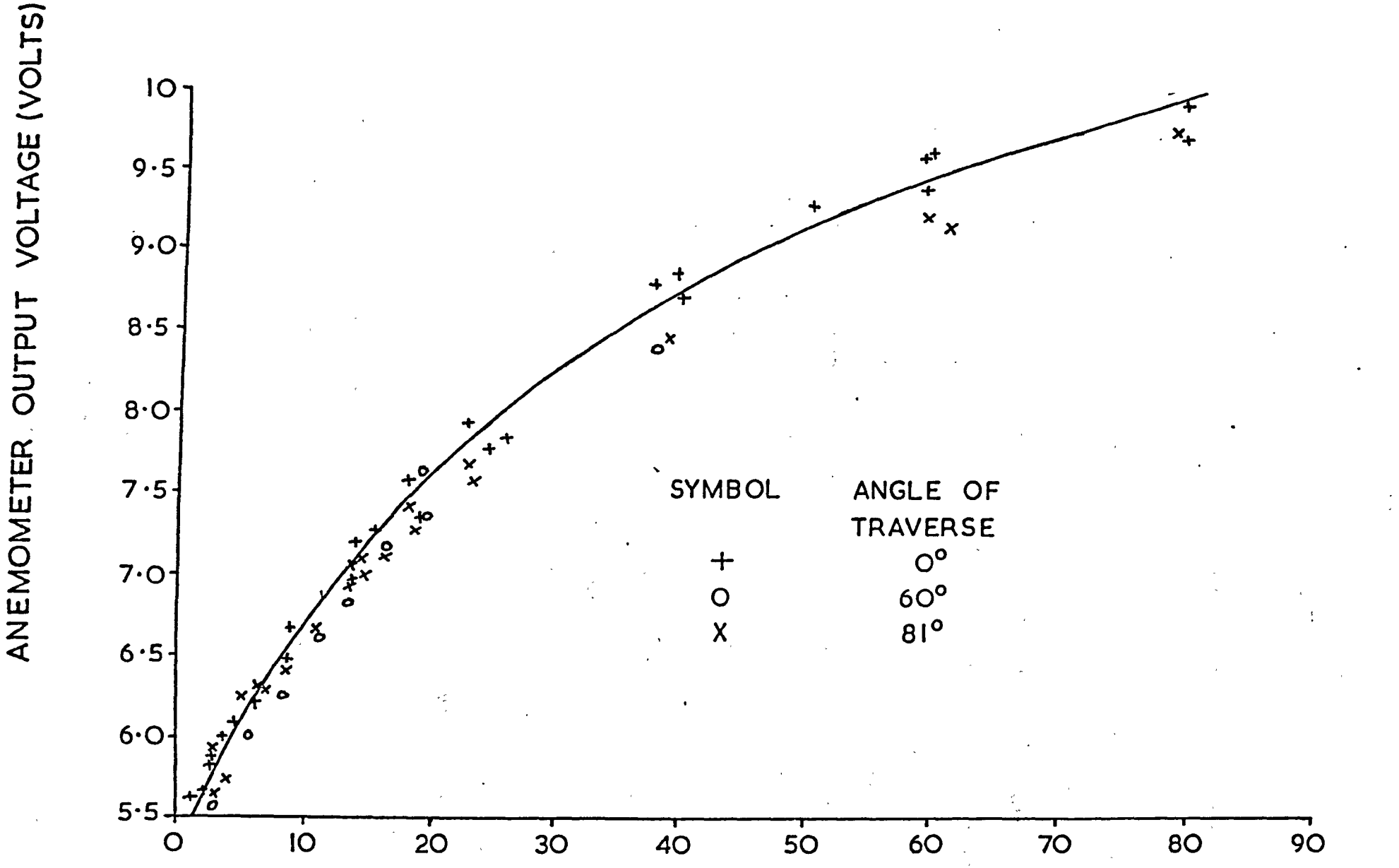

FIGURE 4·5

CALIBRATION CURVE FOR HOT-FIBRE PROBE

CHAPTER 5

EXPERIMENTAL APPARATUS

5.1 INTRODUCTION

This chapter describes the two experimental rigs together with their respective instrumentation. A small rig was built for investigation of the laminar flow region and a large rig for investigation into the transition and turbulent regions.

There are two methods of heating which will produce a uniform heat output from the heated plate, either direct electrical heating of a thin metallic foil or electrical heating elements, for example, mineral insulated cable. Using a thin metallic foil, one can ensure a uniform heat flux provided the foil has a low thermal coefficient of resistance. To obtain a large heat output it is necessary to use a high current because of the low resistance of the foil. Using separate heating elements one cannot guarantee as uniform a heat flux. The small rig used individual heating elements and the large rig used direct heating of a thin metallic foil.

One of the main problems in the design of the rigs was caused by corrosion. The majority of components for use underwater were constructed from copper, brass or stainless steel. It was inevitable that some components were made of mild steel due to the higher cost of, or difficulties in obtaining, the former materials. In this event, the steel was painted to isolate it from the water.

5.2 THE SMALL INCLINED PLATE RIG

5.2.1 A General Description of the Rig

The general arrangement of the rig is shown in Figure 5.1. It consisted of a small galvanized iron water tank (230 ℓ capacity)

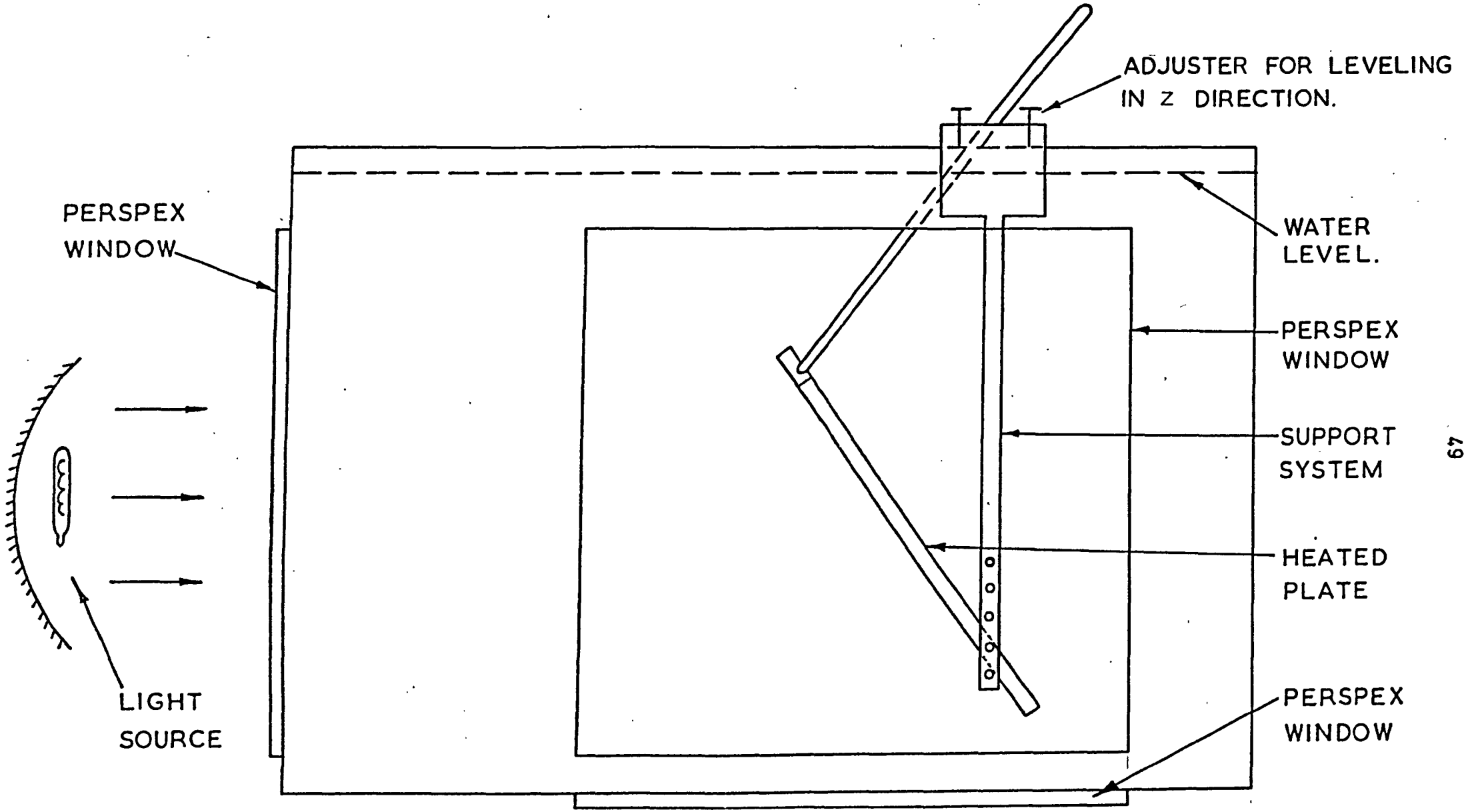

FIGURE 5·1

GENERAL ARRANGEMENT OF THE SMALL RIG.

0.9 m long by 0.6 m high by 0.6 m wide mounted on a steel frame. The tank had several perspex windows so that the heated plate could be viewed from any direction. Both the inside and outside of the tank were painted with matt black paint to reduce stray light when photographing the flow.

The light source used for illuminating the particles for flow visualization gave a narrow parallel beam of light. A commercial 12-volt motor car fog lamp was found to give a suitable light source. The perspex window opposite the plate was covered with thick black paper and a sheet of wood except for a 2 cm wide vertical slit for the light to pass through. The lamp was air-cooled to prevent it from overheating.

The heated plate was suspended from the top of the tank. The support structure was designed such that the plate could be suspended at various heights in the tank. At angles of inclination near the vertical, a large depth of water was required above the trailing edge of the plate. At angles of inclination near the horizontal a greater depth of water was required below the plate. The inclination of the plate could also be adjusted in the z direction (i.e. the width of the plate). This was particularly important when the plate was horizontal.

A drawbridge principle was used to change the angle of inclination of the plate. The angle was set approximately with a protractor and accurately with a plumbline and clinometer.

Plate 5.1 shows a photograph of the rig.

PLATE 5·1

SMALL HEATED PLATE RIG

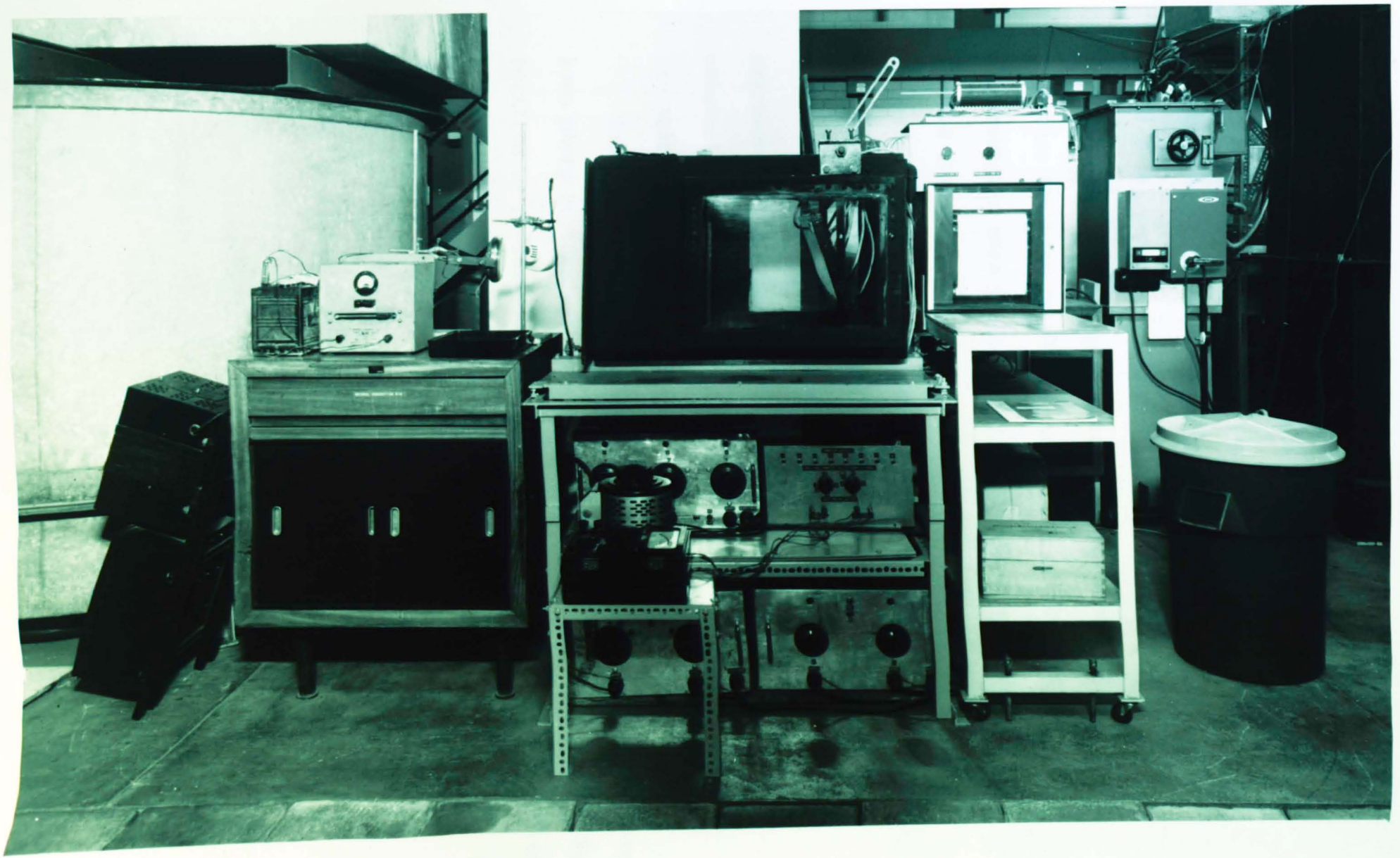

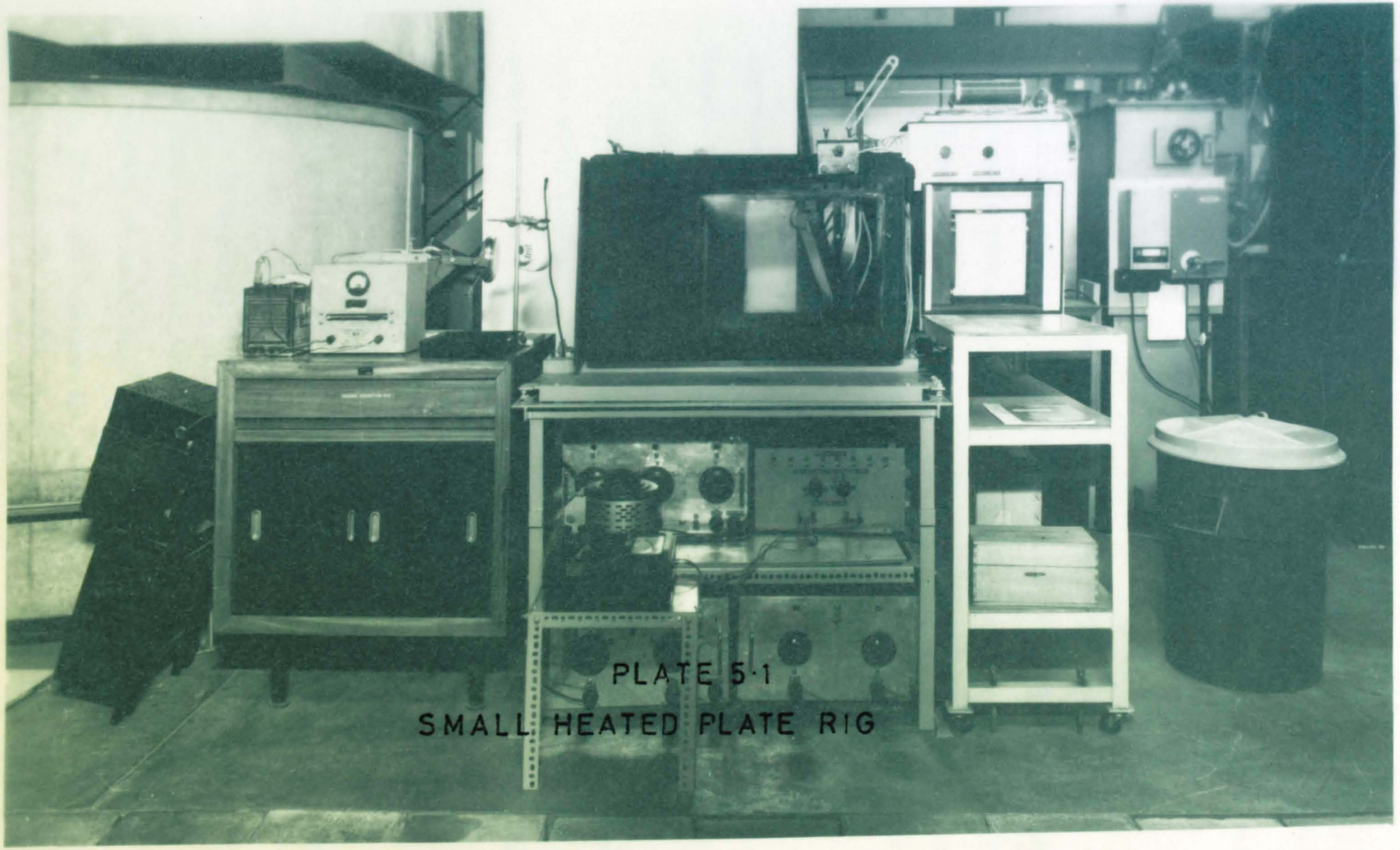

PLATE 5·1

SMALL HEATED PLATE RIG

5.2.2 Details of the Heated Plate

The construction of the heated plate is shown in Figure 5.2. The heat transfer surface was a stainless steel sheet, 29.2 cm long, 51.3 cm wide and 6.35 mm thick. This gave a boundary layer thickness to plate width ratio of 1:20 . Slots, 1.5 mm deep and 1.5 mm wide, were milled along the width of the plate every 25.4 mm from the leading edge to accommodate thermocouples and to reduce the heat flow along the length of the plate. After the thermocouples were installed by glueing down with 'Araldite', the grooves were filled with silicon rubber. With this construction, the effective thermal conductivity in the longitudinal direction is only 83.6% of the effective thermal conductivity in the transverse direction. The thermocouples were manufactured by spark-welding a junction at the end of 36 gauge BS 1828 copper-constantan wire insulated with insuglass. The mean diameter of the thermocouple beads was 0.75 mm.

Behind the heat transfer surface were eight electrical seamless strip heaters each of 400 watts capacity, which were held in position by pressure. The heaters were separated from each other by 6.35 mm tufnol strips, once again to reduce longitudinal conduction.

A 12.7 mm thick layer of Sindanyo insulation (an asbestos cement board) was placed behind the heaters followed by 3.175 mm of low thermal conductivity Refrasil fibre insulation and then 15.67 mm of Sindanyo. Thermocouples similar to those mentioned previously were glued to this sheet of insulation for the calculation of heat loss. The whole assembly was mounted in a tufnol frame and waterproofed with silicon rubber and black nylon paint.

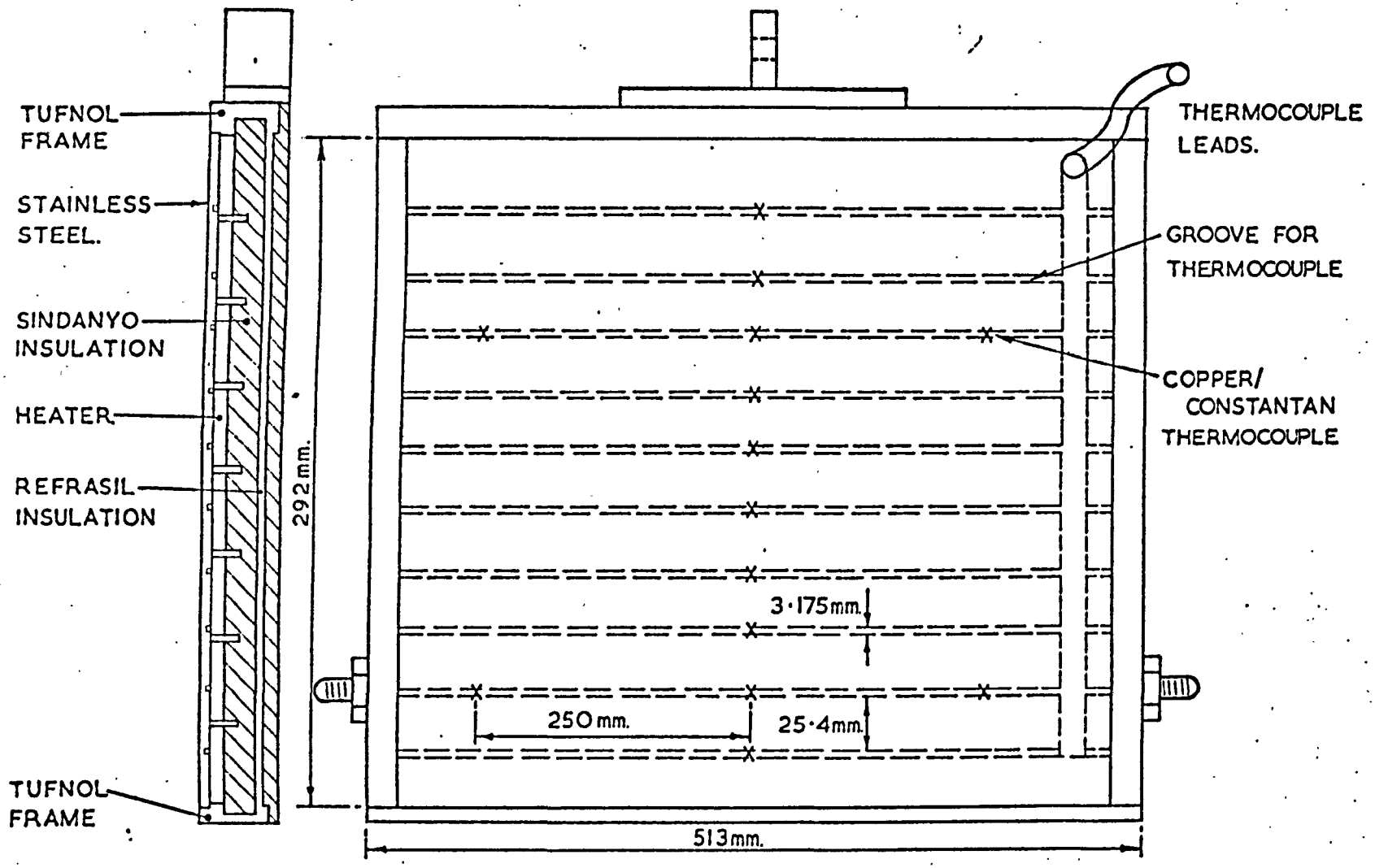

FIGURE 5·2

SKETCH OF SMALL HEATED PLATE

5.2.3 Instrumentation

The power through each heater unit was regulated by an individual variac and was measured with a precision Sangamo-Weston wattmeter with an accuracy of ± ½%. The wattmeter had previously been calibrated. To ensure no voltage fluctuations in the heaters, the power was supplied from a constant voltage regulator with an output voltage of 230 volts rms and a maximum load of 3 kW.

The heated plate thermocouples were recorded on a twelve-point Cambridge P. 180 Chart temperature recorder with a full scale deflection of 50°C. The instrument had good stability and repeatability. An A.E.C. cold junction thermostat was used for the reference temperature. The thermocouples were calibrated in situ between 15°C and 60°C by heating the water to the desired temperature and allowing the rig to attain steady state. The results indicated that the thermocouples were accurate to within ± 1%. Three thermocouples were used to measure the bulk water temperature. These were positioned at heights of 0, 12 and 30 cm above the heated plate leading edge and placed equi-distant between the heated plate and the end of the water tank.

5.2.4 Heat Flux Distribution

A finite element computer program which solves steady state heat conduction problems was used to model the heat flux distribution in the heated plate. In the finite element method, the structure is dissected into small manageable components which are then analysed and merged together. The computer program used here was the PAFEC 70 + Scheme (1972) developed in the Department of Mechanical Engineering, University of Nottingham.

The heated plate was divided into a series of 8 noded two-dimensional quadrilateral elements, with the following boundary conditions:

1. No heat loss from the ends of the plate
2. Heat transfer coefficient on the heat transfer surface = 332 W/m^2K
3. Heat transfer coefficient on the insulated surface of the rig = 84 W/m^2K
4. Heat flux from the heaters = 3700 W/m^2

The resulting heat flux distribution is shown in Figure 5.3. The dips in the curve are caused by either the thermocouple or the insulation separating the heaters. At 0.175 m from the leading edge, there is a sharp drop in the heat flux caused by a thermocouple and the heater separation insulation being next to each other. The graph shows that the heat flux varies by $\pm$ 11%.

5.3 THE LARGE INCLINED PLATE RIG

5.3.1 A General Description of the Rig

Plate 5.2 shows a photograph of the rig. It consisted of a large mild steel water tank (2,500 ℓ capacity), 1.83 m long by 1.83 m high by 0.76 m wide placed on a wooden frame. On one of the larger sides of the tank two plate-glass observation windows were installed and on the adjacent side wall a narrow perspex window was installed. Both the inside and outside of the tank were painted with a polyurethane-based anti-corrosive paint. Details of the design of the tank are given in Appendix C. As there was no electrical insulation between the heated plate and the water, a lid was fitted to the tank.

FIGURE 5·3

THEORETICAL CURVE OF HEAT FLUX

DISTRIBUTION ON SMALL HEATED PLATE

PLATE 5·2

LARGE HEATED PLATE RIG

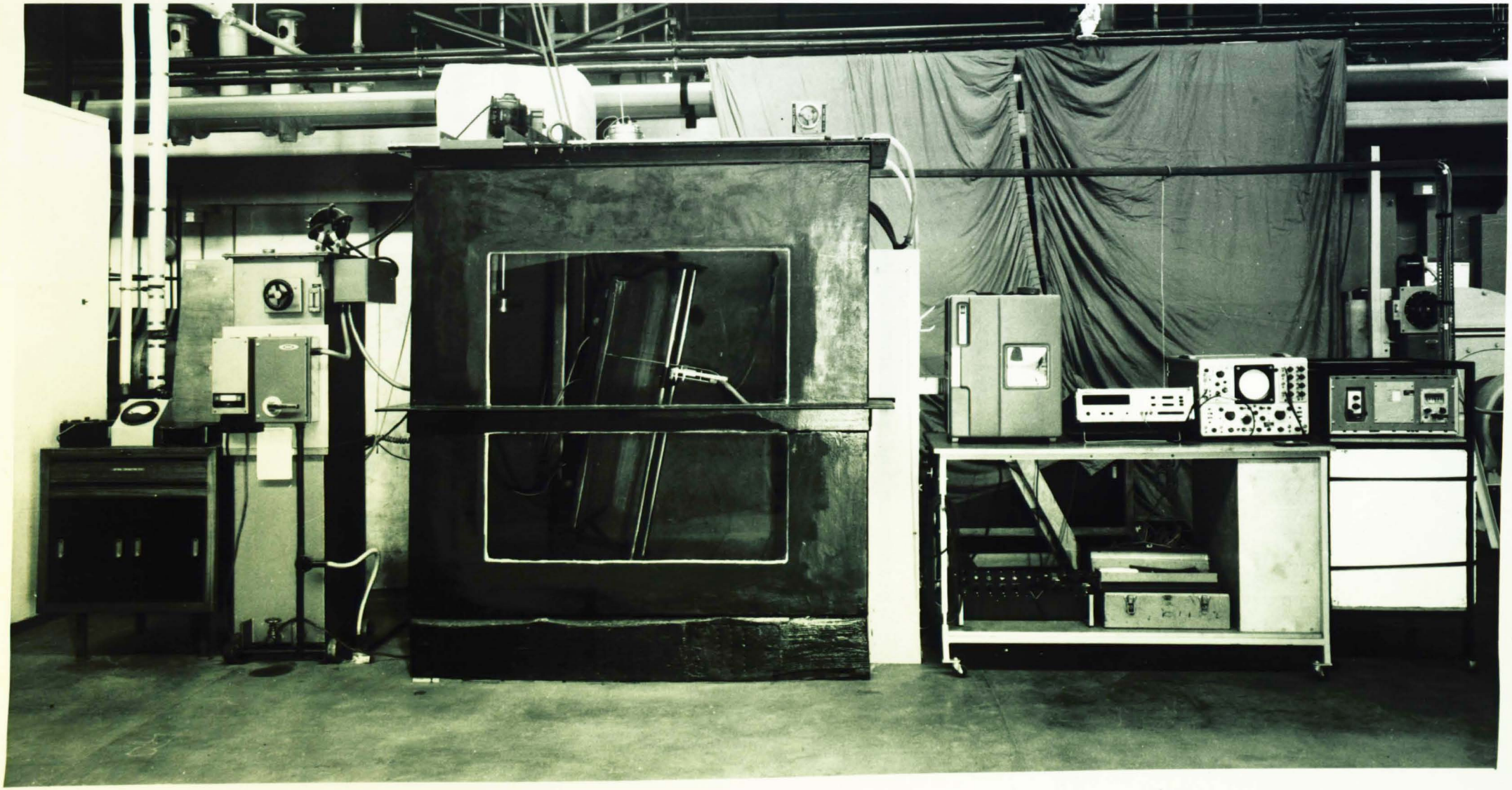

PLATE 5·2

LARGE HEATED PLATE RIG

Microswitches were fitted to the lid such that the rig could not be switched on until it was closed. The light source for flow visualization and the heated plate support structure were similar to those of the small rig (see Section 5.2.1).

5.3.2 Details of the Heated Plate

The heated plate, 1 m long and 0.6125 m wide, consisted of an electrically-heated copper-nickel sheet backed by a phenolic sheet and silicon rubber as shown in Figure 5.4. The heating element consisted of five strips of 0.05 ± 0.002 mm thick and 12.2 ± 0.05 cm wide foil (46% Cu - 54% Ni) heated by alternating current. The strips were placed adjacent to each other with a spacing of 2 mm between them and connected in series. The width of the foil ensured a uniform electrical distribution within ± 6%. The foil had a very stable resistance, its resistance changing by only 0.2% for a 50°C temperature change. The centre foil was the test section with the remaining four foils acting as guard heaters. Thirty-three insulated copper-constantan (0.193 mm dia.) thermocouples were glued to the inner surface of the test section and twelve across the plate to check for any variation due to edge effects. The thermocouple leads were placed along isotherms for approximately 5 cm before being passed through the insulation.

Behind the foil was a 1.58 mm layer of silicon rubber. This was used to fill up the gap between the thermocouple leads and the phenolic insulation and also to allow for thermal expansion of the foil. To ensure a good bond between the foil and the silicon rubber, the foil was first coated with a thin film of 'Evostick' adhesive which was allowed to dry. Careful

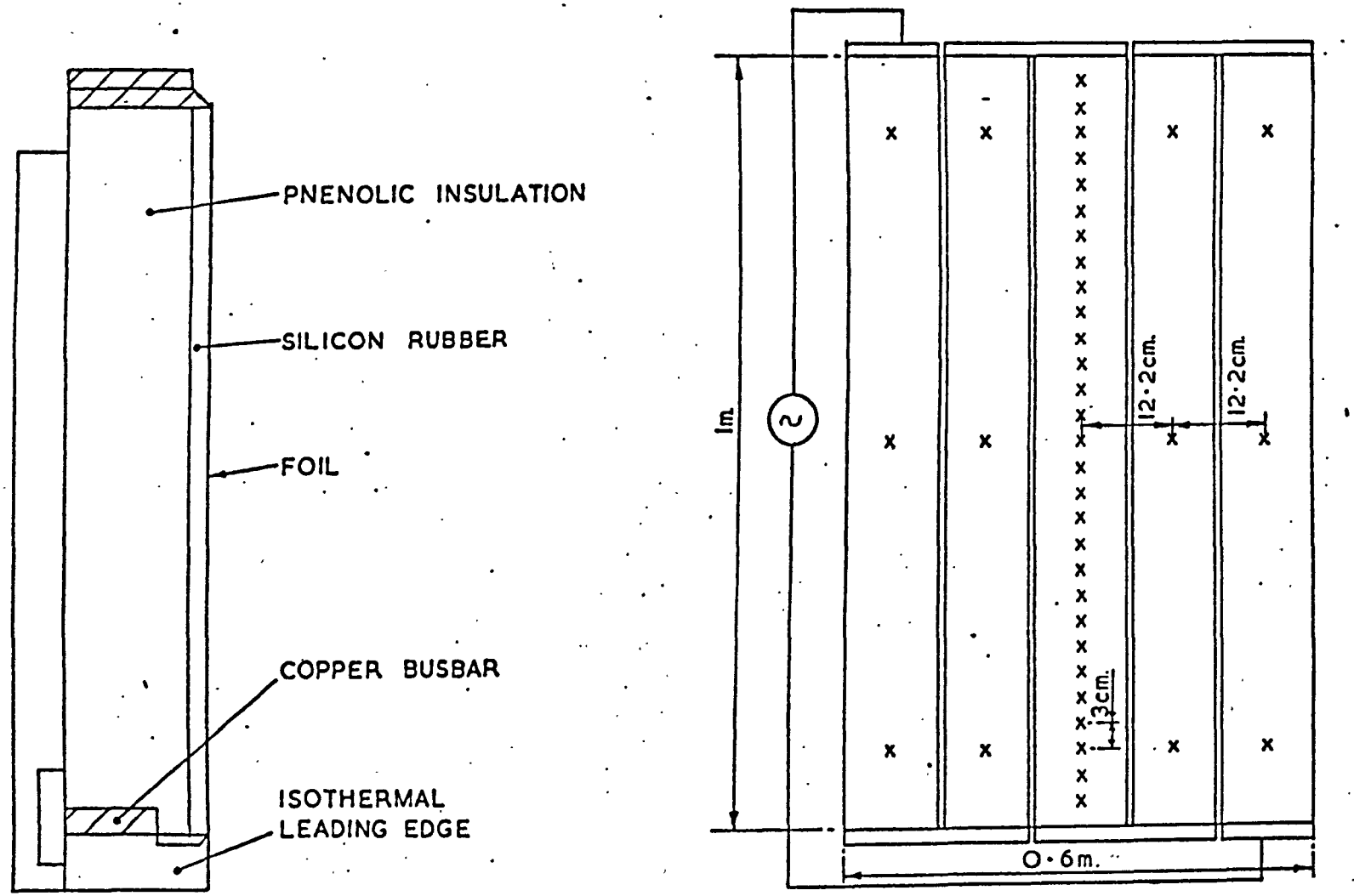

FIGURE 5·4

SKETCH OF LARGE HEATED PLATE

attention was given to ensuring that no air pockets were present in the silicon rubber.

The phenolic insulation was 22.2 ± 0.05 mm thick. Thin film thermocouples were glued to the insulation for the calculation of heat losses.

The whole assembly was mounted on a brass angle frame and waterproofed with black nylon spray except for the heat transfer surface.

5.3.3 Instrumentation

5.3.3.1 Power Supply

The power supply was a Brentford Regulating Unit Type RO 30/04 comprising an autowound regulator together with a double wound stepdown transformer. The regulator was immersed in oil and cooled naturally. With an input of 415 volts at 50 Hz the transformer gave a stepless output of 0 to 82.4 volts with a maximum current of 375 amps.

The output current from the transformer was measured with a Crompton Parkinson ammeter (0 - 5 amps) using a current transformer (B.S. 3938 Class AM/AL) with tappings of 0 - 100 amps and 0 - 200 amps. The voltage drop across the test section was measured with an Avometer calibrated to ± ½%. A check was made on the power factor and within the accuracy of the equipment it was found to be 1.

5.3.3.2 Data Acquisition System

The heated plate and bulk thermocouple emf's were recorded on magnetic tape using a data acquisition system shown in Figure 5.5. The thermocouple leads were taken to an isothermal enclosure where the constantan leads were all connected to the

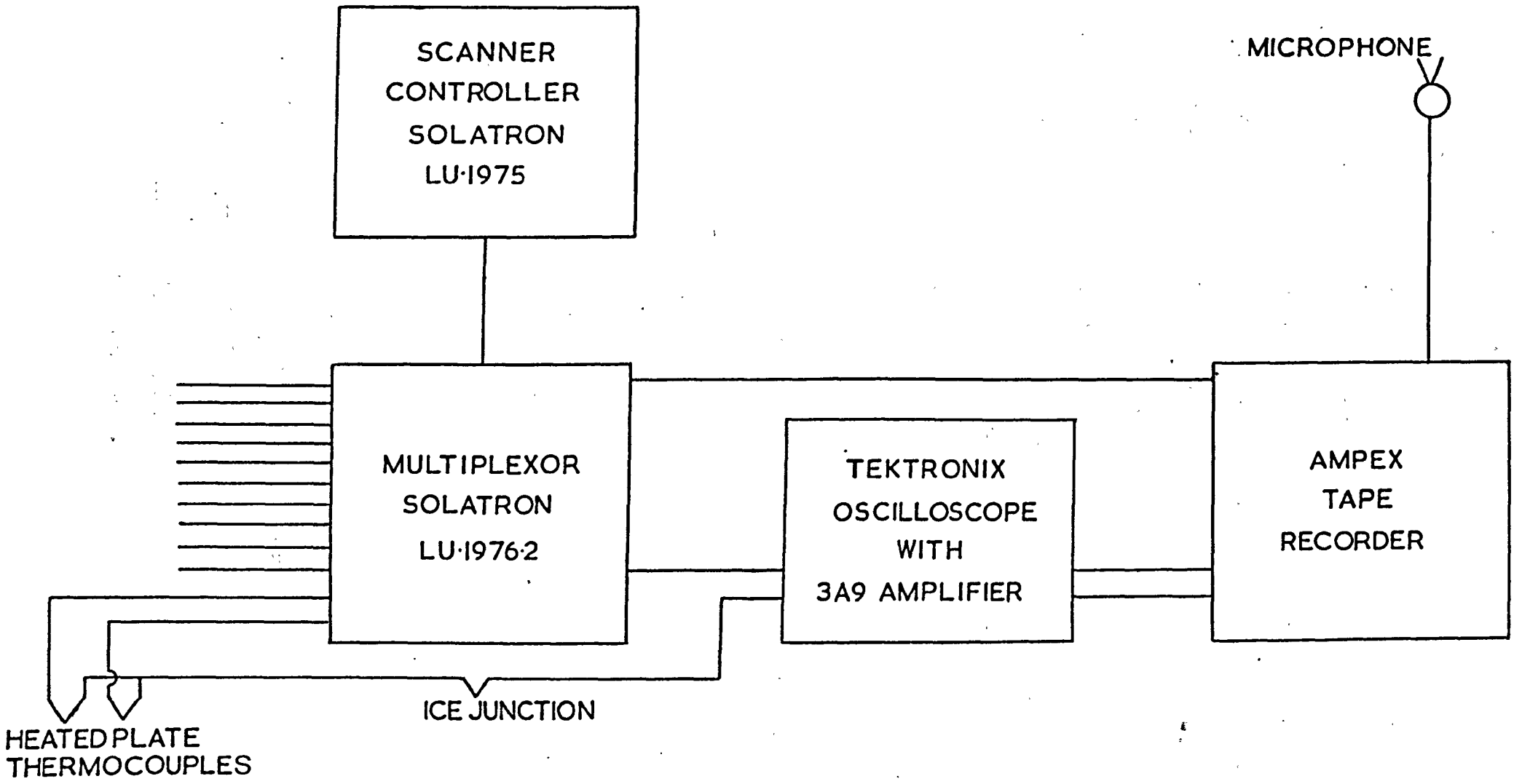

FIGURE 5·5

DATA ACQUISITION SYSTEM

cold junction thermocouple which was placed in crushed ice. The remaining copper leads were then taken through a Solatron multiplexer. The output from the multiplexer and cold junction was fed to a Tektronix 3A9 AC/DC coupled differential amplifier. The amplifier was housed in a Tektronix Oscilloscope (Type 565) which also displayed the signal. The amplifier had excellent common-mode-rejection and high gain characteristics. The amplifier was set for a gain of 500 and its output was fed to an Ampex F.M. tape recorder. Each time the multiplexer switched channel, it sent an electrical impulse which was recorded on another track of the tape recorder.

5.3.3.3 The Processing Software

Figure 5.6 shows the output from the differential amplifier. On switching to the next channel, electrical noise was produced by the multiplexer. The signal then changed to its new value after the electrical transients had died away. The analogue signal was converted to digital form using a PDP 8 minicomputer, the software having been written by Cooper (1974). The timing signal, which initiates the ADC (analogue to digital conversion), was produced 35 ms after the multiplexer had switched. The ADC programme then waited for 600 ms, to allow the transients to die away, before taking 1,000 samples of the signal and averaging them to give a mean value. By taking several samples of the signal after the ADC had started, it was found that after 600 ms the digital value remained constant, indicating that the transients had died away.

5.3.3.4 The Traverse Mechanism

The probe traversing mechanism is shown diagrammatically in

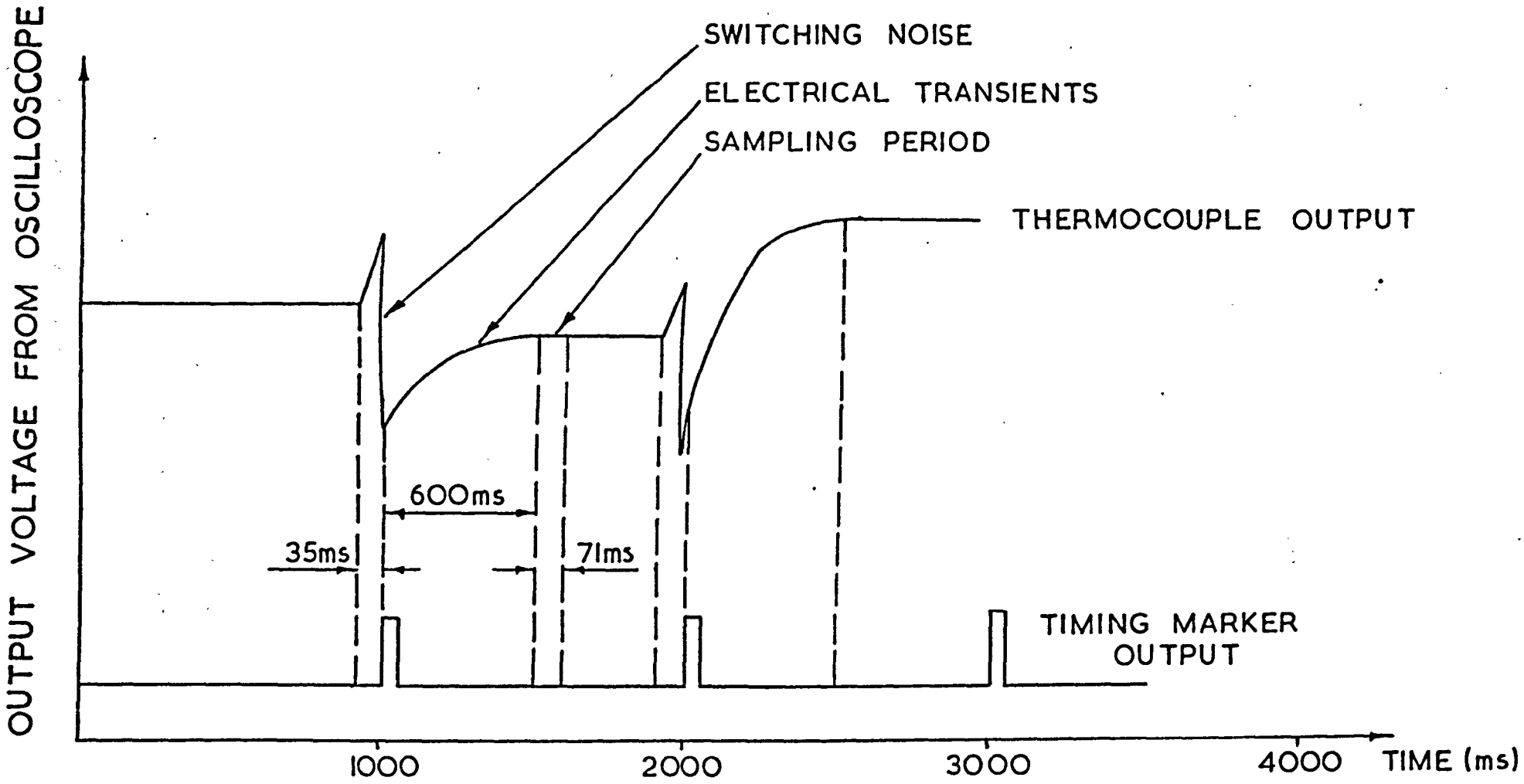

FIGURE 5·6

THERMOCOUPLE OUTPUT FROM OSCILLOSCOPE

Figure 5.7. It was permanently fixed to the rig so that the probe always entered the boundary layer perpendicular to the plate.

The traverse mechanism consisted of a 1 mm pitch screw which was rotated from the outside of the rig via a flexible drive. Due to some play in the flexible drive and screw thread, the movement of the probe carriage was measured with a vernier gauge and ruler. It was read by a telescope through the inspection windows.

The mechanism was bolted to a carriage which moved along the length of the plate on two stainless steel rods at a distance of 20 cm from the plate. The carriage could be set at 10 cm intervals up the plate.

5.3.3.5 The Temperature Probe

The temperature in the boundary layer was measured with a copper-constantan thermocouple probe with 0.2 mm diameter wires, as described earlier in Section 4.1. Two systems were used to record the thermal emf, one for laminar flow and the other for turbulent flow.

In the laminar boundary layer, the emf was measured with a Solatron LM 1604 digital voltmeter. As it was necessary to measure a fluctuating signal in the transition and turbulent regimes, a system similar to that used for measuring the heated plate thermocouples was used. The signal was fed via a high gain D.C. amplifier to an Ampex F.M. tape recorder. The resulting analogue signal was then analysed on a PDP11/05 minicomputer to give mean and r.m.s. values of the temperature. At each position of the probe, the signal was recorded for 100 sec.

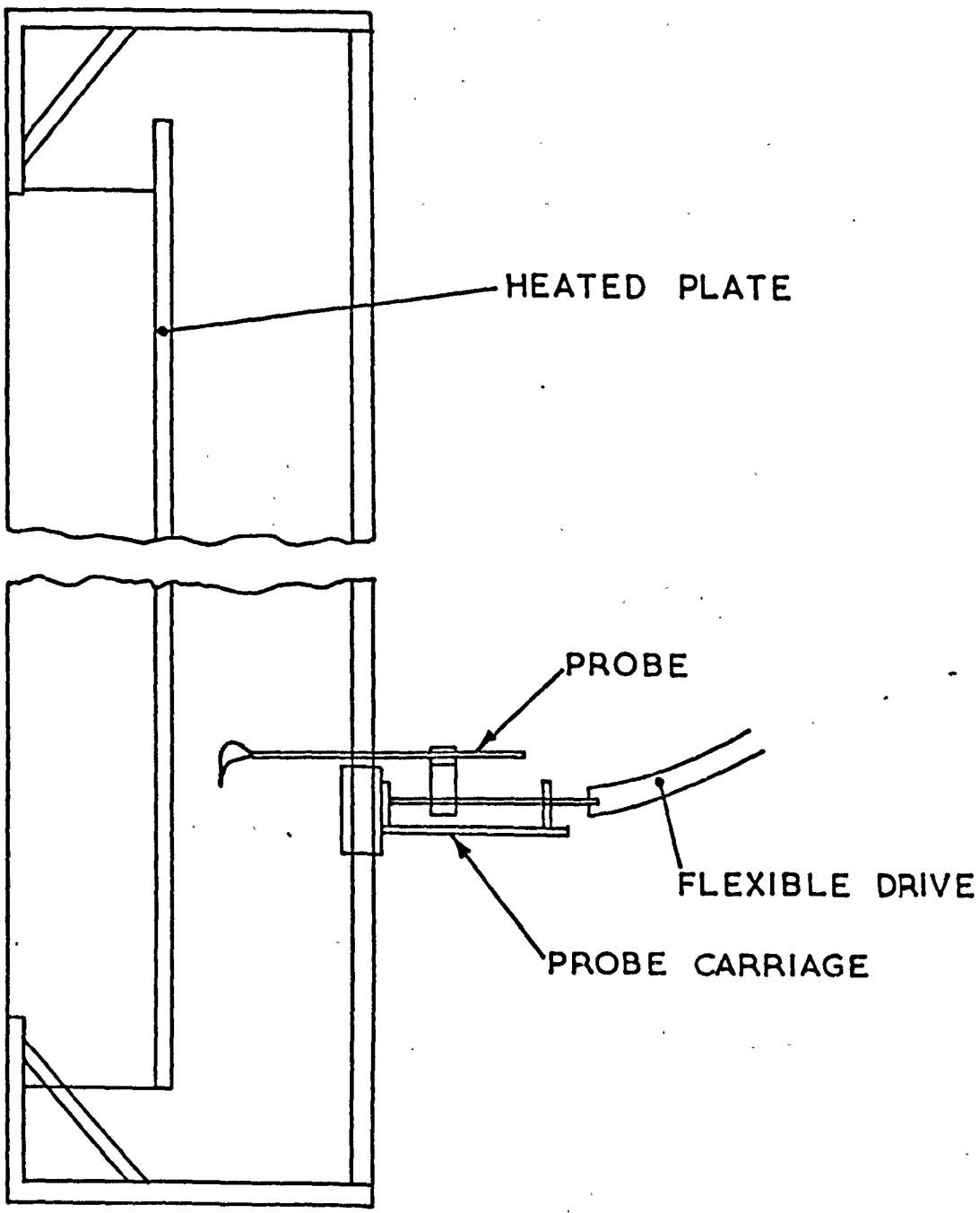

FIGURE 5·7
SKETCH OF THE PROBE TRAVERSING MECHANISM

The position of the plate surface was determined by moving the probe slowly towards the wall until an electrical potential was recorded between the thermocouple and the plate, i.e. the thermocouple was in electrical contact with the uninsulated plate foil. The probe was then slowly moved away from the wall until no electrical contact was evident. Using this procedure, the probe could be positioned to within 0.05 mm.

5.3.3.6 The Velocity Probe

Details of the velocity probe have been given earlier in Section 4.3. The instrumentation was identical to that used in the calibration procedure. The procedure used to determine the plate surface position in Section 5.3.3.5 was not suitable for use with the hot-fibre anemometer. The probe carriage was modified so that the probe would stop 0.39 mm from the plate surface while a thermocouple probe, situated 5 mm to the side of the hot-fibre probe, was in contact with the wall.

The distance between the plate surface and the probe was determined using a theodolite which could measure angles to within $\frac{1}{2}$ second. By measuring the angle between the probe and its reflection from the heated plate, it was possible to calculate the distance of the probe from the wall provided the distance between the probe and the theodolite was known. Tests with a dummy probe showed that the probe could be positioned within 0.05 mm.

5.3.4 Development of the Baffle System

The results from the small rig had shown that care should be taken to ensure that no unwanted flows were present in the

main bulk of the fluid away from the plate. Therefore, bulk flow patterns outside the boundary layer were observed by photographing small particles suspended in the water and illuminated by the light source.

Neutral density polystyrene particles of mean diameter 0.25 mm were used as the tracer particles rather than aluminium particles and introduced into the tank through a funnel and glass tube. The reason was that the heated plate was not insulated and the aluminium particles could have caused a short circuit. The polystyrene particles were not as successful as the aluminium platelets (0.01 mm^2) used in the small rig because of their higher drift velocity. The drift velocity of the aluminium particles was of the order of 1 mm/sec compared with 5 mm/sec for the polystyrene particles. Their drift velocity was also a very strong function of surface tension and fluid temperature. At angles near the horizontal, it was found that the particles drifted upwards and stuck to the plate surface. Using polystyrene particles, it was very difficult to view the motion near the plate surface and because of their fast settling rate it was also difficult to obtain good photographs of the flow.

Initial flow visualization results showed that with the rig running at full power, several large recirculating vortices were produced, similar to those shown in Plate 6.1b. Three vortices were observed, reaching over half-way down the plate. To prevent the vortices forming, several baffle systems were tried and the system found to be most successful will be discussed here. Figure 5.8 shows the baffle and cooler configuration chosen.

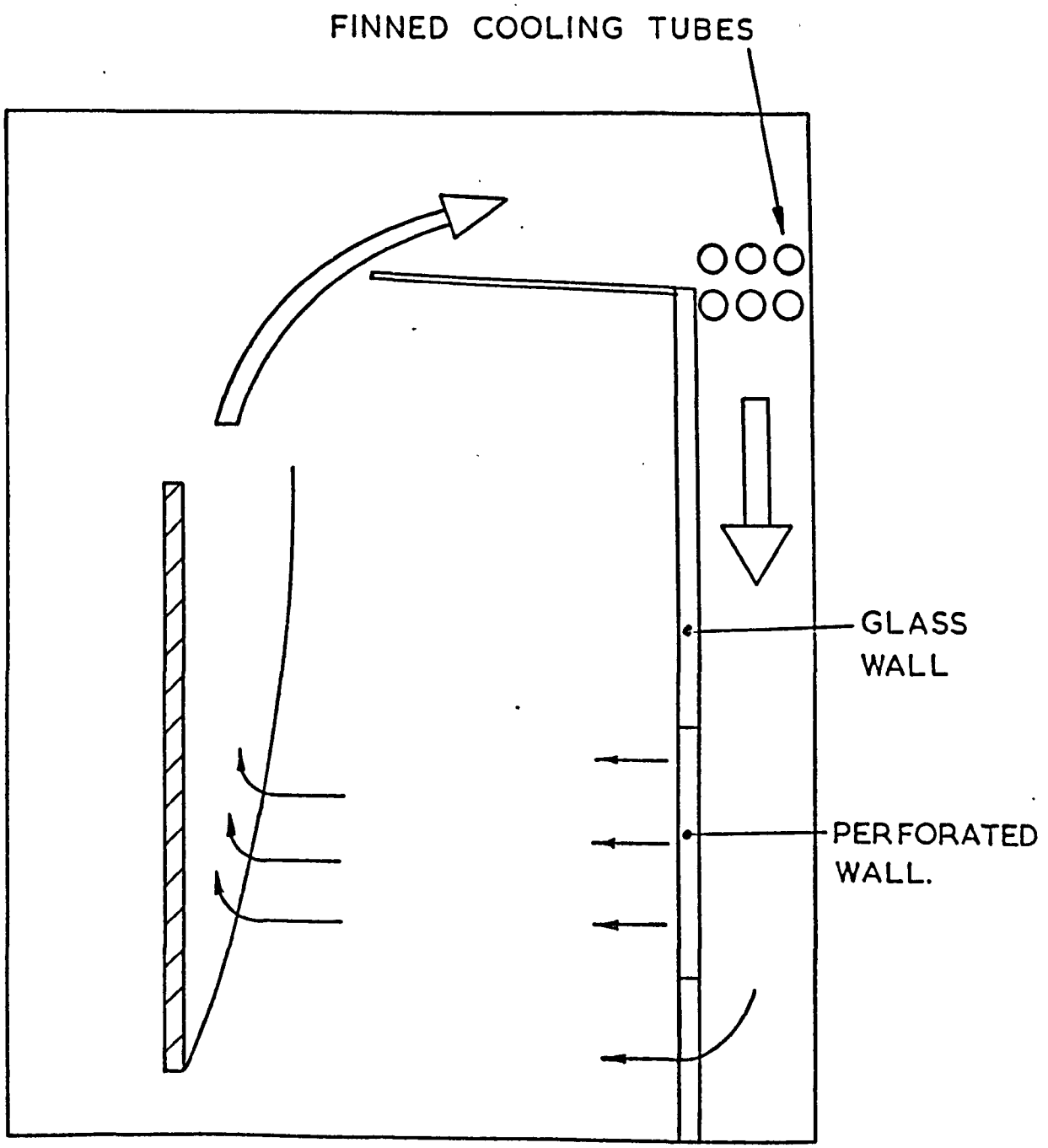

FIGURE 5·8
COOLER AND BAFFLE CONFIGURATION

The plume of water leaving the trailing edge of the plate rose to the surface of the water and extended along the top of the tank producing a vortex. An adjustable baffle was used to prevent the vortex disturbing the main bulk of the fluid. At the top right-hand corner of the tank, a tubular heat exchanger was used to remove the heat input. The heat exchanger consisted of 5 m of 25 mm bore finned tube through which tap water at approximately constant temperature was passed. Typical flow rates through the heat exchanger were 0.3 to 0.4 kg/s removing approximately 30% of the input heat from the heated plate. The remaining heat was either lost by natural convection from the walls of the tank and evaporation of the water or slowly increased the overall water temperature. The cooled water then flowed slowly down a passage at the far end of the tank opposite the heat transfer surface. The water was allowed to filter slowly into the main bulk of the fluid, firstly through a perforated perspex sheet and secondly through a 20 cm gap at the bottom of the tank.

Plates 5.3 and 5.4 show the change in flow pattern for a vertical plate with and without the baffle system. In Plate 5.4, flow particle streaks are very distorted away from the plate and the particles may be seen to be moving horizontally towards the plate surface indicating a vortex. These streaks are not present in Plate 5.3. The adjustable baffle was horizontal.

As the position of the plate was changed, it was necessary to change the angle of the adjustable baffle to retain the gap between the trailing edge of the heated plate and the edge of the baffle. Plate 5.5 shows the flow distribution near the

PLATE 5·3

FLOW PATTERNS WITH THE BAFFLE SYSTEM

PLATE 5·4

FLOW PATTERNS WITHOUT THE BAFFLE SYSTEM

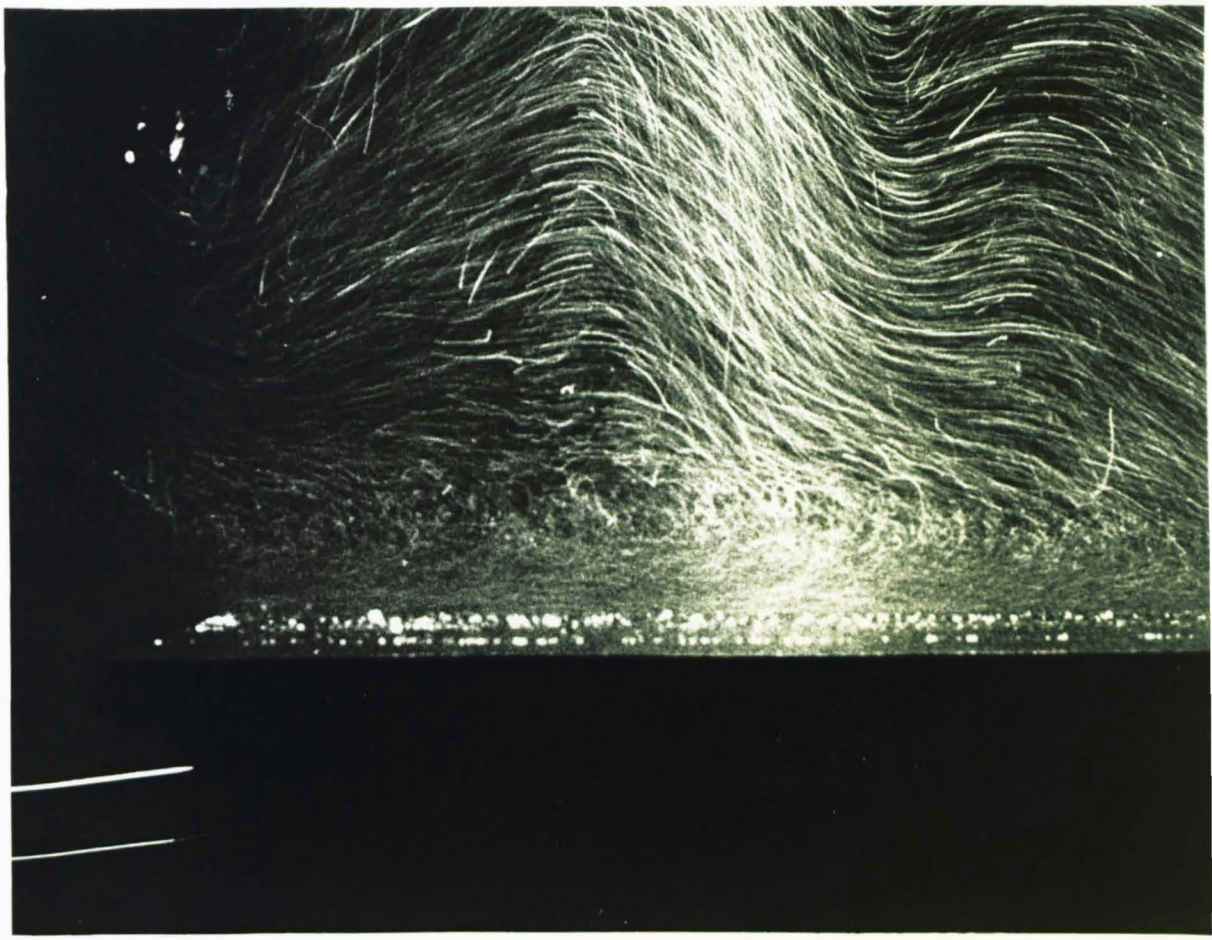

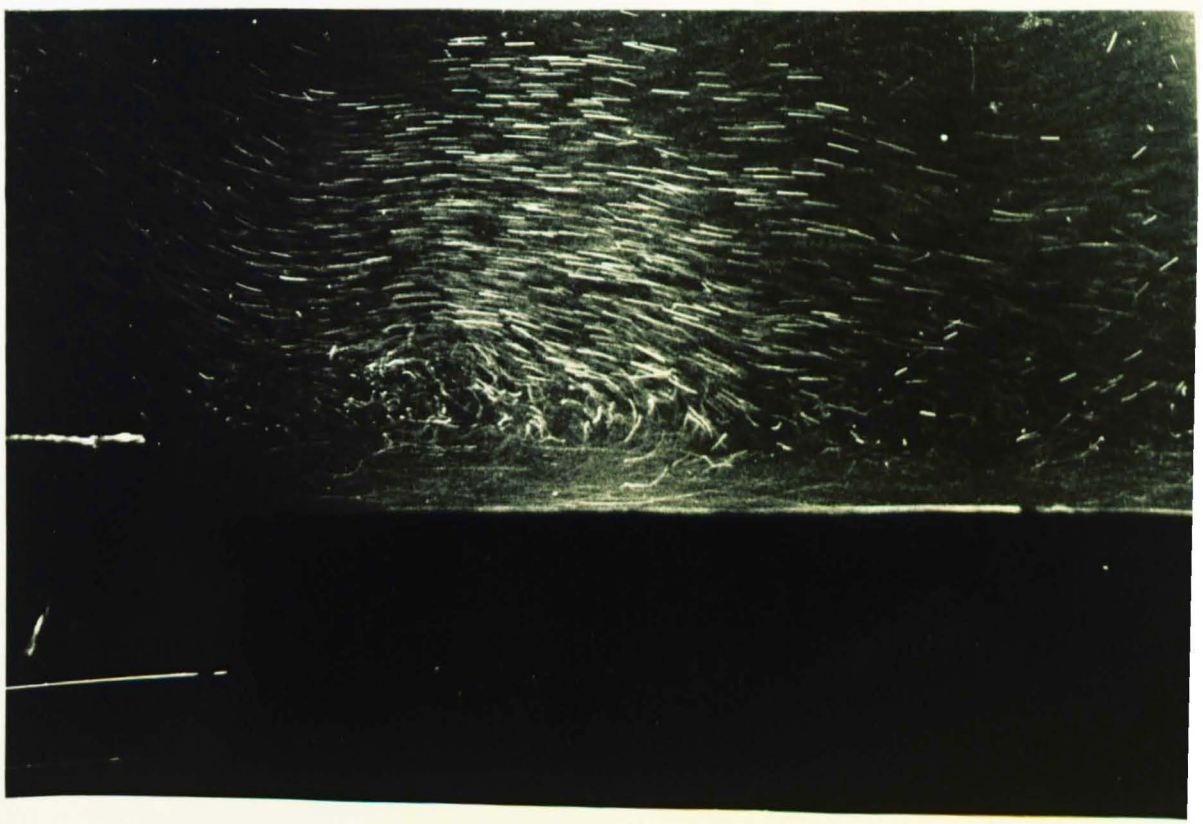

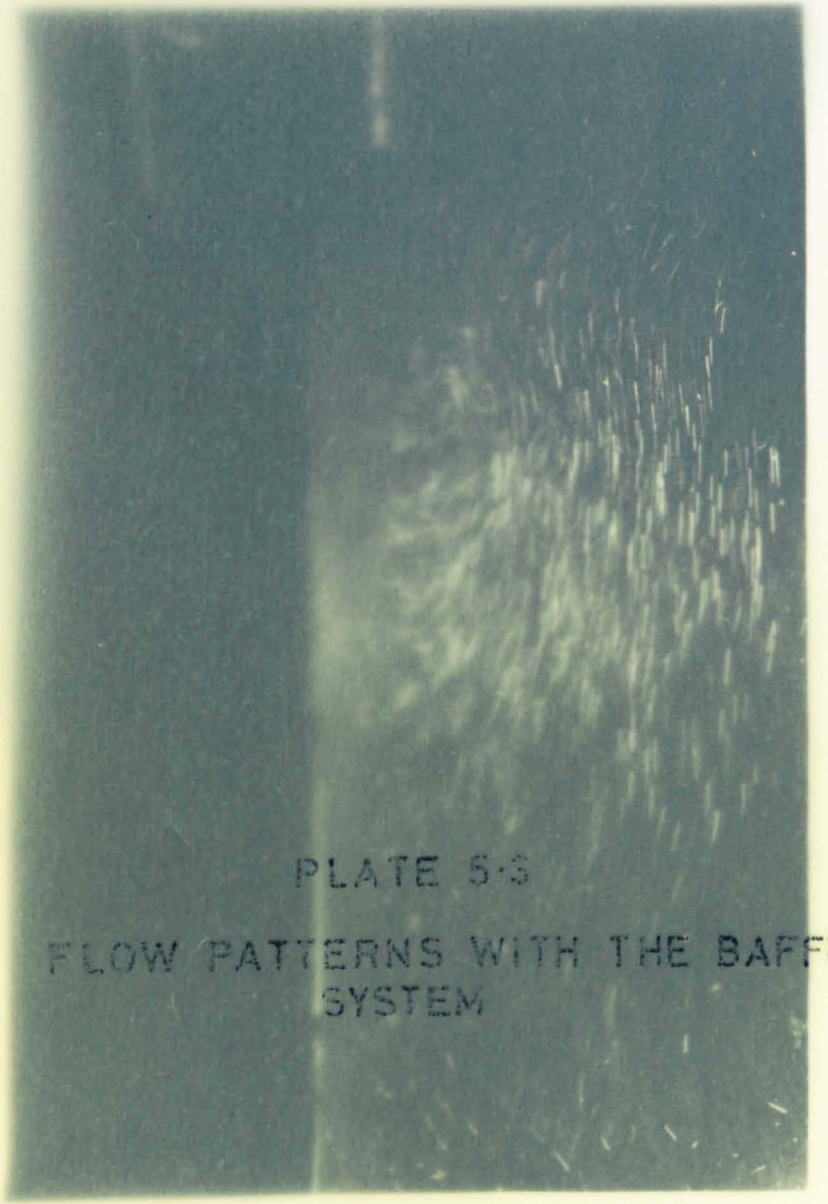

PLATE 5·3

FLOW PATTERNS WITH THE BAFFLE SYSTEM

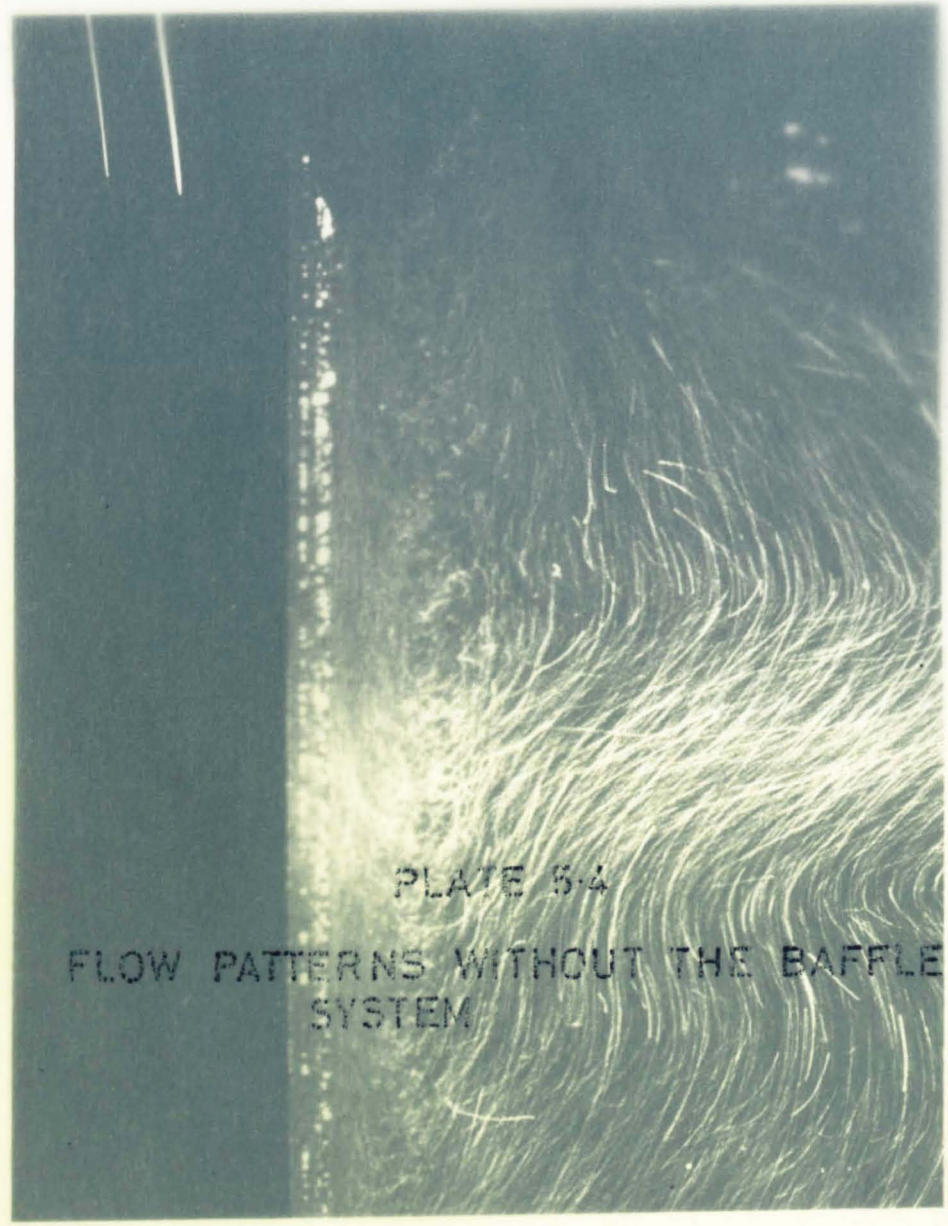

PLATE 5·4

FLOW PATTERNS WITHOUT THE BAFFLE SYSTEM

PLATE 5·5

FLOW PATTERNS WITH THE BAFFLE SYSTEM FOR $\phi = -17{\cdot}5°$

PLATE 5·6

FLOW PATTERNS WITH THE BAFFLE SYSTEM FOR $\phi = -74{\cdot}5°$

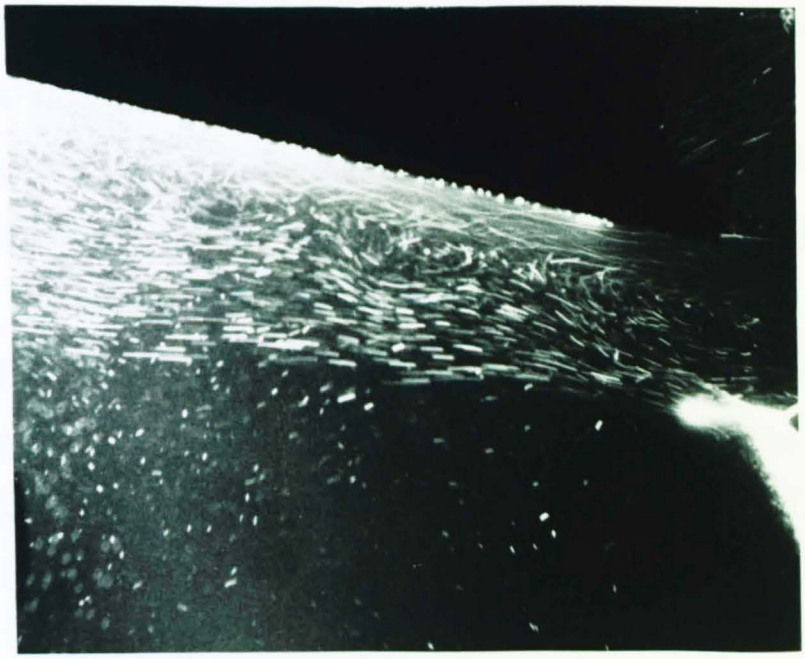

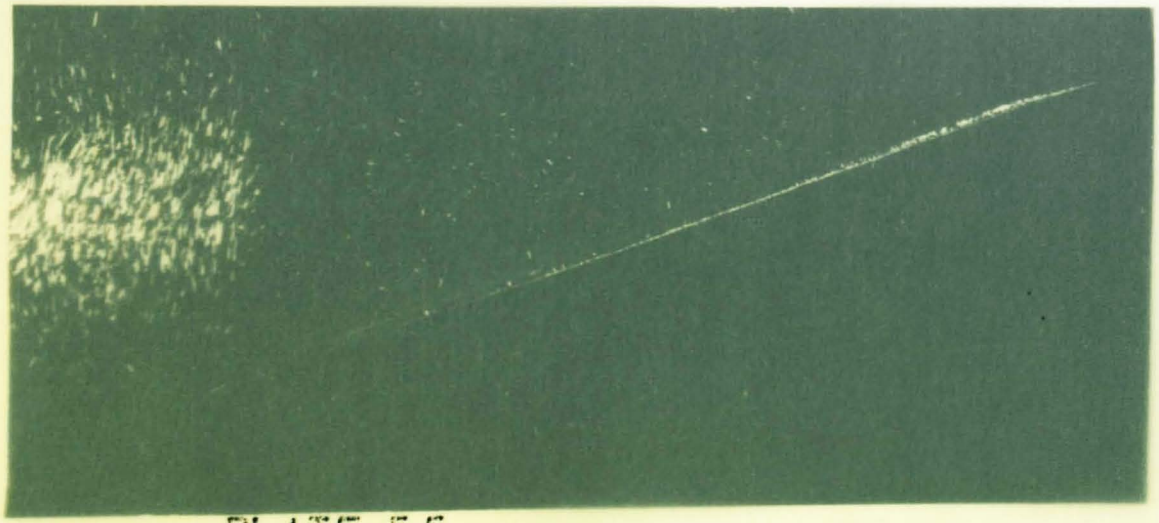

PLATE 5·5

FLOW PATTERNS WITH THE BAFFLE SYSTEM FOR $\emptyset = -17{\cdot}5°$

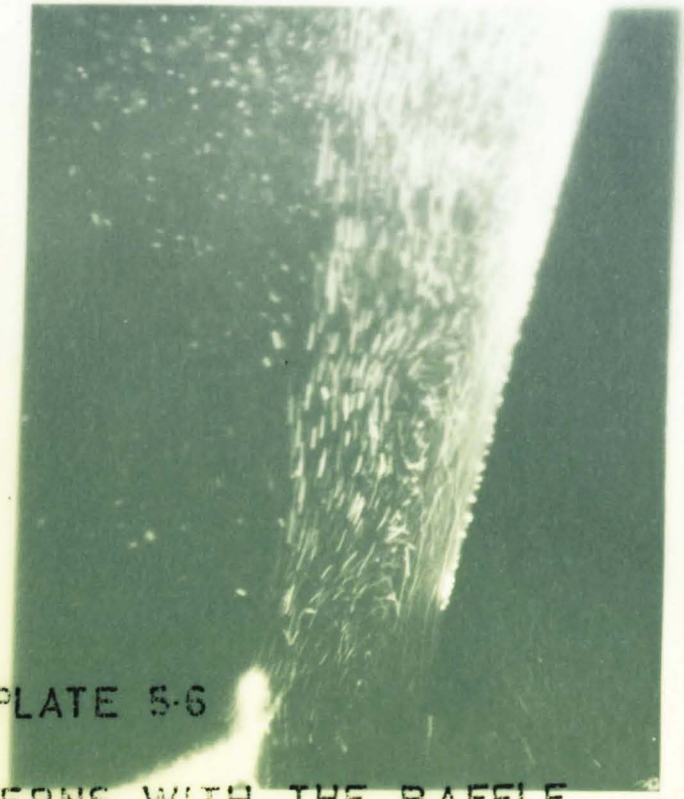

PLATE 5·6

FLOW PATTERNS WITH THE BAFFLE SYSTEM FOR $\emptyset = -74{\cdot}5°$

plate, the adjustable baffle being at 15° from the horizontal. For angles less than -45° the adjustable baffle was not required, a vortex forming above the plate but not interfering with the flow beneath the plate. At angles less than -80° the plate was moved higher in the tank so that a larger volume of water was beneath the plate and the complete baffle system was removed but the cooler retained. Plate 5.6 shows a streak photograph of the polystyrene particles as they fell past the trailing edge of the plate inclined at -74.5°.

CHAPTER 6

EXPERIMENTAL PROCEDURE, RESULTS AND DISCUSSION FOR THE SMALL HEATED PLATE

The heat transfer results for the small and large rigs are presented and discussed separately. The reason for separating the two sets of data is that the small rig is not a true constant-heat-flux surface, as described earlier in Section 5.2.4. Most of the heat transfer results for the small heated plate have been published (see Warneford and Fussey (1974)) and this chapter will elaborate on the method of analysis and presentation.

6.1 EXPERIMENTAL PROCEDURE

Before a series of experimental runs was performed, the water in the tank was de-aerated by heating it electrically to about 60° - 70°C and then cooling it to room temperature. The water remained de-aerated for approximately three weeks, after which time air bubbles began to appear on the heated plate and the water was then changed. The angle of inclination of the plate was set and the heaters switched on to the desired power. Eight of the front plate thermocouples were monitored continuously on the temperature recorder and the remaining thermocouples were switched through into the last four positions of the recorder. For each experimental run, approximately half an hour was required for the plate to reach a quasi-steady state, and it took about five minutes to record a set of experiments. Between each run, the water was stirred to ensure an even temperature distribution in the main bulk. The water was then left for half an hour to allow the disturbances to die down.

The heat transfer measurements were obtained for the following angles of inclination:

$0°$, $-15°$, $-30°$, $-45°$, $-57°$, $-75°$, $-80°$, $-85°$, $-90°$

and heat fluxes of approximately

0.5, 1.0, 1.6, 2.1, 2.6, 3.2, 3.6, 4.2 kW/m^2

Bulk flow patterns outside the boundary layer were observed by photographing small aluminium particles suspended in the water and illuminated by the light source. The aluminium particles were first wetted with 'Teepol' and then introduced into the water with a syringe.

Flow visualization photographs were obtained for the following angles of inclination:

$0°$, $-17°$, $-30°$, $-45°$, $-57°$, $-80°$, $-85°$, $-90°$

with approximate heat fluxes of 1.0 and 2.6 kW/m^2.

6.2 METHOD OF ANALYSIS OF THE RESULTS

The temperatures recorded on the chart recorder were first corrected using the calibration data. The temperature drop across the stainless steel front plate was then calculated and from that a new front plate temperature was obtained. From these temperatures, the Nusselt, Grashof and Prandtl Numbers were calculated using the equations

$$Nu_x = \frac{hx}{k} = \frac{x\,q''}{k\,(T_w - T_\infty)}$$

$$Gr_x^* = \frac{g\beta q''\,x^4}{k\nu^2}$$

$$Pr = \frac{\alpha}{\nu}$$

The physical properties of the water were taken from various sources, details of which are given in Appendix D. Several suggestions have been made as to which temperature should be used to evaluate the fluid properties. Sparrow and Gregg (1958) suggested the reference temperature formula:

$$T_{reference} = T_w - 0.38\,(T_w - T_\infty)$$

As the main effects take place very near the wall, it has been suggested that the wall temperature should be used to evaluate the properties. The most commonly-used reference temperature was the mean film temperature defined by:

$$T_{reference} = \frac{1}{2}(T_w + T_\infty)$$

and this will be used here.

As there was some thermal stratification of the fluid (for one or two runs the temperature rise in the fluid was 80% of the temperature rise up the heated plate), it was necessary to use a local temperature difference. For the vertical plate, this was straightforward but when the plate was inclined one had to decide at what height in the tank the bulk temperature should be taken.

The flow visualization photographs showed that the fluid entered the boundary layer horizontally up to angles of inclination of -85°. The bulk temperature may be evaluated horizontally away from the plate of measurement (T_{∞_1}) or at the edge of the boundary layer perpendicularly away from the plate at some distance from the plate (T_{∞_2}) (see Figure 6.1).

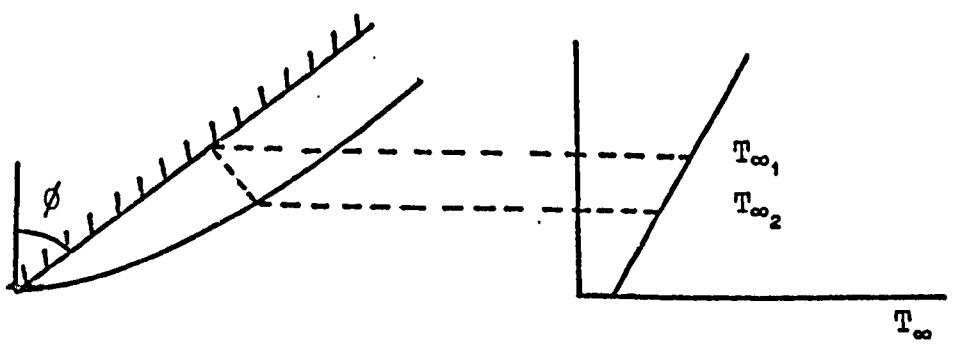

FIGURE 6.1

EFFECT OF STRATIFICATION ON THE BULK TEMPERATURE CALCULATION

There could be up to a 4% difference in the two bulk temperature readings. As it was difficult to estimate the thickness of the boundary layer (unless one used a temperature probe), it was decided to use the temperature T_{∞_1} as in all practical situations this was the position most readily calculable.

The dimensionless groups were correlated for each angle of inclination using the following equations:

$$Nu_x = K_1(Gr_x^* Pr)^{0.2} \qquad \ldots (6.1)$$

$$Nu_x = K_2(Gr_x^* Pr)^{K_3} \qquad \ldots (6.2)$$

The best fit curve was obtained using a least squares fit (see Appendix B). The procedure for correlating the data to the latter equation was to take logarithms of the Nusselt and Rayleigh Numbers and correlate these transformed quantities. As the dependent variable has been transformed, it is necessary to apply a weighting factor. Cox and Hayes (1973) suggest the appropriate weight, w_n, is:

$$w_n = 1\Big/\frac{d}{dNu_x}(\ln Nu_x)$$

evaluated at the nth data point, giving:

$$w_n = Nu_x$$

This procedure was used in the least squares curve fitting routine.

All the data were correlated using the last two equations and the following three correlations suggested by various authors:

$$Nu_x = K_4\frac{(1 + \cos \phi)}{2}(Gr_x^* Pr)^{0.2} \qquad \ldots (6.3)$$

$$Nu_x = K_5 Pr^{\frac{1}{5}}(Pr + 0.8 - K_6 Pr \sin \phi)^{-\frac{1}{5}} (Gr_x^* \cos \phi)^{\frac{1}{5}} \qquad \ldots (6.4)$$

$$Nu_x = K_7 Pr^{\frac{2}{5}} (Pr+0.8)^{-\frac{1}{5}}(1+K_8 f(Pr,Gr_x^*,\phi)\tan\phi)^{\frac{1}{5}}(Gr_x^*\cos\phi)^{\frac{1}{5}} \ldots (6.5)$$

where $f(Pr,Gr_x^*,\phi) = Pr^{-\frac{2}{5}}(0.8+Pr)^{\frac{1}{5}}(Gr_x^*\cos\phi)^{-\frac{1}{5}}$

The constants (K_5, K_6, K_7, K_8) in the latter two equations were evaluated by minimising the sum of the squares of the residuals, i.e.

$$\text{Residual} = \sum_{i=1}^{n} (K_5 Pr_i^{\frac{2}{5}} (Pr_i + 0.8 - K_6 Pr_i \sin \phi_i)^{-\frac{1}{5}} (Gr^*_{x_i} \cos \phi_i)^{\frac{1}{5}} - Nu_{x_i})$$

See Appendix B.

In all the correlations, the standard deviation was defined as:

$$S D = \sqrt{\frac{1}{n-1} \Sigma (Nu_{CALC} - Nu_{EXP})^2}$$

In all experimental work, there are some data points which look dubious in comparison with the main bulk of the data. Holman (1971) suggests the use of Chauvent's criterion to eliminate these dubious points. Chauvent's criterion says that a reading may be rejected if the probability of obtaining the particular deviation from the mean is less than $\frac{1}{2n}$ where n is the number of readings. The data were re-correlated after the dubious points had been eliminated.

6.3 LOCAL HEAT TRANSFER DATA

6.3.1 The Vertical and Inclined Plate

Figure 6.2 shows the temperature difference between the plate and the fluid along the plate for various heat fluxes for the vertical plate. From this graph, it may be seen that:

$$\Delta T \propto x^{\frac{1}{5}}$$

as predicted by theory (see Section 3.2.1). The thermocouple nearest the trailing edge always indicated a lower temperature and this was thought to be caused by either the effect of the trailing edge or recirculating flows. The difference between the thermocouples on the centre line and those near the edge of the plate was less than 3%, indicating that the flow was two-dimensional.

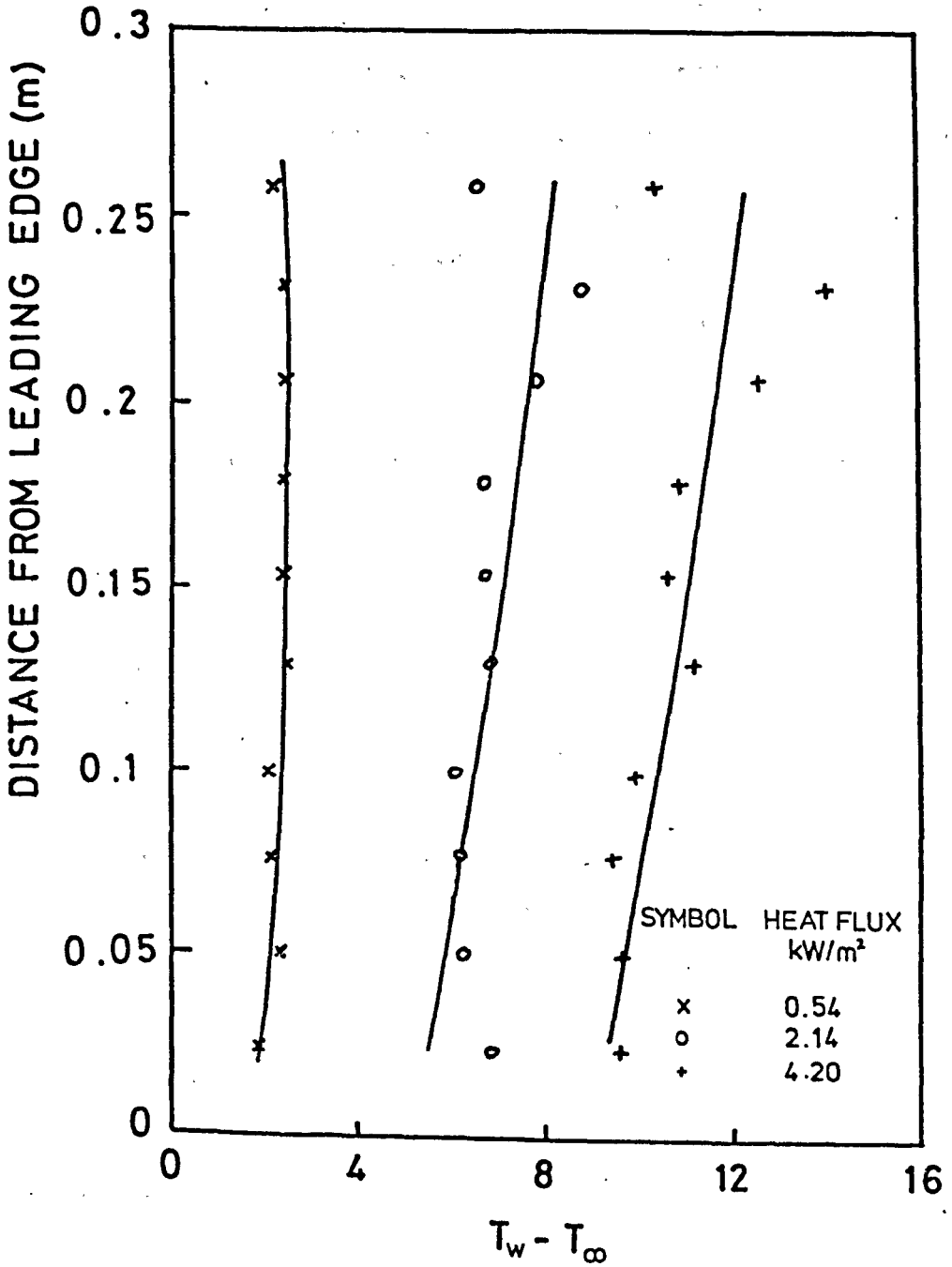

FIGURE 6·2

DISTRIBUTION OF $T_w - T_\infty$ AS A FUNCTION OF HEAT FLUX FOR $\phi = 0°$

Figure 6.3 shows the wall temperature distribution as a function of angle of inclination. As the angle of inclination neared the horizontal position, the effect of inclination became more prominent and produced larger temperature differences (ΔT_w) because of the thicker boundary layer.

Table 6.1 gives the values of the constants in equations (6.1) and (6.2) together with their percentage standard deviations.

Angle of Inclination	Equation (6.1)		Equation (6.2)		
	K_1	SD(%)	K_2	K_3	SD(%)
0.0	.587	10.28	.506	.207	9.54
- 15.0	.563	10.06	.415	.214	8.48
- 31.0	.557	5.97	.600	.197	6.02
- 45.0	.521	6.70	.538	.199	6.80
- 57.0	.468	6.41	.437	.203	6.12
- 75.0	.412	5.86	.435	.198	5.98
- 80.0	.359	6.83	.358	.200	6.79
- 85.0	.312	4.53	.292	.203	4.28

TABLE 6.1

THE VALUES OF THE CONSTANTS IN EQUATIONS (6.1) AND (6.2)

In some cases the percentage standard deviation for equation (6.2) was higher than for equation (6.1). This was due to the weighting employed in the least squares fit for equation (6.2).

The variation of Nu_x against $Gr_x^* Pr \cos \phi$ is shown in Figure 6.4 for all the experimental data obtained, and the following two expressions were obtained:

$$Nu_x = 0.546 \ (Gr_x^* Pr \cos \phi)^{0.2} \qquad \ldots (6.6)$$

$$Nu_x = 0.455 \ (Gr_x^* Pr \cos \phi)^{0.208} \qquad \ldots (6.7)$$

with standard deviations of 9.04% and 8.34% respectively. For

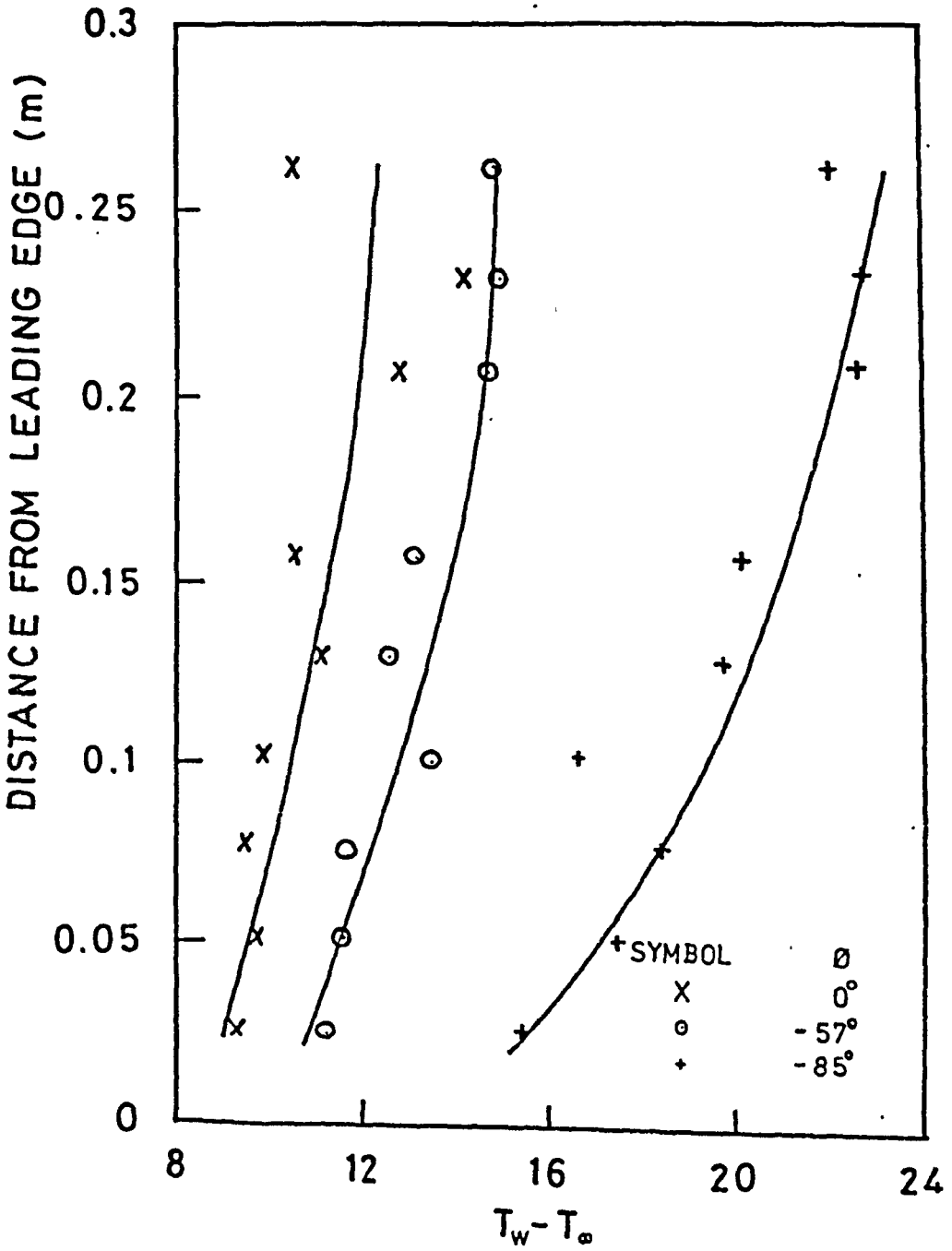

FIGURE 6·3

DISTRIBUTION OF $T_w - T_\infty$ AS A FUNCTION OF INCLINATION

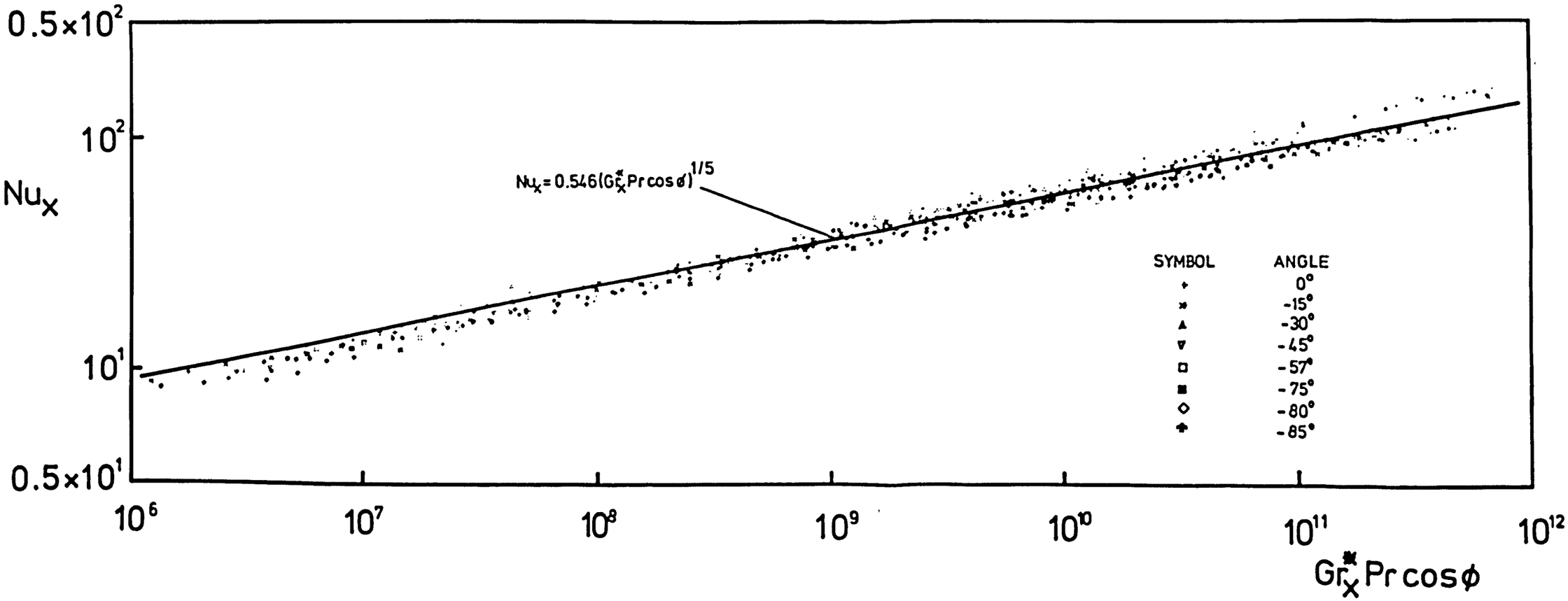

FIGURE 6·4

LAMINAR NATURAL CONVECTION FROM THE SMALL RIG

$\phi = 0^{\circ}$, the data agree well (within 9%) with the experimental results for a laminar constant-heat-flux vertical plate solution of Vliet and Liu (1969) and with the theoretical predictions for the same situation by Sparrow and Gregg (1956). Yung and Oetting's (1969) correlation

$$Nu_x = \frac{0.602}{2}(1 + \cos\phi)(Gr_x^* Pr)^{\frac{1}{5}} \qquad \ldots (6.8)$$

proved to correlate the data satisfactorily. The main disadvantage of this equation is that when $\phi = -90^{\circ}$, the correlation gives $Nu_x \alpha Gr_x^{*\frac{1}{5}}$ rather than $Nu_x \alpha Gr_x^{*\frac{1}{6}}$ as predicted in Section 3.2.2.

The data were also correlated using equation (6.4). The result, which determines the constants in this equation, is:

$$Nu_x = 0.609\, Pr^{\frac{2}{5}}[(Pr+0.8) - 0.938\, Pr \sin\phi]^{-\frac{1}{5}}(Gr_x^* \cos\phi)^{\frac{1}{5}} \ldots (6.9)$$

with a standard deviation of 7.79%. The constant K_5 differs by 1% and K_6 by 30% from those predicted by theory. It was not possible to minimise the constants in equation (6.5). This was because the function

$$\sqrt[5]{\frac{K_8 f(Pr, Gr_x^*, \phi)\tan\phi}{(1+K_8 f(Pr, Gr_x^*, \phi)\tan\phi}} \quad < -1$$

caused to become complex. This indicates that equation (6.5) does not take the effect of inclination into account as much as is necessary.

The various correlations are compared in Figure 6.5 with the experimental data. The results for Michiyoshi's analysis (1964) have been modified from the ordinary Grashof Number to the modified Grashof Number and equation (6.9) has been evaluated at Pr = 5. Michiyoshi's solution lies below the others, but this was to be expected as the solution was for an isothermal plate. In spite of this, if his results were normalised against

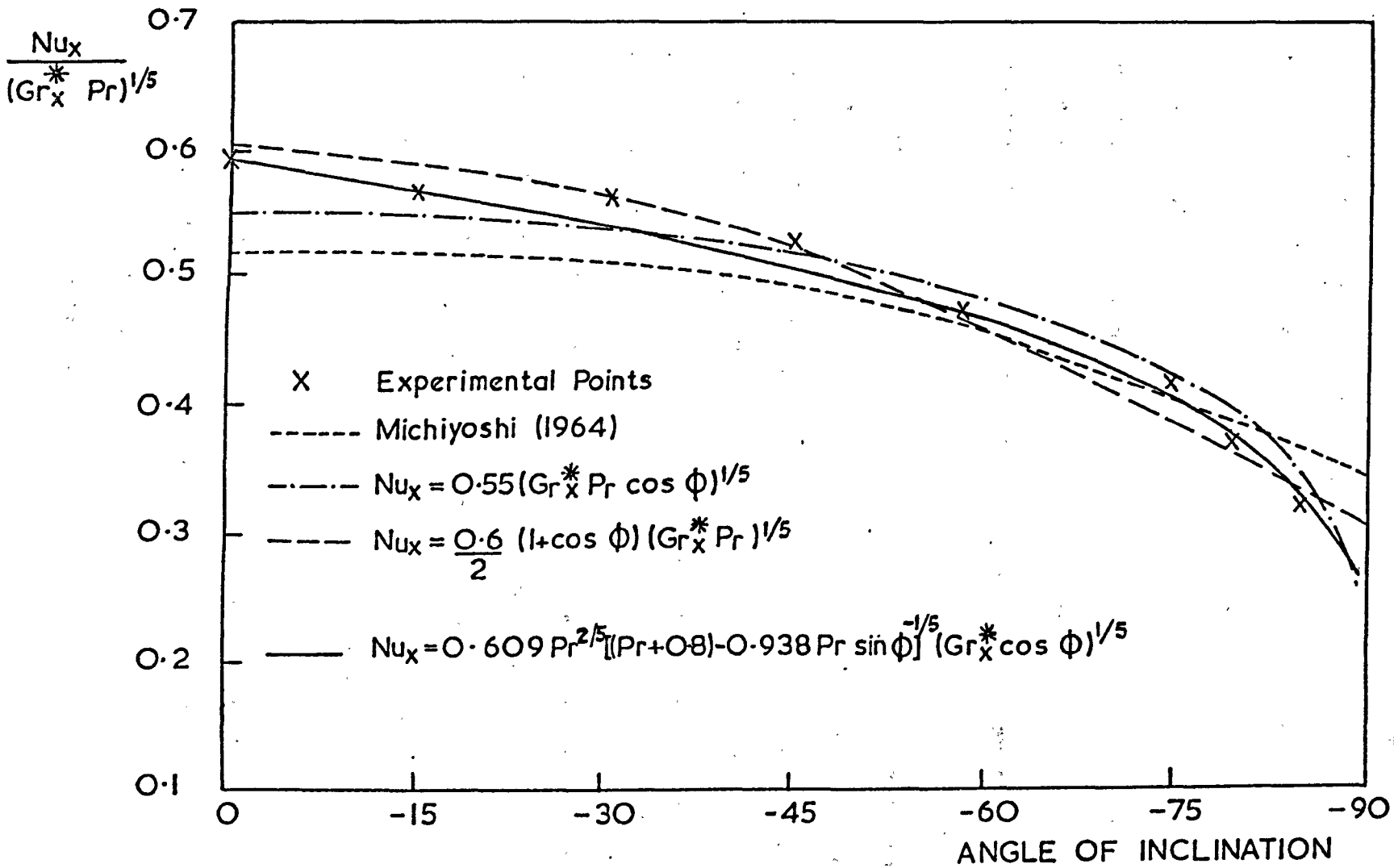

FIGURE 6·5
COMPARISON OF EXPERIMENTAL RESULTS.

the vertical plate, then from 60° to 90° his solution would lie above the remaining three correlations.

6.3.2 The Horizontal Plate

At the outset, it was not the intention of studying in great detail the heat transfer from a downward-facing horizontal plate but it was thought useful to obtain some heat transfer coefficients. In recent years, there has been an upsurge in interest in the horizontal plate. It is generally agreed that a boundary layer develops on the plate, the fluid flowing from the centre of the plate to the edges. It may be shown from hydrostatics that the pressure at the centre of the plate is higher than at the edges, causing the flow to move to the plate edges. All theoretical analyses have assumed that the boundary layer approximations are valid but Rotem (1970) questioned this assumption and gave evidence that the thermal boundary layer increased with increasing Rayleigh Number. More recently Aihara, Yamada and Endō (1972) have shown experimentally that the possibility of obtaining similarity solutions is denied.

Two other problems which were apparent when studying the horizontal plate were the effects of the edge conditions and whether the problem was two- or three-dimensional. Restrepo and Glicksman (1974) have shown that edge conditions are very important and that the heat transfer coefficient may be affected by up to 30%.

As the small heated plate was not designed with the intention of studying the horizontal plate in detail, the leading and trailing edges were not identical and this could have caused a preferential flow in one direction.

Many authors have used side walls to try to make the flow two-dimensional. If care is not taken, then secondary flows are produced by the side walls and these may stretch across the plate. Flow visualization photographs by Aihara, Yamada and Endō (1972) show these secondary flows very well. When the flow is unrestrained, the heat transfer coefficient is dependent on the size of the plate as shown theoretically by Singh, Birkebak and Drake (1969) who derived the expression:

$$Nu_x = 0.495\, \chi^{-\frac{1}{4}} (Gr_x\, Pr)^{\frac{1}{5}}$$

where χ is a function defined by the geometry of the plate.

The temperature distribution along the length of the plate is shown in Figure 6.6 for several heat fluxes. For the range of heat fluxes considered, the graph shows that over most of the plate the heat transfer coefficient is independent of the distance x. Only near the edges does the heat transfer coefficient increase, as would be expected. The best fit curve through all the data gave:

$$Nu_x = 0.116\, (Gr_x^*\, Pr)^{0.237} \qquad \ldots (6.10)$$

in contrast to the theoretical work of Section 3.2.2, which gives $Nu_x \alpha Gr_x^{*\,0.167}$.

Figure 6.7 shows a graph of $Nu_x/(Gr_x^*\, Pr)^{\frac{1}{6}}$ against x/l where l is the half length of the plate. Near the centre of the plate, the heat transfer coefficient was seen to be low and in this region a stagnation point was observed visually. Moving away from the centre of the plate

$$h \alpha\ x^{-\frac{1}{3}}$$

and near the edges of the plate, the heat transfer coefficient increased as the boundary layer decreased. Over the region

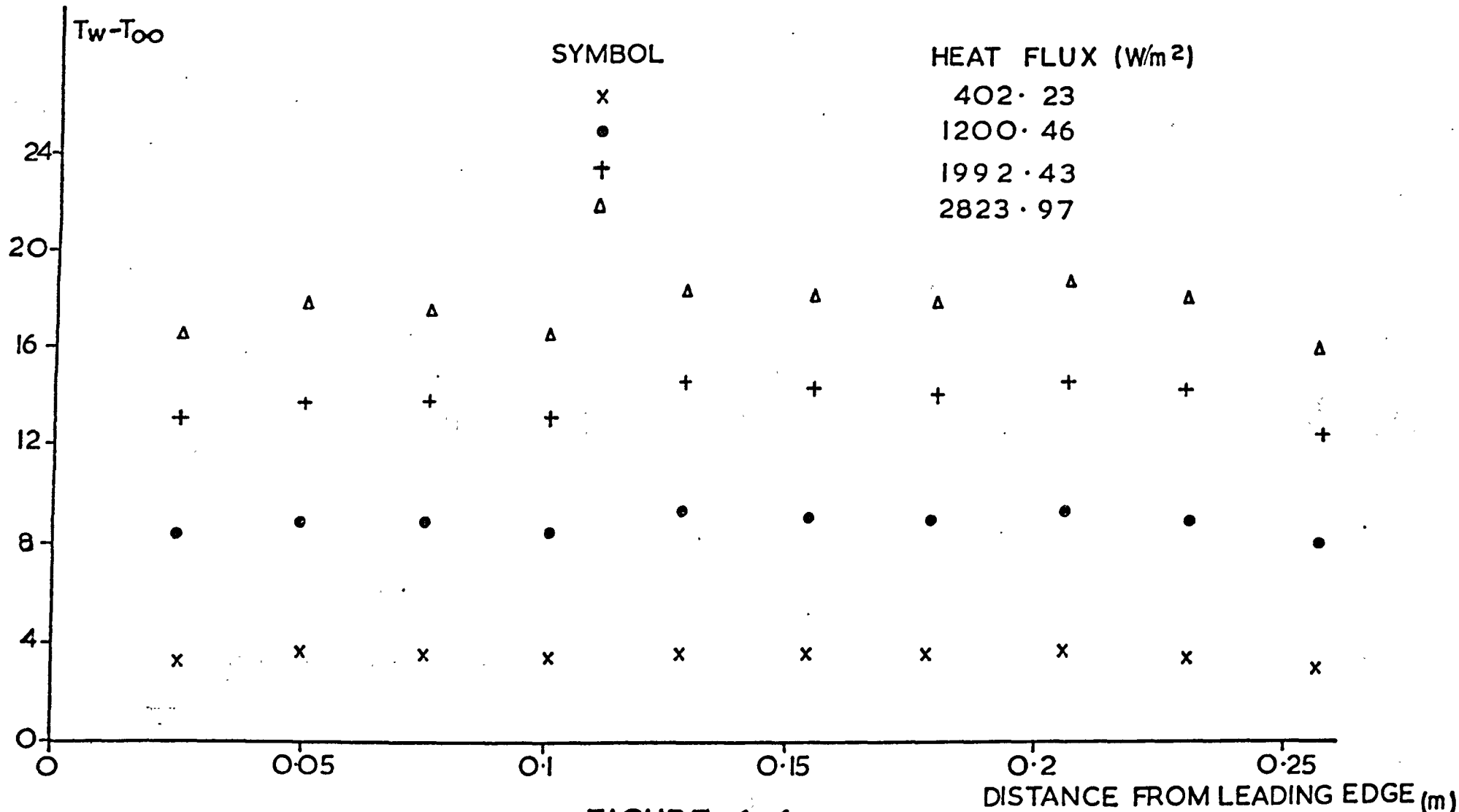

FIGURE 6·6
TEMPERATURE DISTRIBUTION ALONG THE LENGTH OF THE PLATE FOR AN ANGLE OF INCLINATION = −90°

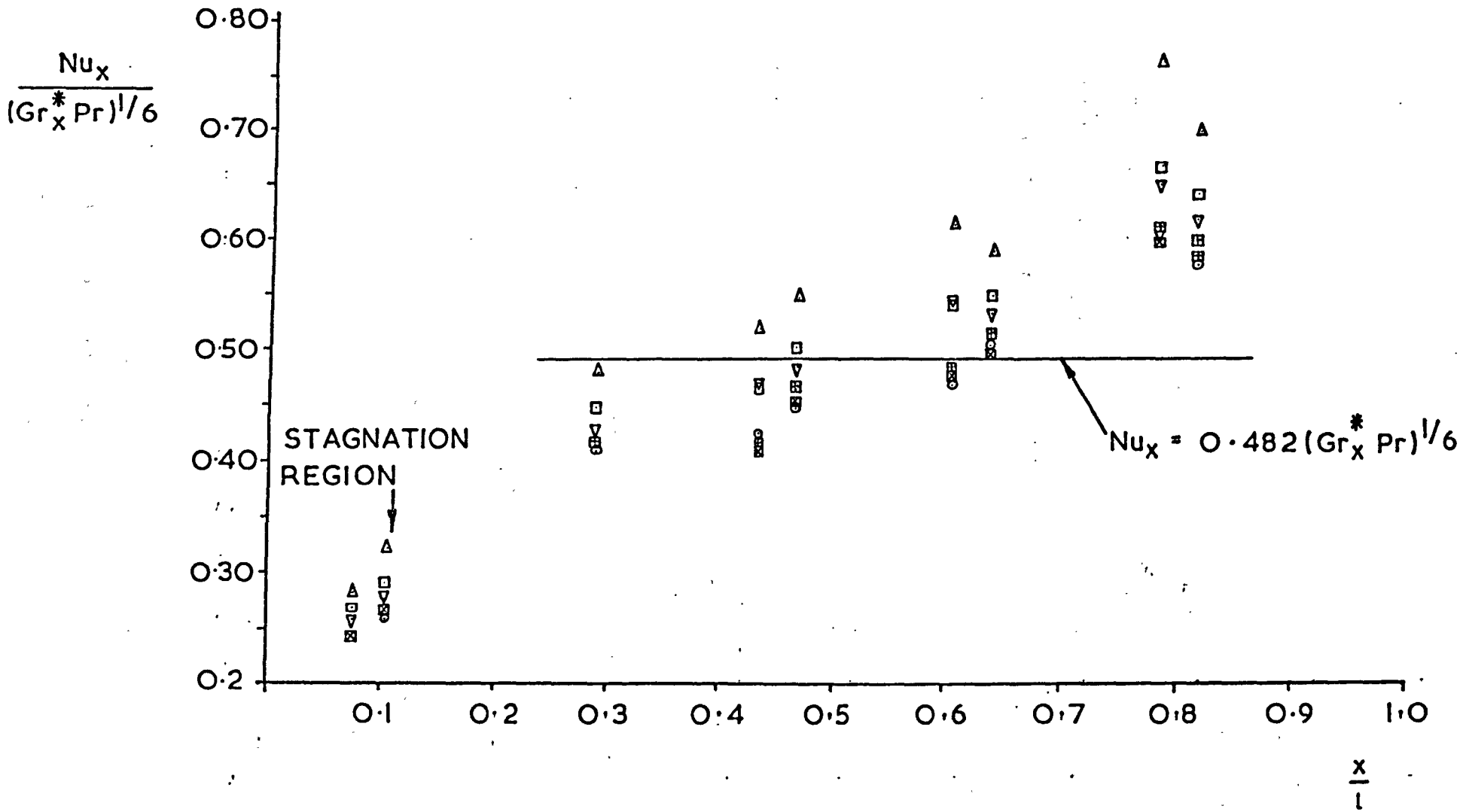

FIGURE 6·7

LOCAL HEAT TRANSFER FROM A DOWNWARD FACING HORIZONTAL PLATE

where $h \propto x^{-\frac{1}{5}}$ we obtained the correlation

$$Nu_x = 0.482 \, (Gr_x^* \, Pr)^{\frac{1}{6}} \qquad \ldots (6.11)$$

6.4 FLOW VISUALIZATION RESULTS

The flow visualization programme was undertaken to ensure that there was no flow in the main bulk of the fluid away from the plate. In these experiments, for angles near to the vertical, the trailing edge was near the free surface of the water. When the boundary layer left the trailing edge of the plate, the hot water rose to the surface and moved away from the face of the plate. This caused a vortex to be produced along the top of the tank, the vortex being 10 cm deep. This tended to break up the boundary layer (see Plate 6.1) which would have led to erroneous heat transfer results in this region. The effect was removed by placing a larger volume of water above the plate.

Flow patterns outside the boundary layer are shown in Plates 6.2, 6.3 and 6.4 for angles of inclination of 0°, -45° and -85°. In all cases the flow moved in horizontally towards the plate in a similar way to the experiments of Fujii and Imura (1972). Plate 6.5 shows a typical photograph for the horizontal plate together with a sketch of the flow pattern. The flow was seen to move towards the centre of the plate where it entered the boundary layer, a stagnation region being formed slightly from the centre of the plate. This was caused by the plate not being exactly in the centre of the tank and the differing edge conditions.

6.5 ADDITIONAL EXPERIMENTS

Some additional experiments were also undertaken to aid the design of a sodium natural convection rig being constructed by

PLATE 6·1a PLATE 6·1b PLATE 6·2

FLOW PATTERNS OUTSIDE THE BOUNDARY LAYER FOR $\phi = 0°$

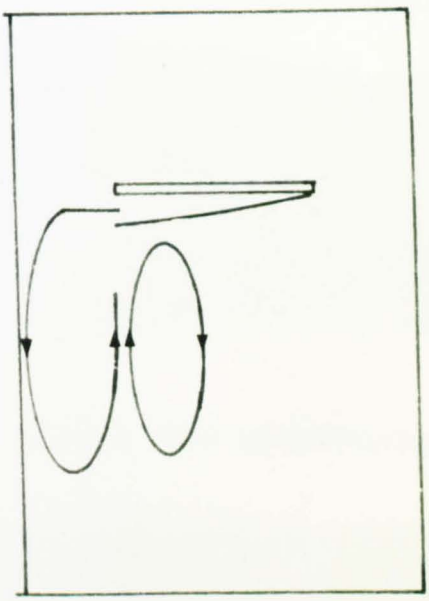

PLATE 6·1a

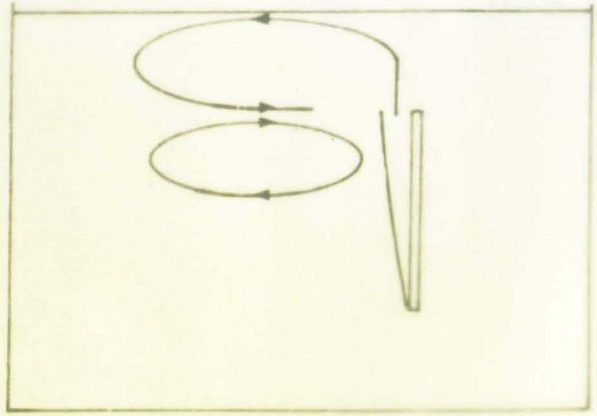

PLATE 6·1b

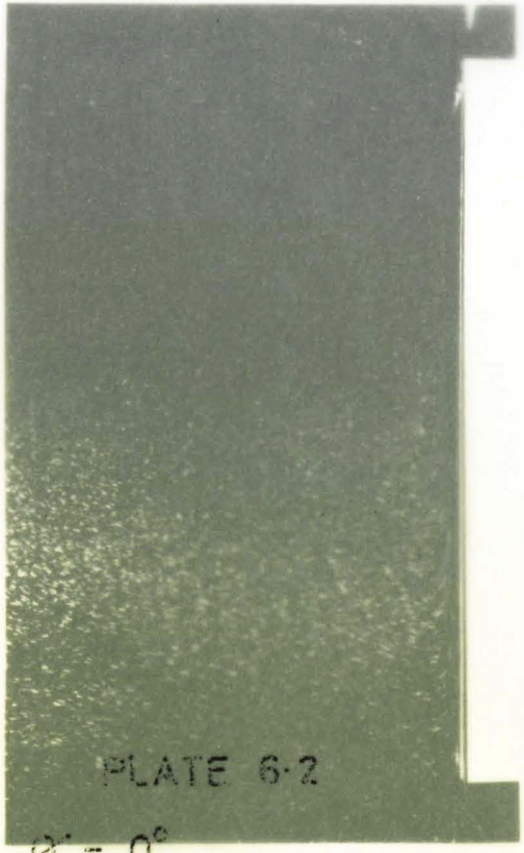

PLATE 6·2

FLOW PATTERNS OUTSIDE THE BOUNDARY LAYER FOR $\beta = 0°$

PLATE 6·3

FLOW PATTERNS FOR $\phi = -45°$

PLATE 6·4

FLOW PATTERNS FOR $\phi = -85°$

PLATE 6·5a

FLOW PATTERNS FOR $\phi = -90°$

PLATE 6·5b

SKETCH OF FLOW PATTERNS FOR $\phi = -90°$

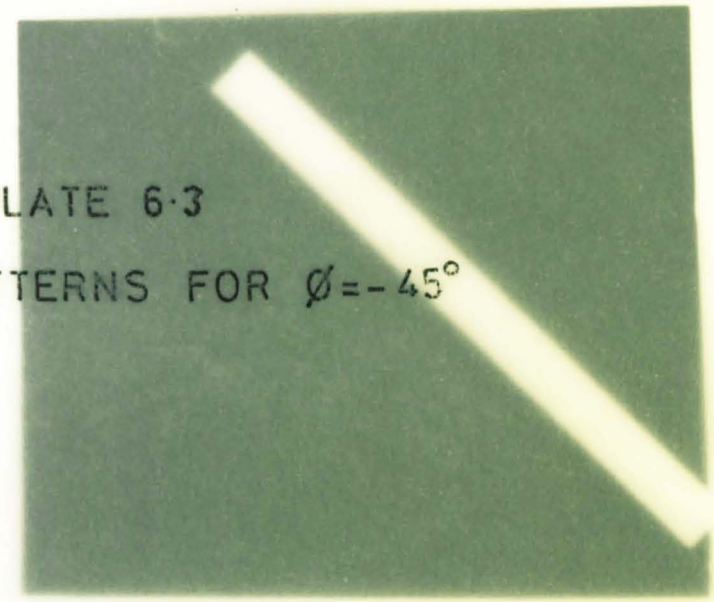

PLATE 6·3

FLOW PATTERNS FOR Ø=-45°

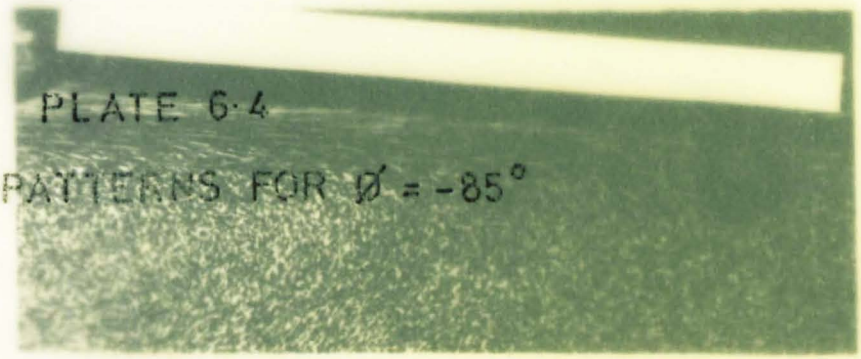

PLATE 6·4

FLOW PATTERNS FOR Ø = -85°

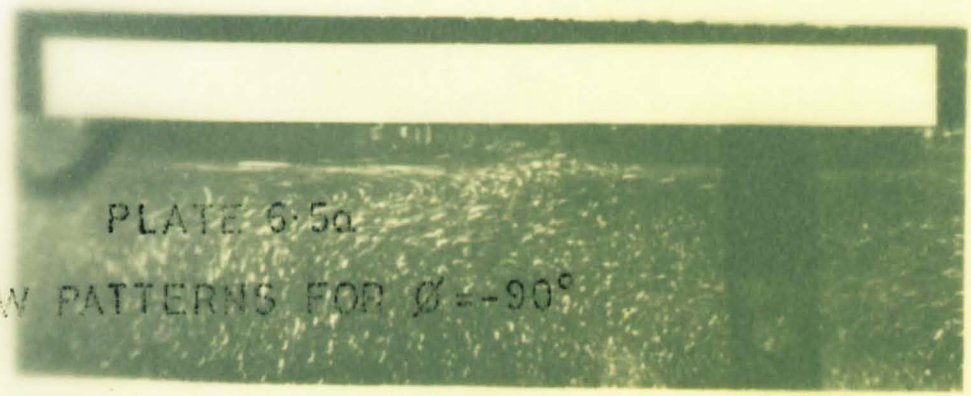

PLATE 6·5a

FLOW PATTERNS FOR Ø=-90°

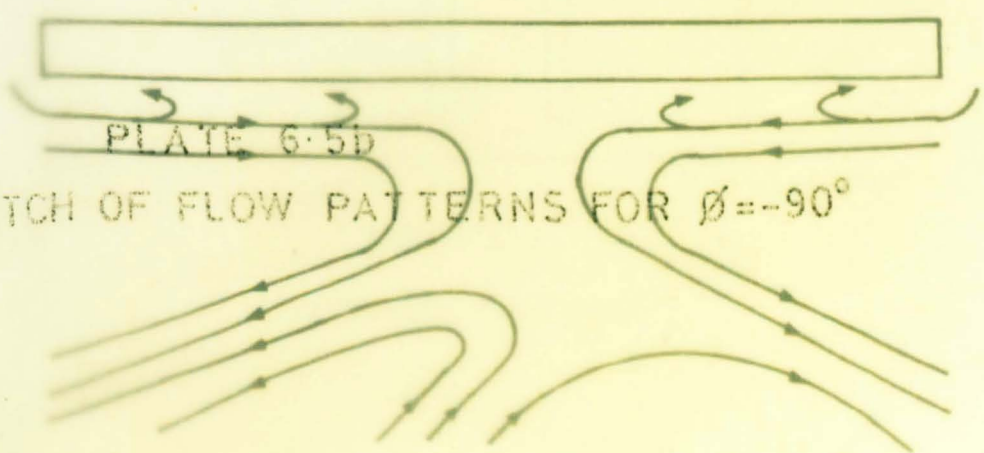

PLATE 6·5b

SKETCH OF FLOW PATTERNS FOR Ø=-90°

the United Kingdom Atomic Energy Authority, Risley, in their Reactor Engineering and Materials Laboratory, and also to aid the design of the large rig. These experiments involved a study of the effects of a vertical isothermal leading edge and the position of a suitable cooler to reduce stratification of the bulk fluid.

In the sodium experiment there will be a vertical isothermal wall which represents the line of symmetry of a reactor core catcher. To represent this in the water experiments, a sheet of perspex was placed beneath the leading edge of the heated plate. Both heat transfer and flow visualization results were obtained at an approximate heat flux of 2 kW/m^2 for angles of inclination of

$$0^\circ, -31^\circ, -57^\circ \text{ and } -79^\circ$$

To observe the effects of a cooler on the overall flow patterns and thermal stratification of the flow, a commercial car radiator, through which cold water was passed, was placed vertically in the tank and parallel to the heated plate (see Figure 6.8).

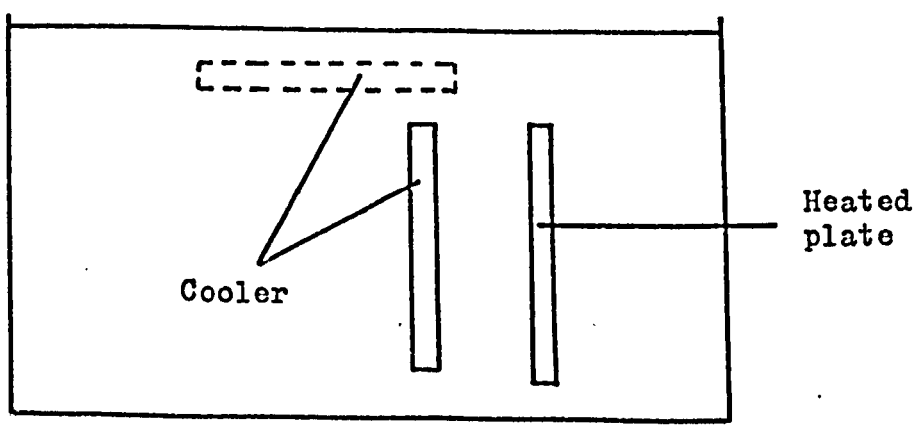

FIGURE 6.8

ARRANGEMENT WITH COOLER

The cooler was used to simulate approximately the situation of the proposed cooler in the sodium experiments. Direct comparison was not possible because of the much thicker boundary layer in sodium. Four sets of experimental runs were carried out at an approximate heat flux of 2 kW/m^2:

1. Heater vertical, heated plate - cooler separation 34 cm
2. Heater vertical, heated plate - cooler separation 10 cm
3. Heater vertical, heated plate - cooler separation 10 cm
4. Heater-$55\frac{1}{2}^{o}$ from vertical, heated plate - cooler separation 15 cm

In each case, two runs were carried out; firstly with no cooling water flow, and secondly with the cooling water flow on.

In all experiments, the inlet and outlet temperatures of the cooling water were monitored with mercury in glass thermometers and the cooling water flow rate was measured by timing a given volume of water.

Further experiments were carried out with the cooler placed horizontally near the free surface of the water and displaced 10 cm horizontally from the heated plate (see Figure 6.8). Only one experimental run was carried out at a nominal heat flux of 2 kW/m^2; firstly with the cooling water flow on, secondly with no cooling water and finally with the cooling water on.

6.5.1 The effect of a vertical isothermal wall below the leading edge

It was found that for angles of inclination of up to -79^{o} to the vertical, there was no flow in the region of the vertical wall below the leading edge, as shown in Plates 6.6 and 6.7. However, a change in behaviour was observed with the heated plate in the horizontal position. This was to be expected, since with

PLATE 6·6

FLOW PATTERNS WITH AN ISOTHERMAL LEADING EDGE FOR $\phi = -57°$

PLATE 6·7

FLOW PATTERNS WITH AN ISOTHERMAL LEADING EDGE FOR $\phi = -79°$

PLATE 6·8

FLOW PATTERNS WITH AN ISOTHERMAL LEADING EDGE FOR $\phi = -90°$

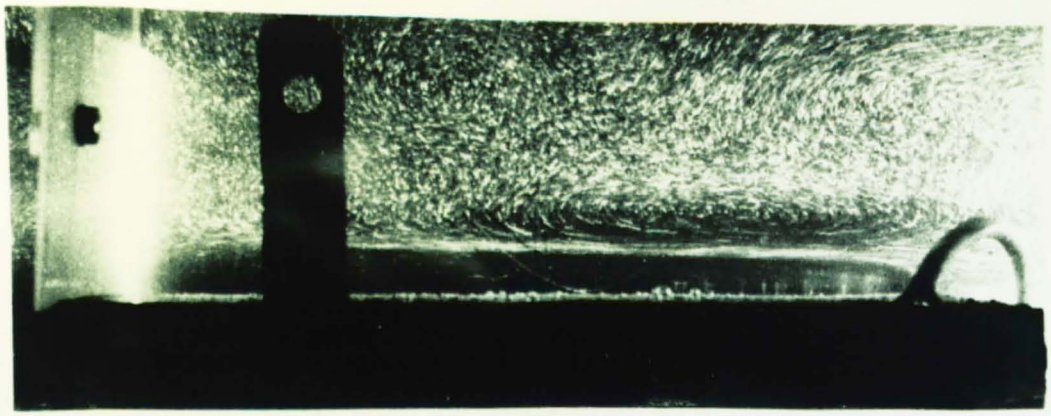

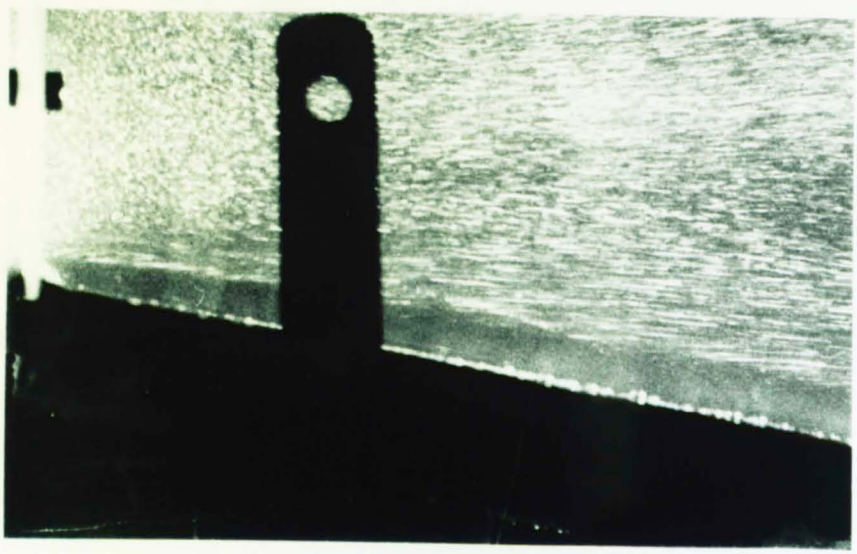

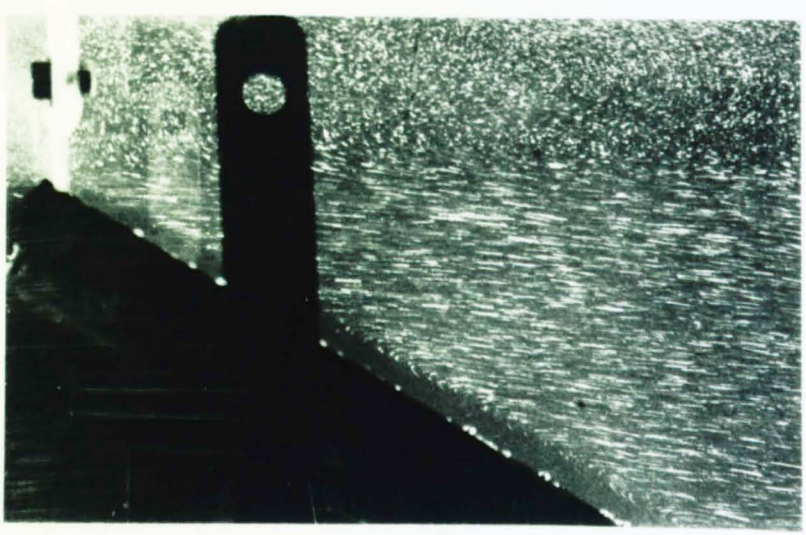

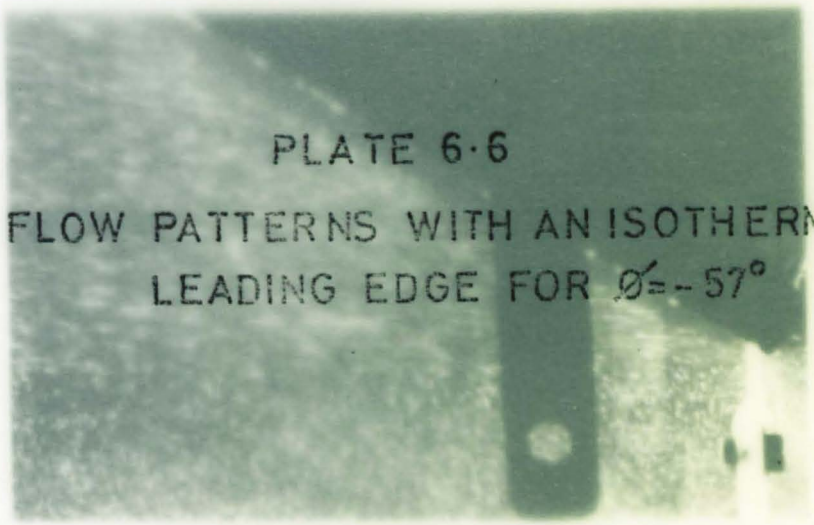

PLATE 6·6

FLOW PATTERNS WITH AN ISOTHERMAL LEADING EDGE FOR $\emptyset = -57°$

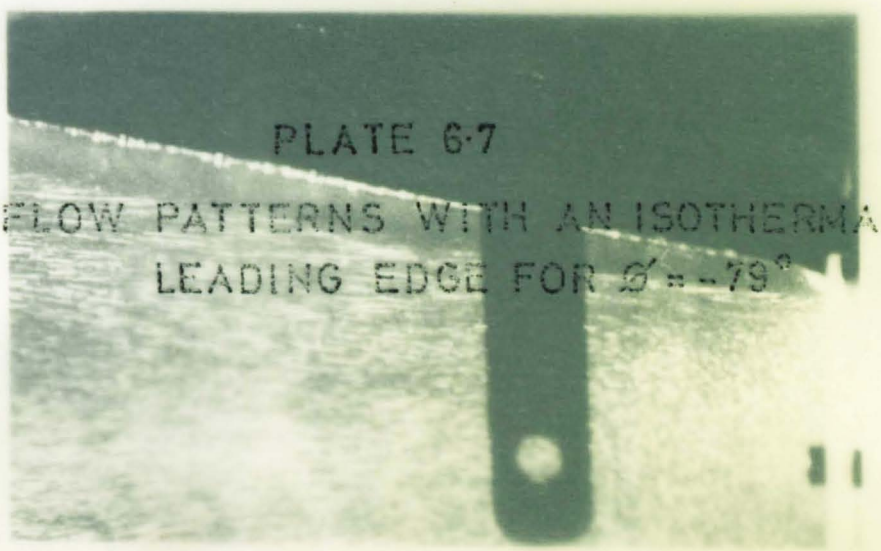

PLATE 6·7

FLOW PATTERNS WITH AN ISOTHERMAL LEADING EDGE FOR $\emptyset = -79°$

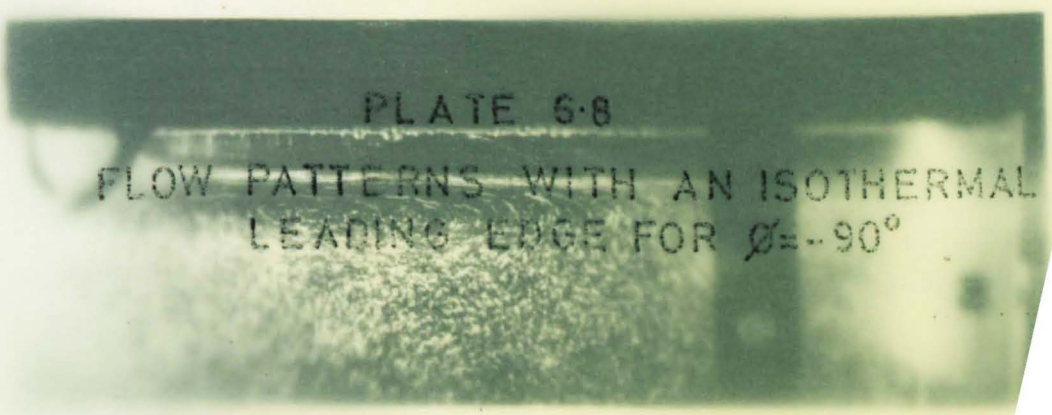

PLATE 6·8

FLOW PATTERNS WITH AN ISOTHERMAL LEADING EDGE FOR $\emptyset = -90°$

a vertical wall against one edge (see Plate 6.8) the heater has only one free edge instead of two without any wall.

Once again, plotting a graph of $Nu_x/(Gr_x^* Pr)^{\frac{1}{6}}$ against x (Figure 6.9) we see the heat transfer coefficient is low near the false wall, levels off near the centre of the plate and increases as the boundary layer decreases near the trailing edge.

6.5.2 The effect of a vertical cooler on the thermal stratification

The situation with a vertical cooler near the plate surface is a very difficult geometry to analyse. Effectively we were considering natural convection in an enclosure with one wall heated and one cooled. The situation was much worse as there was also a free surface and the enclosure had many openings in it.

Consider the case of a vertical cooler and heated plate with a separation of 10 cm. This had a height to separation ratio of 3. With no flow through the cooler, the flow patterns are shown in Figure 6.10.

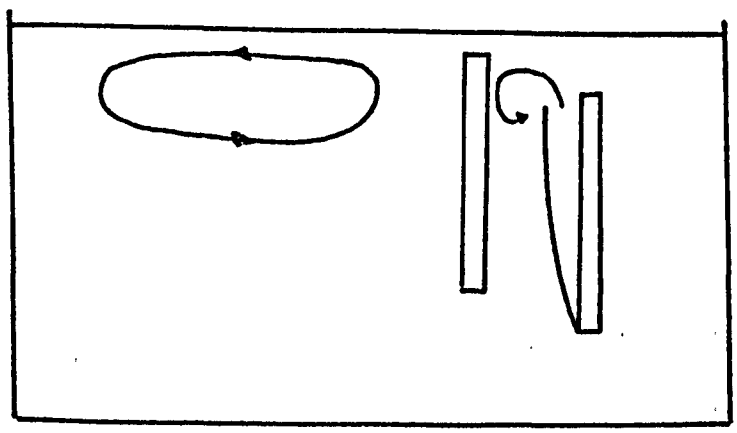

FIGURE 6.10

FLOW PATTERNS WITH THE COOLER OFF

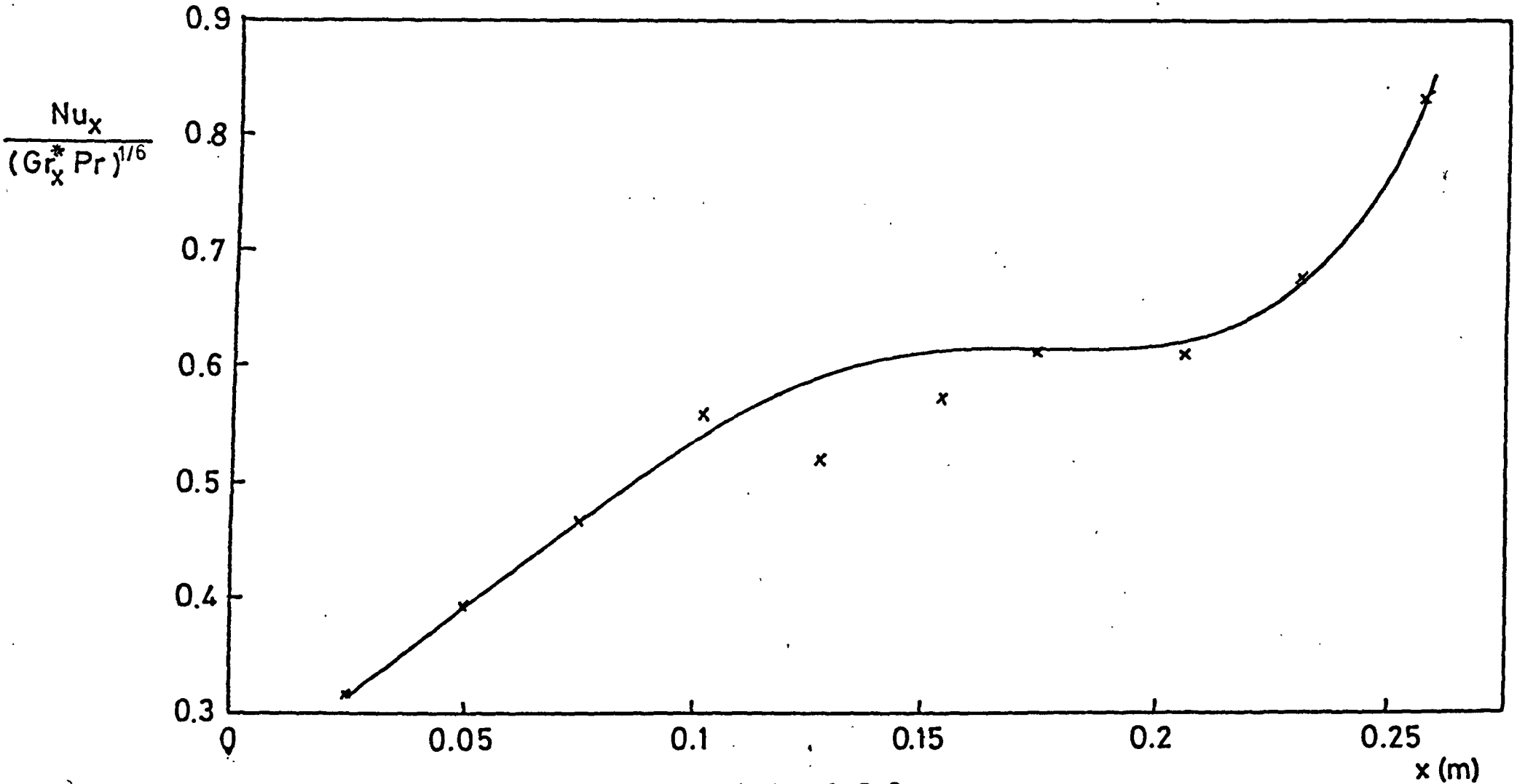

FIGURE 6·9

LOCAL HEAT TRANSFER FROM A DOWNWARD FACING HORIZONTAL PLATE WITH AN ISOTHERMAL WALL AT ONE EDGE

When the plume of hot water left the heated plate, it cooled on reaching the free surface and a recirculating vortex was formed. A vortex was also formed behind the cooler as the hotter water on the surface spread through the spaces in the cooler.

With water flowing through the cooler, the flow pattern changed to that shown in Figure 6.11. In this case, the recirculating vortex behind the cooler had been removed. A boundary layer was formed on the cooler which began to break up near the bottom of the cooler and this caused some disturbance to the boundary layer on the heated plate.

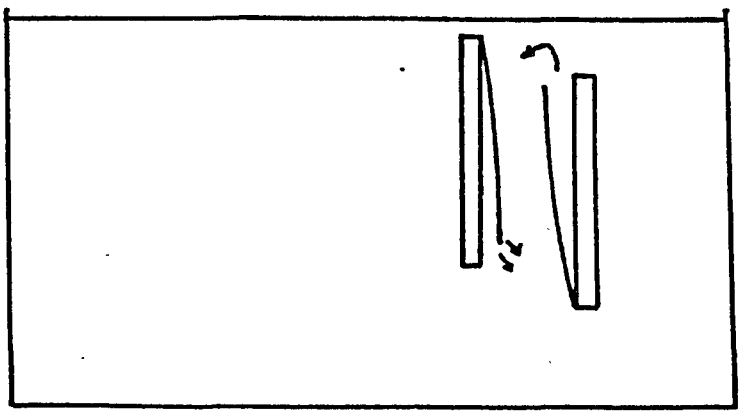

FIGURE 6.11

FLOW PATTERNS WITH THE COOLER ON

Table 6.2 shows the effect the cooler had on the bulk temperature gradient.

Position of heated plate in relation to cooler	Cooling water flow rate kg/s	Temperature Gradient °C/m
Heated plate vertical, separation 34 cm	0	17.7
" " " " " "	.029	12.7
" " " " 10 "	0	1.67
" " " " " "	.028	9.33
" " " " " "	0	5.2
" " " " " "	.028	13.0
Heated plate-55½° from vertical, separation 15 cm	0	1.66
" " " " " " "	.029	8.65

TABLE 6.2

THE EFFECT OF A VERTICAL COOLER ON THE BULK TEMPERATURE GRADIENT

In most cases the cooler made the stratification worse. The experiments of Eckert and Carlson (1961) on natural convection in enclosures with one wall heated and another cooled showed that in the central region between the two boundary layers the temperature was isothermal in a horizontal direction and increased in the vertical direction.

6.5.3 The effect of a horizontal cooler on the thermal stratification

The presence of a horizontal cooler near the free surface (Figure 6.8) was very effective in reducing the bulk temperature gradients. This effect might be expected, since without a cooler the plume of hot water rising from the boundary layer at the trailing edge of the plate tended to accumulate near the surface of the water, and therefore the cooler was absorbing the heat from the hot water where it was collecting.

For example, on one run, the bulk temperature gradient was allowed to reach 8°C/m and on passing water through the cooler

this was reduced to zero after half an hour. The heat absorbed by the cooler was approximately equal to the total heat input to the heated plate.

CHAPTER 7

EXPERIMENTAL PROCEDURE, RESULTS AND DISCUSSION FOR THE LARGE HEATED PLATE

This chapter is concerned with the results obtained from the large rig which include heat transfer data and boundary layer temperature profiles for the laminar, transition and turbulent flow regimes. It had been the intention to obtain boundary layer velocity profiles but because of several problems only one profile was obtained for an angle of inclination of -83.67°.

7.1 EXPERIMENTAL PROCEDURE

Throughout all the experimental runs, care was taken to ensure that the water remained de-aerated insofar as no air bubbles were formed on the heated plate. All electronic equipment was switched on two hours prior to any tests being taken. After the angle of inclination of the plate had been set, the water was thoroughly stirred to ensure a uniform temperature in the tank. The heated plate was then switched on after the disturbances in the water had died away (approximately half-an-hour).

It took approximately forty minutes for the rig to reach a quasi-steady state. For the heat transfer readings, it took approximately one minute to record the heated plate and bulk thermocouple emf's using the data acquisition system described in Section 5.3.3.2. The heat transfer measurements were obtained for the following angles of inclination:

0°, -17.5°, -31.67°, -45.33°, -60.17°, -73.5°, -80.0°, -86.5°

and heat fluxes of approximately:

$$3.0\ ,\ 6.5\ ,\ 13.0\ ,\ 20.0\quad kW/m^2$$

The boundary layer temperature profiles were obtained by

taking thermocouple readings every 0.1 mm away from the plate surface. For the laminar flow region it took approximately fifteen minutes to record a series of readings. For the transition and turbulent regions, approximately 45 minutes were required when using the data acquisition system described in Section 5.3.3.5. Boundary layer temperature profiles were obtained for the following angles of inclination:

0°, -16.8°, -31.5°, -60°, -75.37°, -80°, -84.5°, -85°, -88.5°

with a range of heat fluxes from 1 kW/m^2 to 13 kW/m^2.

One velocity profile was obtained at an angle of -83.67° from the vertical.

7.2 LOCAL HEAT TRANSFER MEASUREMENTS

The thermal emf analogue signal on the tape recorder was converted to digital form using a PDP 8 minicomputer. The resulting output was then processed on the University's 1906A computer to give plate surface temperatures, Nusselt, Grashof and Prandtl Numbers. It was assumed that the heat flux was uniform along the length of the heater foil. The data were then analysed in the same manner as described in Section 6.2 for the small heated plate. The difference between the centre line thermocouples and those near the plate edges was less than 5% for all angles of inclination, indicating that the flow was approximately two-dimensional.

7.2.1 Plate Wall Temperature Distributions

Figure 7.1 shows the wall temperature distribution along the vertical plate. As the heat flux was increased, the point of transition occurred earlier up the plate as was expected. In the turbulent region there was a gradual increase in temperature along the plate.

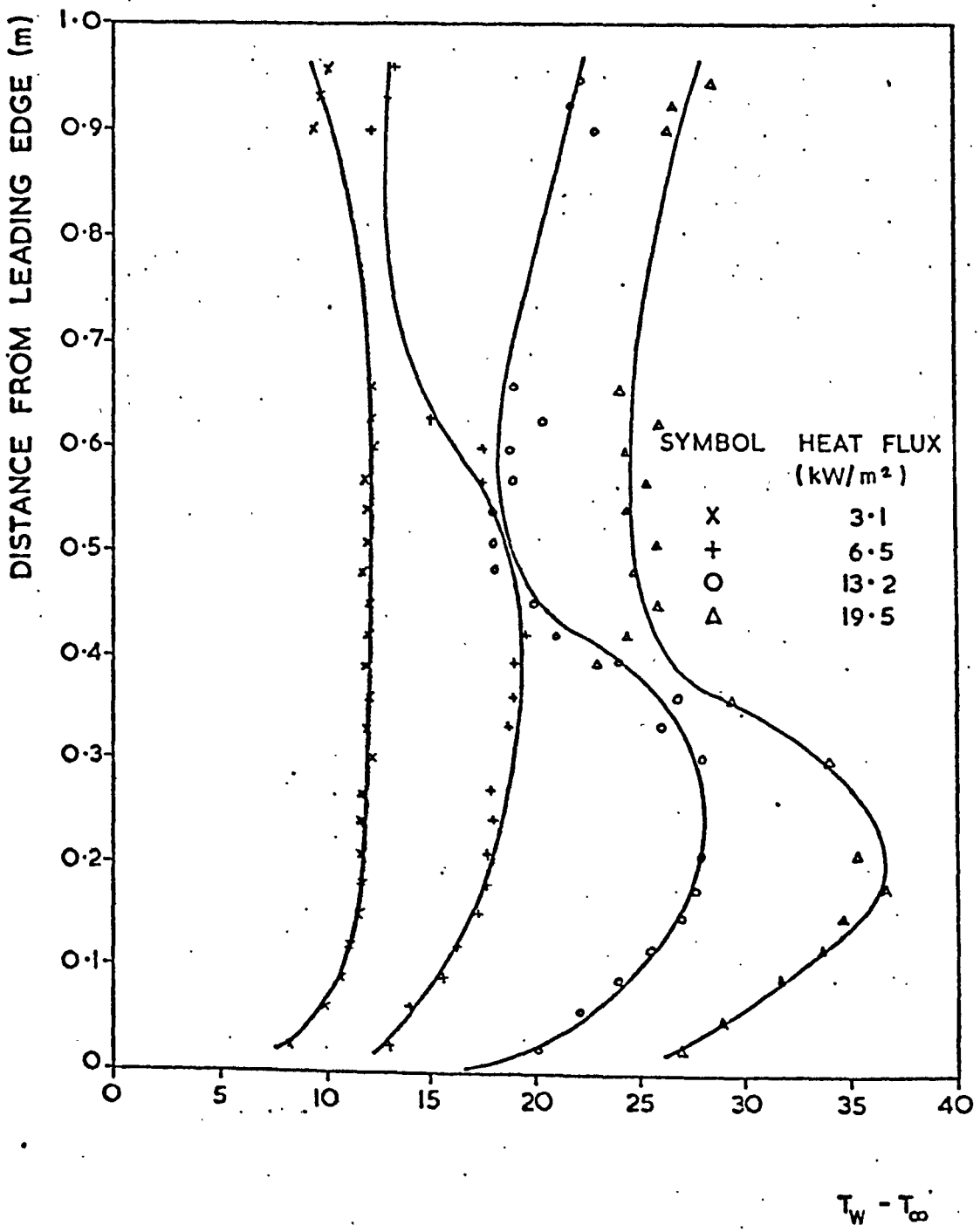

FIGURE 7·1

WALL TEMPERATURE DISTRIBUTION ALONG THE VERTICAL PLATE

The variation of wall temperature distribution against distance along the plate for three angles of inclination is shown in Figure 7.2. The graph is for runs with approximately equal heat fluxes. As the angle of inclination changed from the vertical to -80°, the point of transition is seen to begin further up the plate. This is to be expected because the flow becomes more stable, the further the plate is from the vertical.

7.2.2. Laminar Natural Convection Data

Theory predicts for laminar flow that $Nu_x \propto (Gr_x^* Pr)^{\frac{1}{5}}$. By plotting the heat transfer results as a graph of $Nu_x/(Gr_x^* Pr)^{\frac{1}{5}}$ against log $(Gr_x^* Pr)$, as suggested by Lloyd, Sparrow and Eckert (1972a), it is easier to see whether this relationship is obeyed by the data and the point of transition is made much clearer. Figure 7.3 shows a typical graph for an angle of inclination of -45.33°. Transition is seen to begin at $Ra_x^* = 1.88 \times 10^{14}$. The scatter for $Ra_x^* < 10^9$ is due to leading edge effects.

Table 7.1 gives the values of the constants in equations (6.1) and (6.2) together with their percentage standard deviations.

Angle of Inclination	Equation (6.1)		Equation (6.2)		
	K_1	S D (%)	K_2	K_3	S D (%)
0	0.595	3.47	0.507	0.206	3.46
-17.5	0.591	3.23	0.514	0.205	3.45
-31.67	0.579	4.56	0.549	0.202	4.63
-45.33	0.559	4.72	0.468	0.206	4.64
-60.17	0.524	4.53	0.487	0.202	4.68
-73.50	0.411	6.09	0.242	0.218	5.70
-80.00	0.449	6.18	0.399	0.204	6.59
-86.50	0.334	4.86	0.290	0.205	4.83

TABLE 7.1

THE VALUES OF THE CONSTANTS IN EQUATIONS (6.1) AND (6.2)

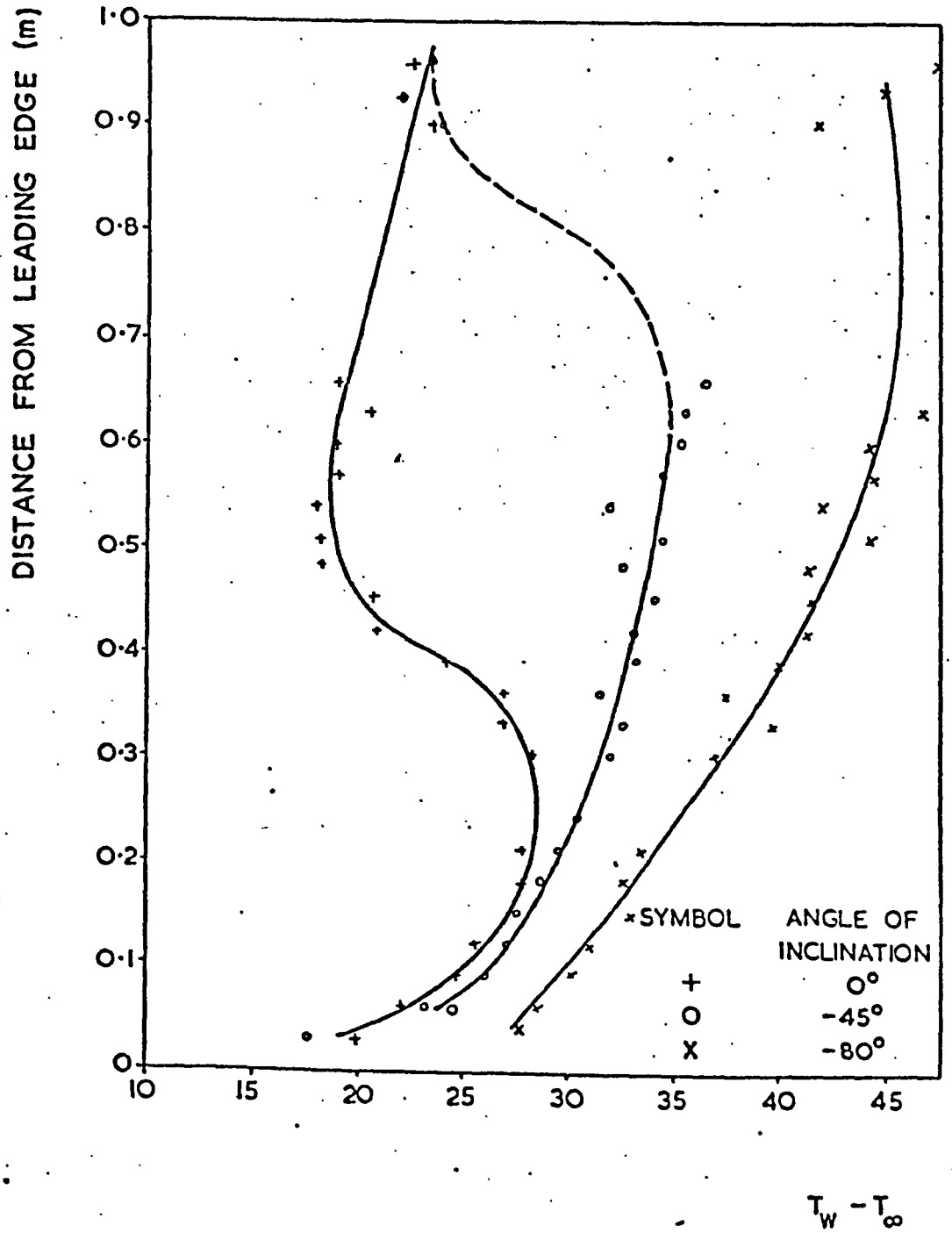

FIGURE 7·2

WALL TEMPERATURE DISTRIBUTION ALONG THE PLATE FOR INCLINATIONS OF 0°, -45°, -80°

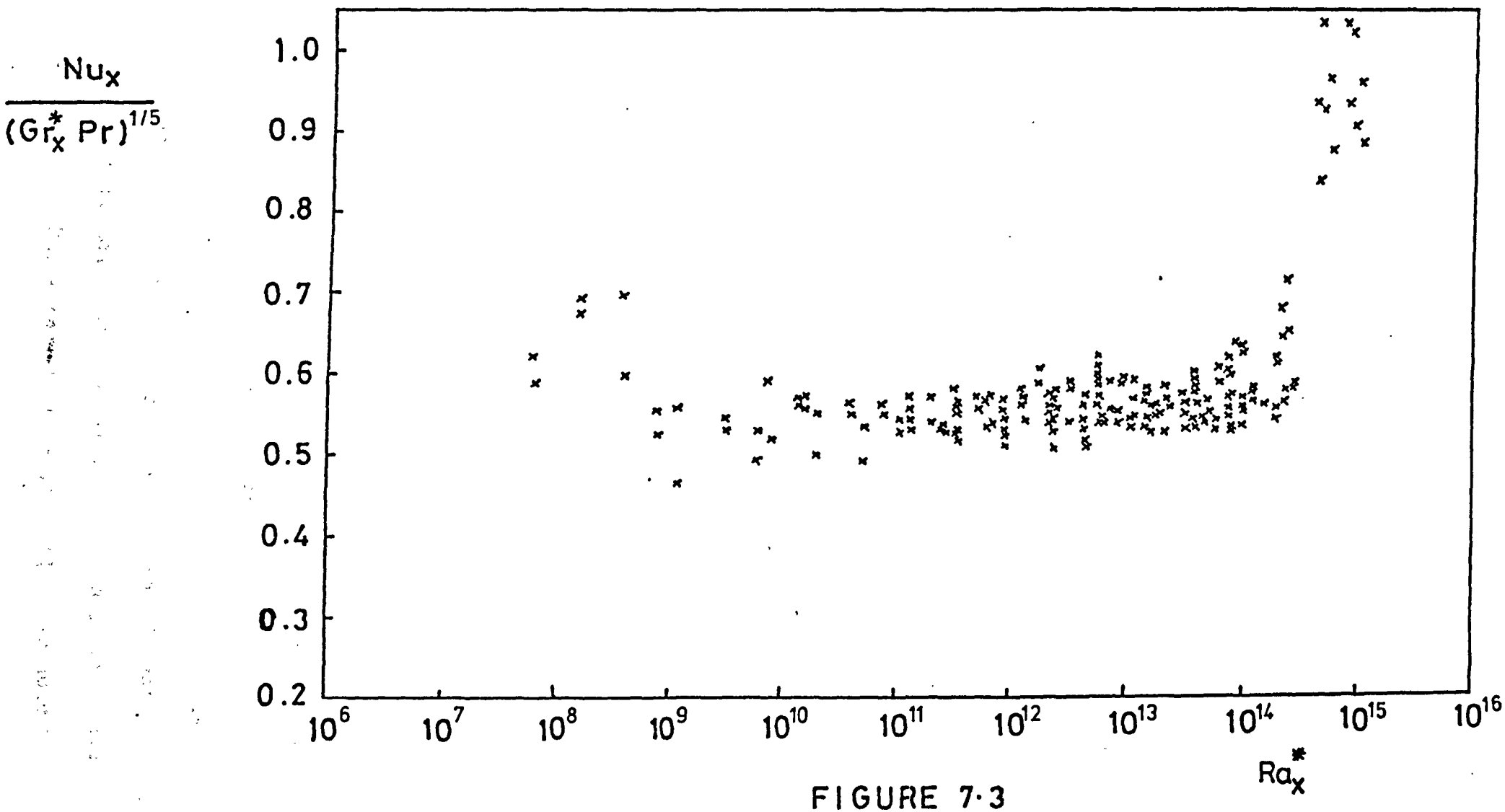

FIGURE 7·3

LOCAL HEAT TRANSFER DATA FOR $\phi = -45°$

The variation of Nu_x against $Gr_x^* Pr \cos \phi$ is shown in Figure 7.4 for all the experimental data obtained and the following two expressions were obtained:

$$Nu_x = 0.592 (Gr_x^* Pr \cos \phi)^{\frac{1}{5}} \quad \ldots (7.1)$$

$$Nu_x = 0.535 (Gr_x^* Pr \cos \phi)^{0.204} \quad \ldots (7.2)$$

with standard deviations of 7.47% and 7.55% respectively. Using Yung and Oetting's correlation, we obtained the equation:

$$Nu_x = \frac{0.668}{2} (1 + \cos \phi)(Gr_x^* Pr)^{\frac{1}{5}} \quad \ldots (7.3)$$

with a standard deviation of 9.3%. Correlating the data with equations (6.4) and (6.5) resulted in the following two expressions

$$Nu_x = 0.630 Pr^{\frac{2}{5}} (Pr + 0.8 - 0.15 Pr \sin \phi)^{-\frac{1}{5}} (Gr_x^* \cos \phi)^{\frac{1}{5}} \ldots (7.4)$$

and

$$Nu_x = 0.619 Pr^{\frac{2}{5}} (Pr+0.8)^{-\frac{1}{5}} (1+0.798 f(Pr, Gr_x^*, \phi) \tan \phi)^{\frac{1}{5}} (Gr_x^* \cos \phi)^{\frac{1}{5}} \quad \ldots (7.5)$$

both with standard deviations of 7.46%. Comparing the constants in equations (7.4) and (7.5) with those in equations (3.23) and (3.25), equation (7.5) gave a closer correlation to the theory.

The various correlations are compared in Figure 7.5 for Pr = 5. Only equation (7.3) differed appreciably from the remaining three correlations.

7.2.3 Transition Data

The criterion used to decide the point of transition was the change in slope of the $Nu_x/(Gr_x^* Pr)^{\frac{1}{5}}$ - log Ra_x^* graph. Figure 7.6 shows a graph of the transition Rayleigh Number against angle of inclination together with the data from the work of Vliet (1969), Lock, Gort and Pond (1967), Pera and Gebhart (1973b) and Lloyd and Sparrow (1970). As the latter three papers used isothermal plates, their data were modified from the ordinary Rayleigh Number (Ra_x) to the modified Rayleigh Number (Ra_x^*). (This was done by assuming

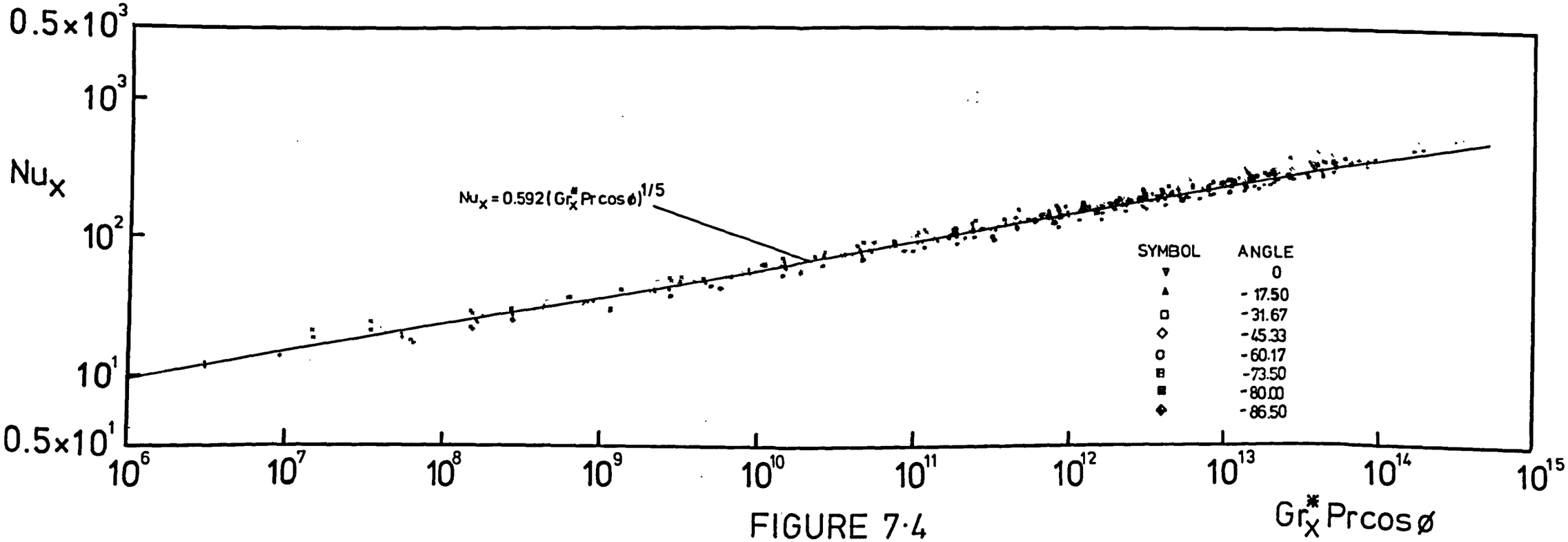

FIGURE 7·4

LAMINAR NATURAL CONVECTION FROM THE LARGE RIG

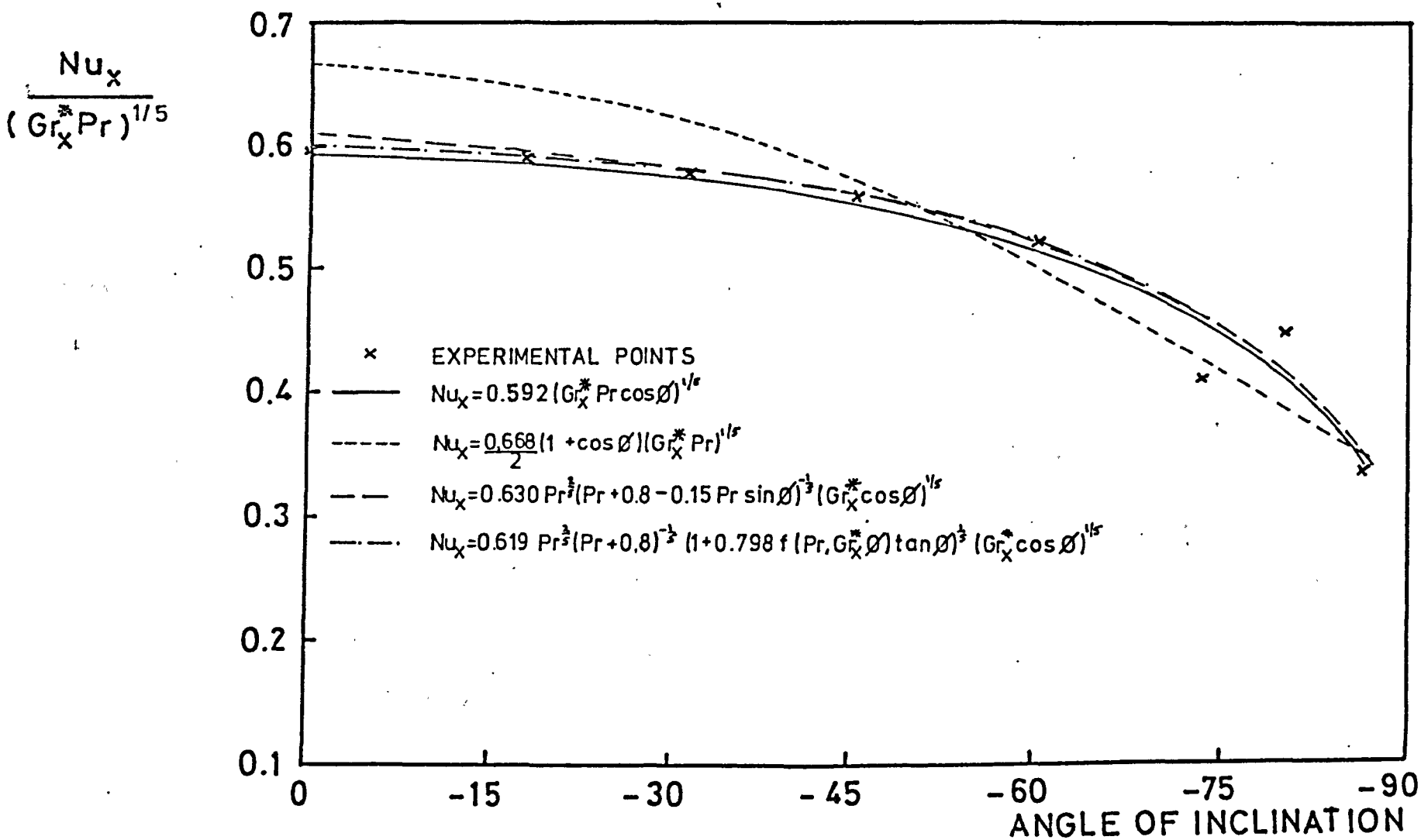

FIGURE 7·5

COMPARISON OF EXPERIMENTAL RESULTS

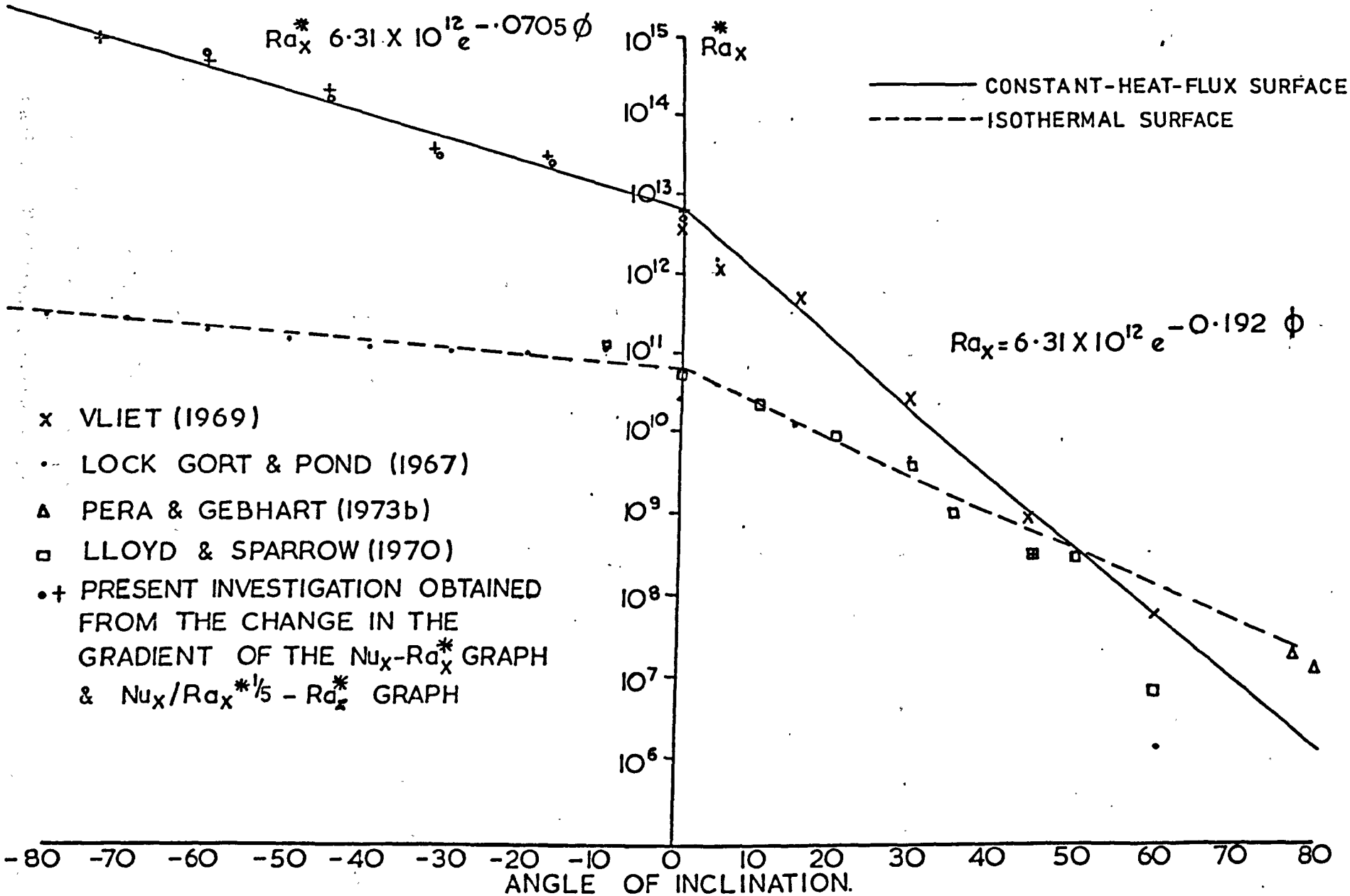

FIGURE 7·6

NATURAL CONVECTION TRANSITION DATA FOR THE LARGE RIG

that the laminar flow heat transfer relationship held up to the point of transition so that the Nusselt Number could be calculated. The modified Rayleigh Number is then obtained from the relationship $Ra_x^* = Ra_x\, Nu_x$.) From the constant-heat-flux results, the following two correlations were derived to calculate the transition Rayleigh Number:

$$Ra_x^* = 6.31 \times 10^{12}\ e^{-0.192\,\phi} \qquad 60 \geq \phi \geq 0$$

$$Ra_x^* = 6.31 \times 10^{12}\ e^{-0.0705\,\phi} \qquad -70 \leq \phi \leq 0 \qquad \ldots (7.6)$$

It will be seen that the majority of results for the isothermal plate lie beneath those of the constant-heat-flux plate. For an upward-facing plate at angles greater than 55° from the vertical, there is a great deal of scatter in the published data. As the angle of inclination changed from positive to negative, the two lines defining the two boundary conditions began to diverge. The divergence was more pronounced for positive angles of inclination. Between the range of angles $-70° \leq \phi \leq 80°$, the transition Rayleigh Number changed by nine orders of magnitude.

7.2.4 Turbulent Data

The experimental data did not cover as large a range of Rayleigh Numbers and angles of inclination as originally intended. Turbulent heat transfer data were obtained for angles of inclination of 0°, -17.5° and -31.67° and covered a range of Rayleigh Numbers of:

5.3×10^{13} to 9.23×10^{14} $\qquad \phi = 0°$

1.3×10^{14} to 9.07×10^{14} $\qquad \phi = -17.5°$

1.48×10^{14} to 9.05×10^{14} $\qquad \phi = -31.67°$

To obtain a realistic relationship between the Nusselt and Rayleigh Numbers, a range of Rayleigh Number of at least three

orders of magnitude is required whereas here we only had one. Nevertheless, a least squares routine was used to correlate the data, the best fit curve being:

$$Nu_x = 0.889\ (Gr_x^* Pr \cos \phi)^{0.205} \qquad \ldots (7.7)$$

with a standard deviation of 6.59%. It was found that the gravity component parallel to the plate correlated the data better than the ordinary gravity component, as found by Vliet (1969). Figure 7.7 shows the turbulent data.

There is little agreement on the power of the Rayleigh Number amongst the various investigations that have been undertaken. The analysis of Section 3.3 gives a dependence of 0.286 whereas the results of Bayley* (1955) give 0.25. Table 7.2 gives a brief résumé of the results.

The slope of the data for the present investigation is less than the other correlations but the data points lie within the large band of scatter of the correlations. At present, no explanation can be put forward for this.

The difference in turbulent heat transfer coefficients between an upward- and downward-facing inclined plate may be due to the separation of the boundary layer from the plate which occurs for an upward-facing plate but not for a downward-facing one. The separation could cause an increase in heat transfer coefficient.

7.3 BOUNDARY LAYER TEMPERATURE AND VELOCITY MEASUREMENTS

7.3.1 Laminar Boundary Layer Temperature Profiles

Laminar boundary layer temperature profiles were obtained over a wide range of angles and Rayleigh Numbers. Table 7.3 gives

---

* where necessary, the correlation has been re-calculated in the form involving the modified Grashof Number

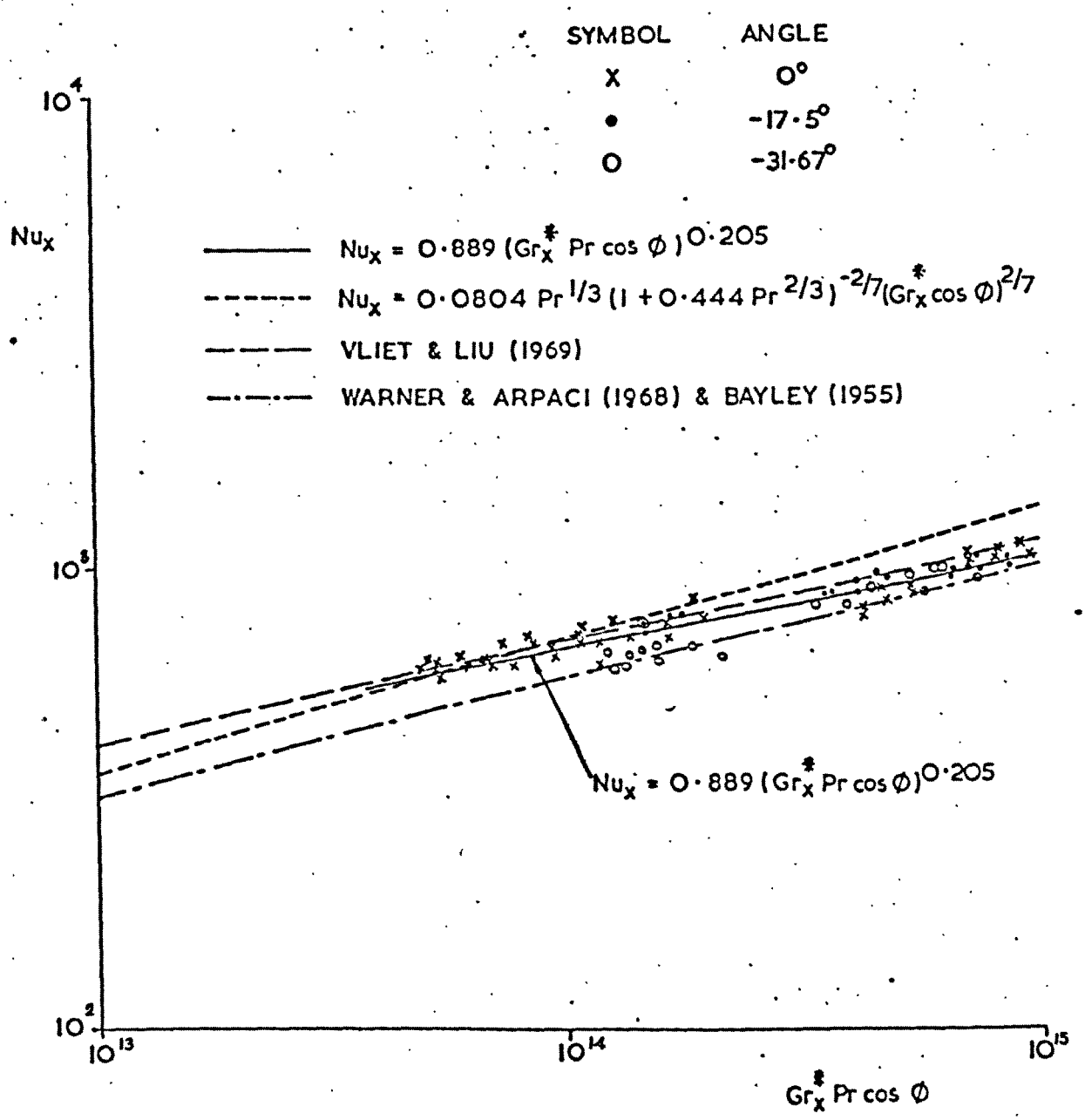

FIGURE 7·7

TURBULENT NATURAL CONVECTION FROM A DOWNWARD FACING INCLINED FLAT PLATE

Investigator	Index of Gr_x^*	Boundary Conditions	Plate Orientation
Bayley (1955)	0.25	Isothermal	Vertical
Warner and Arpaci (1968)	0.25	"	"
Cheesewright (1968)	0.267	"	"
Kato, Nishiwaki and Hirata (1968)	0.237–0.265	"	"
Coutanceau (1969)	0.291	"	"
Vliet and Liu (1969)	0.219	Constant-heat-flux	"
Vliet (1969)	0.24	"	Inclined plate ϕ positive
Lloyd, Sparrow and Eckert (1972a)	0.25	Uniform concentration	" " " "
Present investigation: experimental	0.205	Constant-heat-flux	Inclined plate ϕ negative
theoretical	0.286	"	Inclined plate ϕ positive or negative

TABLE 7.2

GRASHOF DEPENDENCE FOR TURBULENT NATURAL CONVECTION

details of the range of angles, distance up the plate and Rayleigh Numbers.

Angle of Inclination	Distance from leading edge (m)	Range of Ra_x^*
0°	0.1625, 0.3620	2.8×10^{10} - 8.6×10^{11}
-16.83°	0.1625	3.5×10^{10} - 1.5×10^{11}
-31.5°	0.1625	2.2×10^{10} - 1.5×10^{11}
-60.0°	0.1580, 0.8575	3.1×10^{10} - 9.1×10^{13}
-75.37°	0.1580	2.5×10^{10} - 1.3×10^{11}
-80.00°	0.1580	2.4×10^{10} - 1.2×10^{11}
-84.5° to -85°	0.1580, 0.4260, 0.7270, 0.8750	3.1×10^{10} - 1.9×10^{14}
-88.5°	0.4260, 0.7270	1.2×10^{12} - 1.0×10^{14}

TABLE 7.3

RANGE OF LAMINAR BOUNDARY LAYER TEMPERATURE PROFILES

All runs were taken at low heat fluxes so that bulk temperature stratification did not become a problem.

The heat flux and plate surface temperature were obtained by extrapolating the temperature to the wall, the gradient of the curve giving the heat flux. Agreement within 5% was obtained with the heat flux and plate surface temperatures obtained from the plate surface thermocouples.

The temperature data are usually normalised using $\frac{T - T_\infty}{T_w - T_\infty}$ and the distance from the plate by $\frac{y}{x}\left(\frac{Gr_x^* Pr}{5}\right)^{\frac{1}{5}}$. Figures 7.8 to 7.15 show the variation of normalised temperature as a function of distance from the wall for angles of inclination of 0°, -16.83°, -31.5°, -60°, -75.37°, -80°, -85° and -88.5° from the vertical. The data covered a range of Prandtl Number from 4.5 to 6.5. The

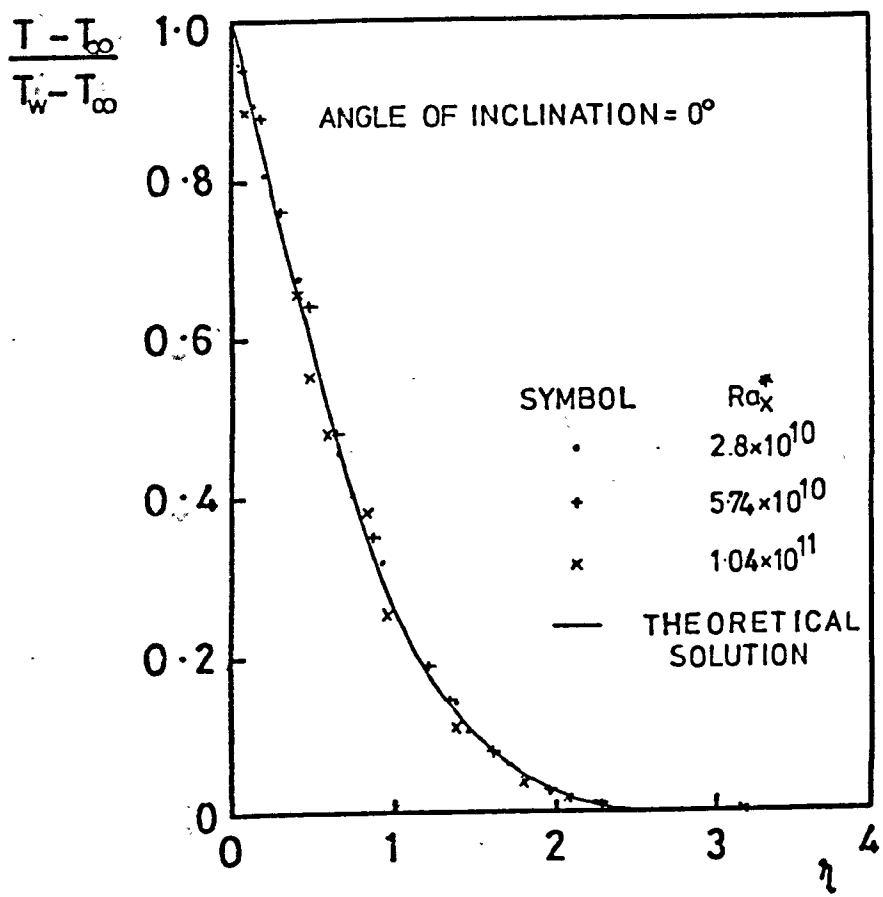

FIGURE 7·8

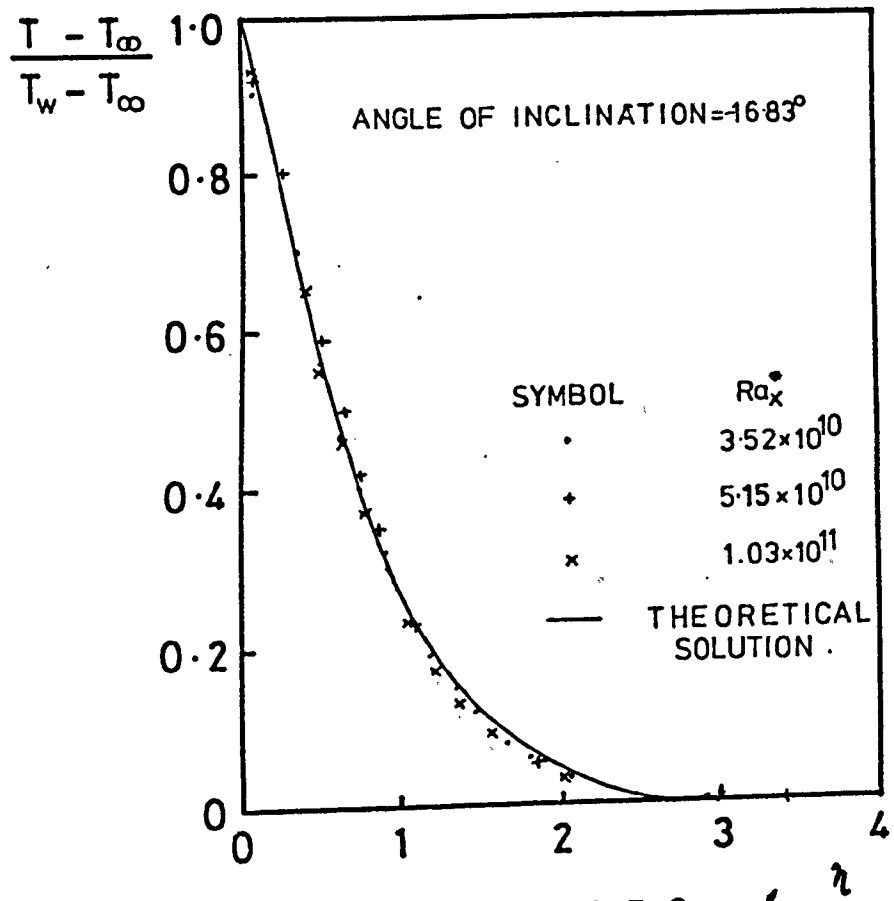

FIGURE 7·9

LAMINAR BOUNDARY LAYER TEMPERATURE PROFILES

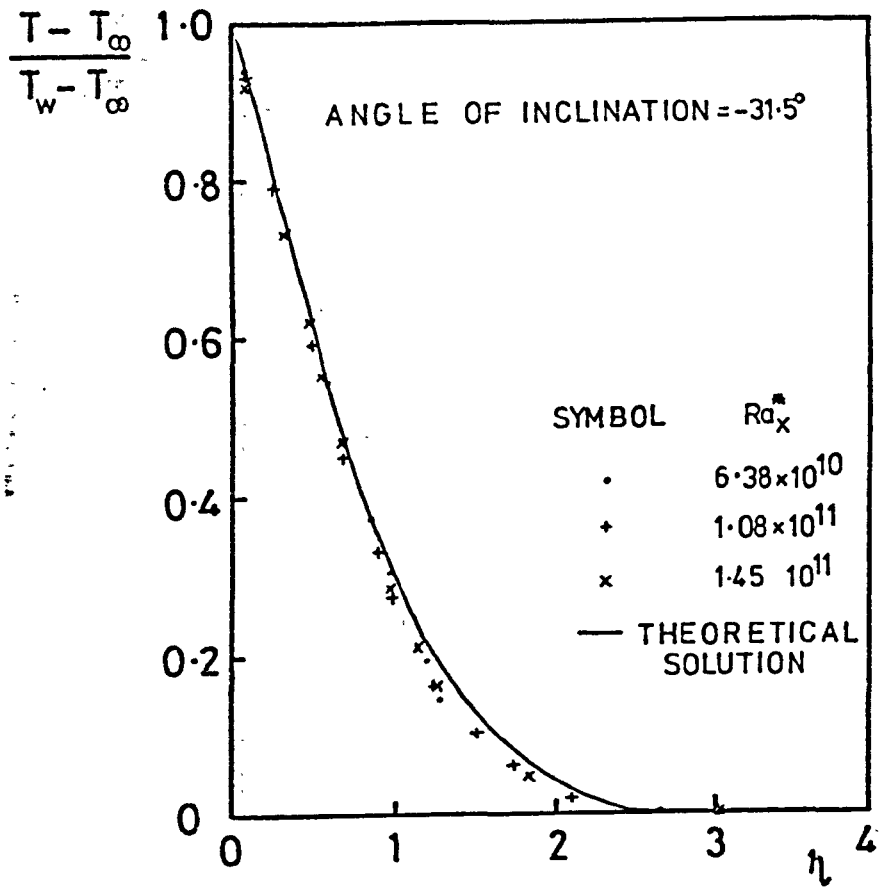

FIGURE 7·10

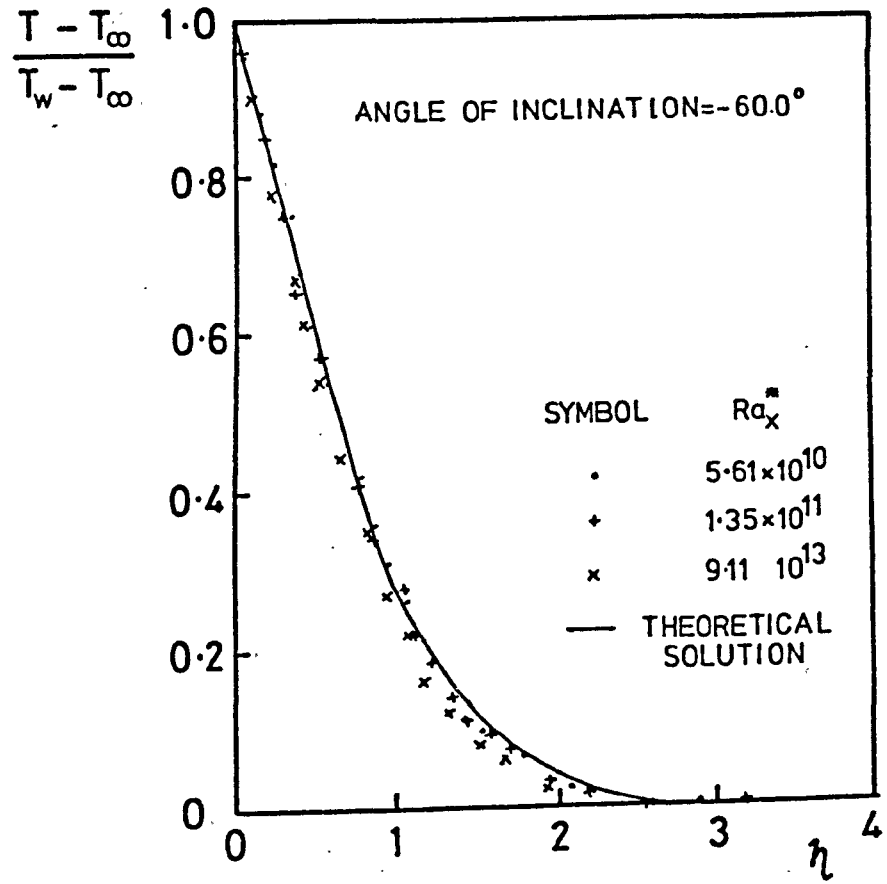

FIGURE 7·11

LAMINAR BOUNDARY LAYER TEMPERATURE PROFILES

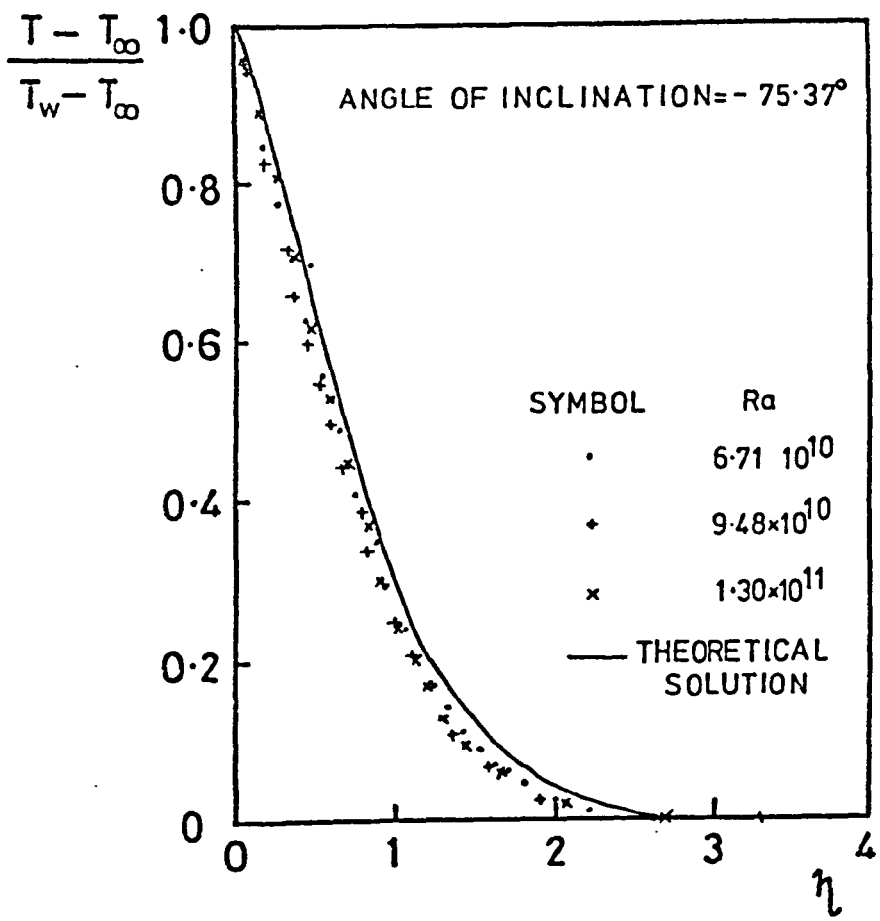

FIGURE 7·12

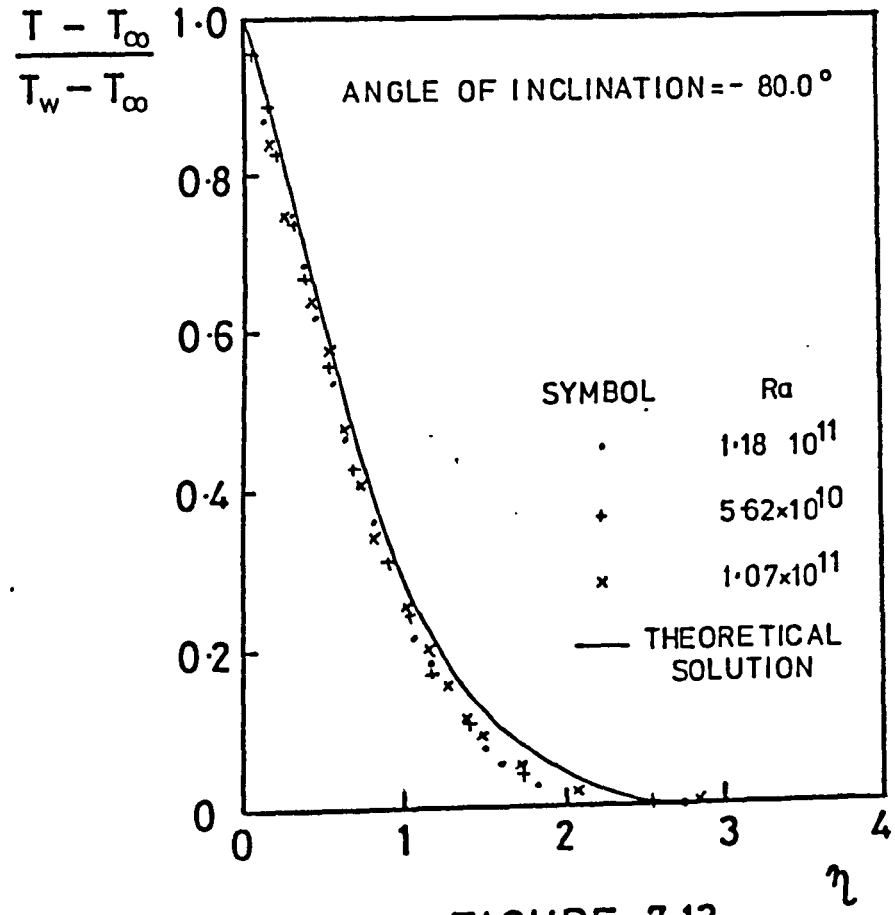

FIGURE 7·13

LAMINAR BOUNDARY LAYER TEMPERATURE PROFILES

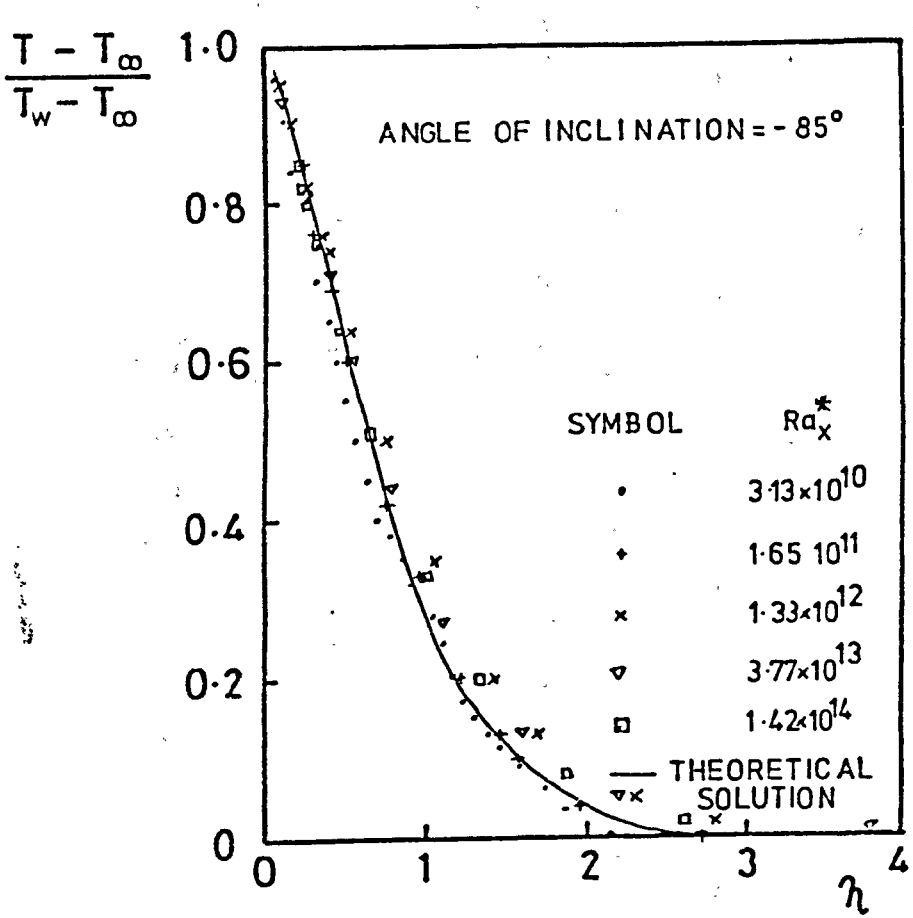

FIGURE 7·14

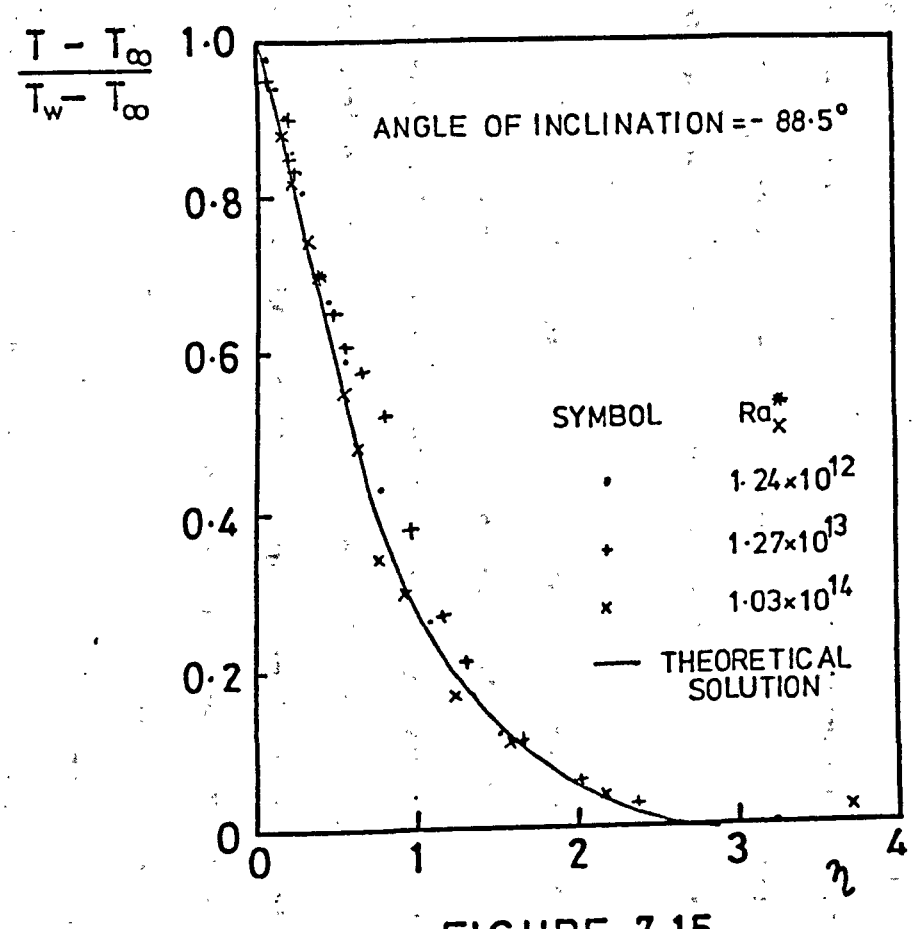

FIGURE 7·15

LAMINAR BOUNDARY LAYER TEMPERATURE PROFILES

experimental data were also compared with the vertical plate theory, the theoretical curves being interpolated from the results of Chang, Akins, Burris and Bankoff (1964). For the inclined plate, the theoretical data were modified to include the cos ϕ correction.

For the vertical plate, there was excellent agreement between theory and experiment. As the angle of inclination began to decrease, the experimental points began deviating from the theoretical curve up to -80° from the vertical. At angles between -80° and -90°, the results taken at small x were below the curve but at higher x they were above the curve. The theoretical curves were based on boundary layer theory rather than perturbation analysis which gives more accurate results. The results of Yang and Jerger (1964) for laminar natural convection on an isothermal vertical plate using a perturbation analysis showed that there was very little effect on the temperature profile in the boundary layer, the perturbation analysis being slightly above the boundary layer analysis of Ostrach (1952). This result was confirmed by Pera and Gebhart (1973a). They plotted graphs of $\frac{T - T_{\infty}}{T_W - T_{\infty}}$ against $\frac{y}{x}\left(\frac{Gr_x \sin \phi}{5}\right)^{\frac{1}{5}}$ for various values of $\epsilon = \sqrt[5]{\frac{Gr_x \sin \phi}{5}} \cot \phi$. When $\epsilon < 0.7$, they found good agreement between theory and experiment but for values of $\epsilon > 0.7$ the experimental points were lower than the theoretical curve.

An alternative method of presenting the results is to calculate the thermal displacement thickness, used by Warner and Arpaci (1968), and defined by:

$$\delta_h = \frac{1}{T_W - T_{\infty}} \int_0^{\infty} (T - T_{\infty})\, dy$$

The polynomial used in the laminar boundary layer theory for the temperature profile (Section 3.2) gave:

$$\delta_h = 0.3\delta$$

From equation (3.16)

$$\frac{\delta}{x} = 360^{\frac{1}{5}}\ Pr^{-\frac{2}{5}}\ (Pr + 0.8)^{\frac{1}{5}}\ (Gr_x^* \cos\phi)^{-\frac{1}{5}}$$

giving

$$\frac{\delta_h}{x} = \frac{1}{3}\ 360^{\frac{1}{5}}\ Pr^{-\frac{2}{5}}\ (Pr + 0.8)^{\frac{1}{5}}\ (Gr_x^* \cos\phi)^{-\frac{1}{5}} \qquad \ldots (7.8)$$

Hence it may be assumed that

$$\frac{\delta_h}{x} = \text{function}\ (Gr_x^*,\ Pr,\ \cos\phi)$$

The results of Chang, Akins, Burris and Bankoff (1964) for a vertical plate were analysed and gave the solution:

$$\frac{\delta_h}{x} = 0.361\ Pr^{-0.267}\ Gr_x^{*-0.1395} \qquad \ldots (7.9)$$

The experimental data were correlated in the two forms discussed and the following two equations were obtained:

$$\frac{\delta_h}{x} = 0.606\ Pr^{-\frac{2}{5}}\ (Pr + 0.8)^{\frac{1}{5}}\ (Gr_x^* \cos\phi)^{-0.177} \qquad \ldots (7.10)$$

and

$$\frac{\delta_h}{x} = 0.917\ Pr^{-0.383}\ (Gr_x^* \cos\phi)^{-0.180} \qquad \ldots (7.11)$$

with standard deviations of 9.59% and 9.58% respectively.

Comparison of equations (7.8) and (7.10) showed that the index of the Grashof Number had decreased as well as the constant. Figure 7.16 shows the variation of δ_h/x against log $(Gr_x^*\ Pr \cos\phi)$ at Pr = 5 together with equations (7.10) and (7.11). There was very little difference between the two correlations.

7.3.2 Transition and Turbulent Boundary Layer Temperature Profiles

In the transition and turbulent regimes, the frequency of

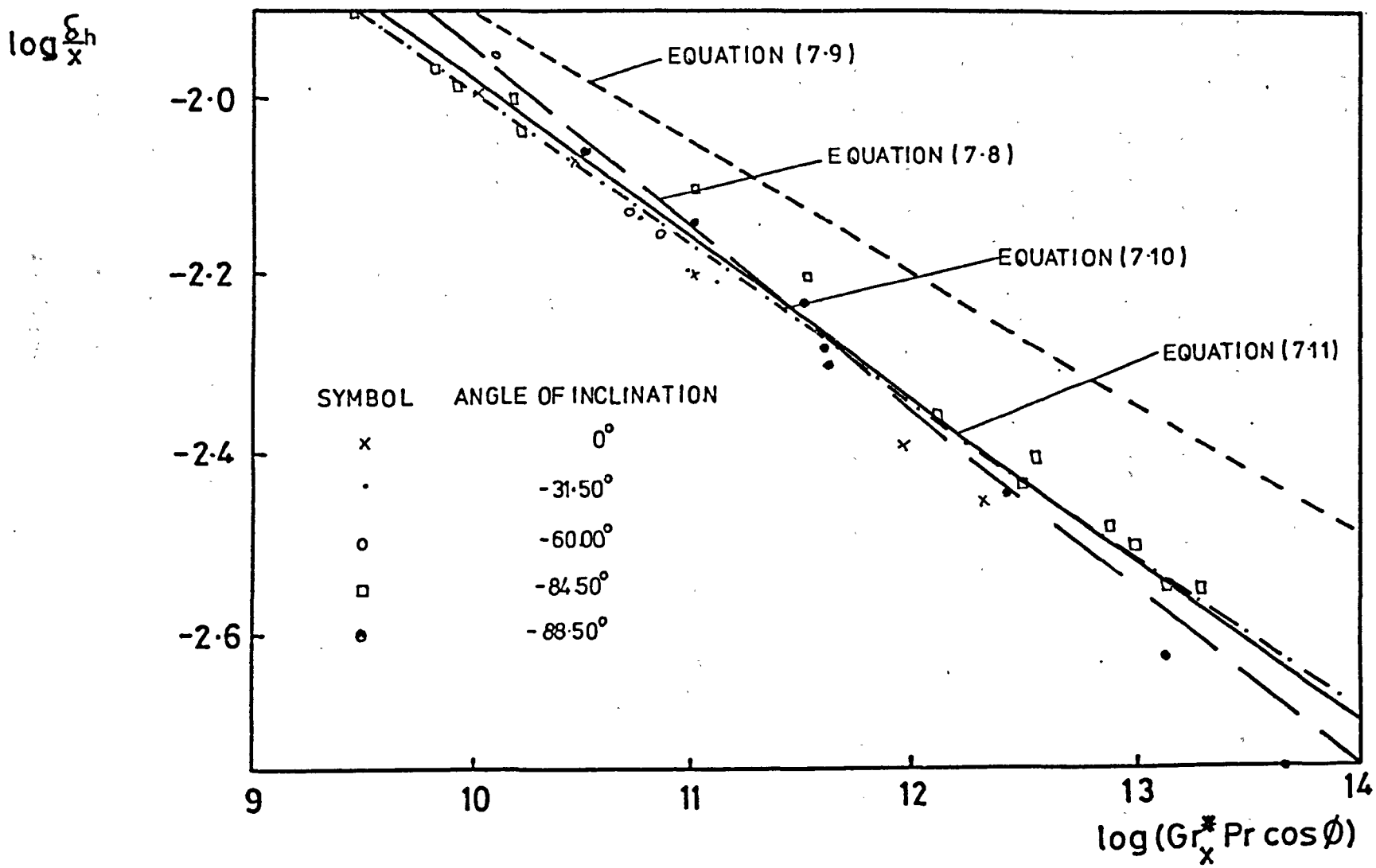

FIGURE 7·16

DISTRIBUTION OF THERMAL DISPLACEMENT THICKNESS FOR LAMINAR FLOW

fluctuations is less than 10 Hz, necessitating a long averaging time. Cheesewright (1968) used a 300-second averaging time whereas Vliet and Liu (1969) recorded signals over a period ranging from 30 to 60 seconds. In the present investigation, the thermocouple signal was recorded for 100 seconds and the ADC programme took samples of the data every 0.1 seconds to obtain an average of 1,000 points. A check was made to see if 100 seconds was a reasonable time for obtaining a mean value and it was found that above 100 seconds there was little change in the value.

At the present time, there is no general agreement as to which is the best method of presenting the results in the transition and turbulent regimes. The following suggestions have been made:

Fujii (1959)	$\frac{T - T_\infty}{T_w - T_\infty}$	$Nu_x \left(\frac{y}{2x}\right)$
Cheesewright (1968)	"	$\frac{y}{x} Gr_x^{0.1}$
Warner and Arpaci (1968)	"	y
Lock and Trotter (1968)	"	y
Vliet and Liu (1969)	"	y/δ_h

Of the various suggestions for correlating the data, the method of Vliet and Liu (1969) gave the best fit. The use of a boundary layer thickness for normalising distances has been found to be quite good for laminar natural convection and is also used extensively in forced convection work. The method also provided a useful method of comparing the laminar, transition and turbulent boundary layer profiles.

The development of the thermal boundary layer profile from laminar through transition, to turbulence is shown in Figure 7.17.

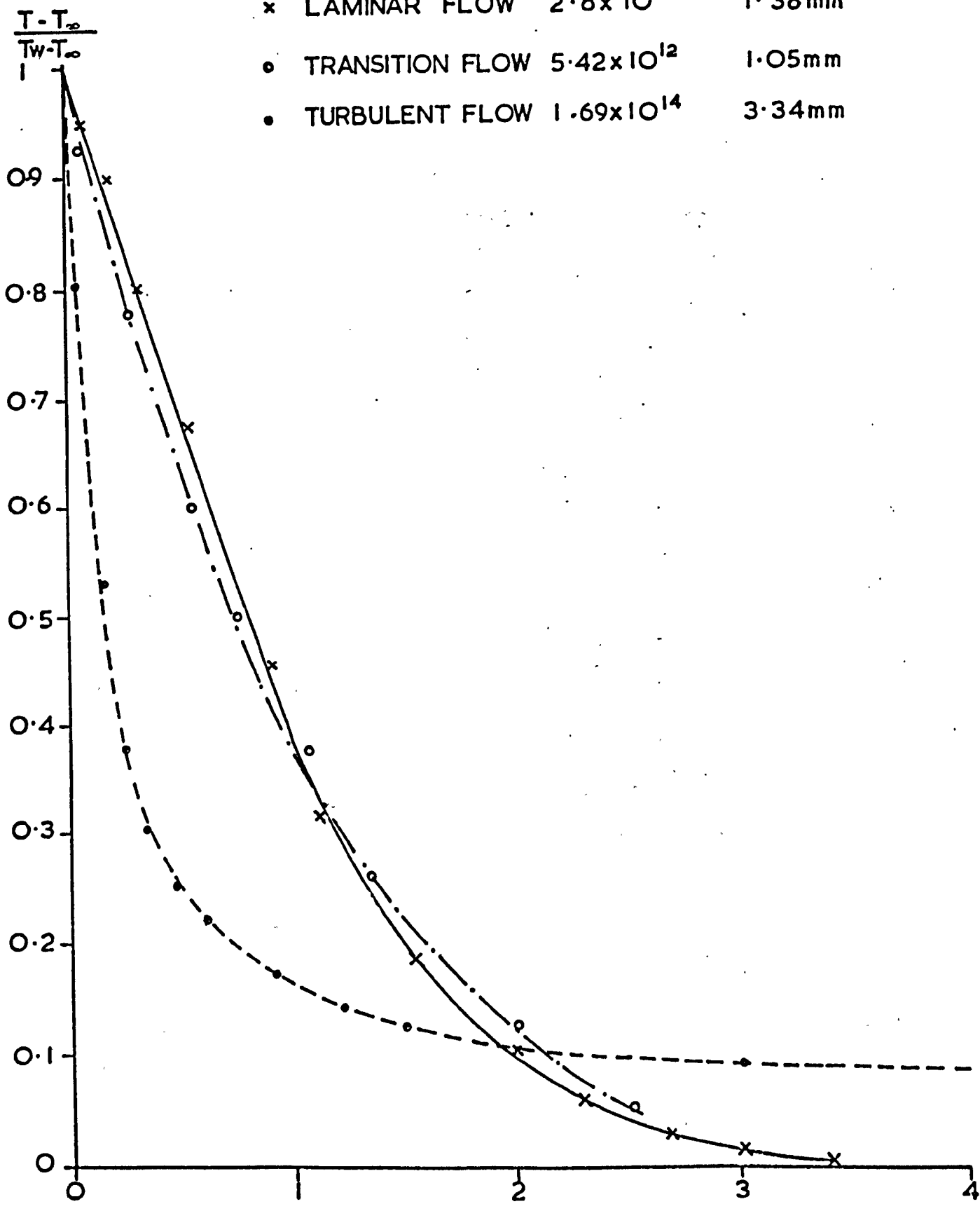

FIGURE 7·17

LAMINAR, TRANSITION & TURBULENT TEMPERATURE PROFILES FOR A VERTICAL PLATE.

These curves show the steepening of the profile as the flow became more turbulent. Figure 7.18 compares the vertical plate mean turbulent boundary layer temperature profiles with the data of Vliet and Liu (1969). Excellent agreement was found between the two sets of data.

Mean profiles were obtained for angles of inclination of 0°, -14.5° and -30° and these are shown in Figure 7.19. These profiles cover a range of modified Rayleigh Numbers from 5.13×10^{13} to 7.8×10^{14}. There was some scatter in the data but this was to be expected as the averaging time was not as long as was desired.

Strip chart recordings were taken at various points throughout the boundary layer and a typical set of traces is shown in Figure 7.20 for an angle of inclination of -14.5° and $Ra_x^* = 5.28 \times 10^{14}$. Figure 7.20(a), taken at the outer edge of the boundary layer, shows the high intermittency and asymmetry of the turbulent process. As one proceeded towards the wall, the asymmetry began to disappear (Figures 7.20(b), (c) and (d)) until at $y = 0.1\delta_h$ (Figure 7.20(e)) the turbulence was symmetric. It should be noted from Figure 7.20 that the turbulent frequency increased up to $y/\delta_h = 0.1$ and then began to decrease.

The root-mean-square values of the turbulent temperature fluctuations as a function of y/δ_h are presented in Figure 7.21. The intensity increased as one proceeded towards the wall until it reached a maximum of $y/\delta_h = 0.25$ where it began to decrease. A similar graph of turbulent velocity fluctuations in the boundary layer from Vliet and Liu (1969) also showed a maximum at a similar value.

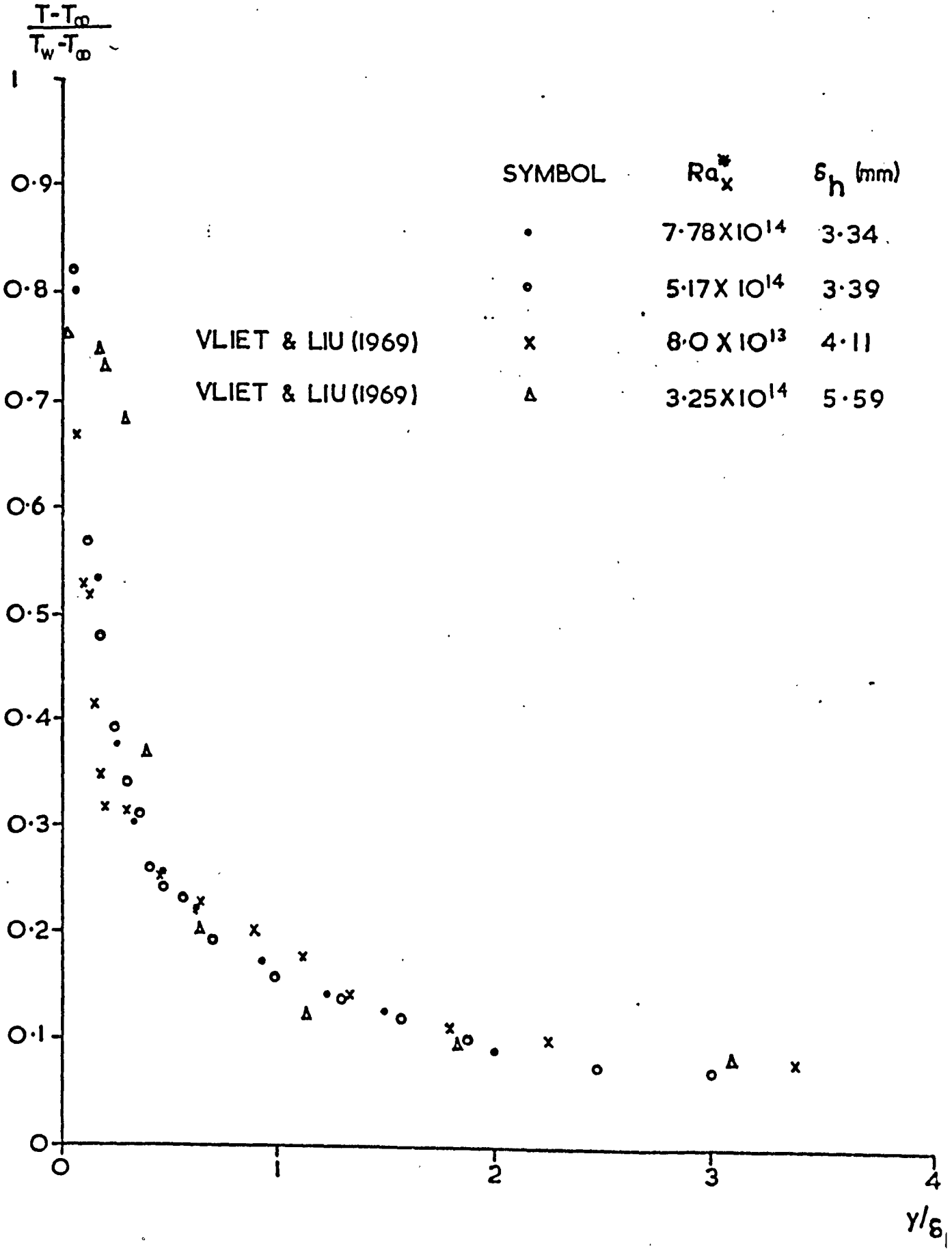

FIGURE 7·18

MEAN TEMPERATURE DISTRIBUTION IN TURBULENT BOUNDARY LAYER FOR VERTICAL PLATE.

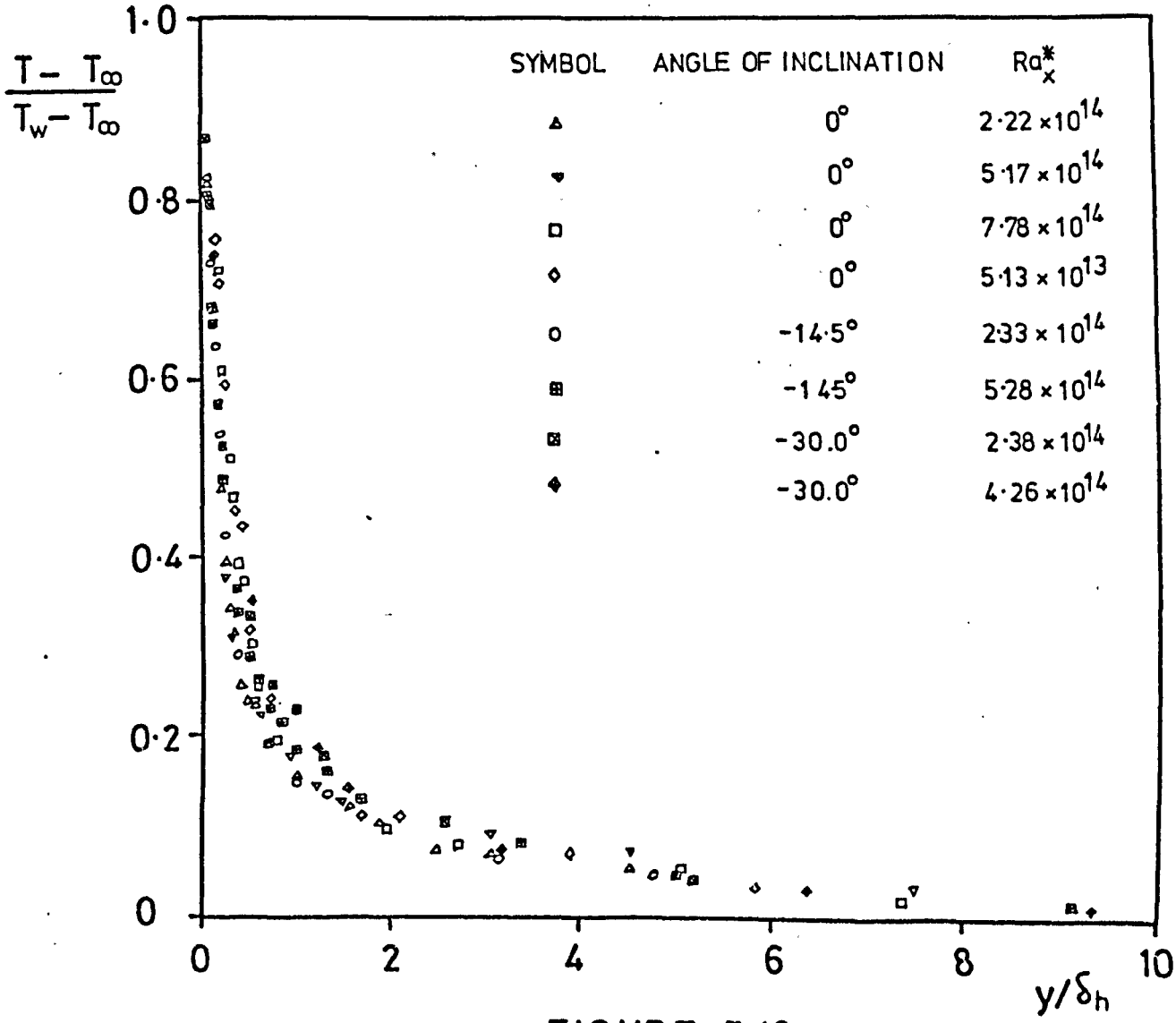

FIGURE 7·19

TURBULENT BOUNDARY LAYER TEMPERATURE PROFILES

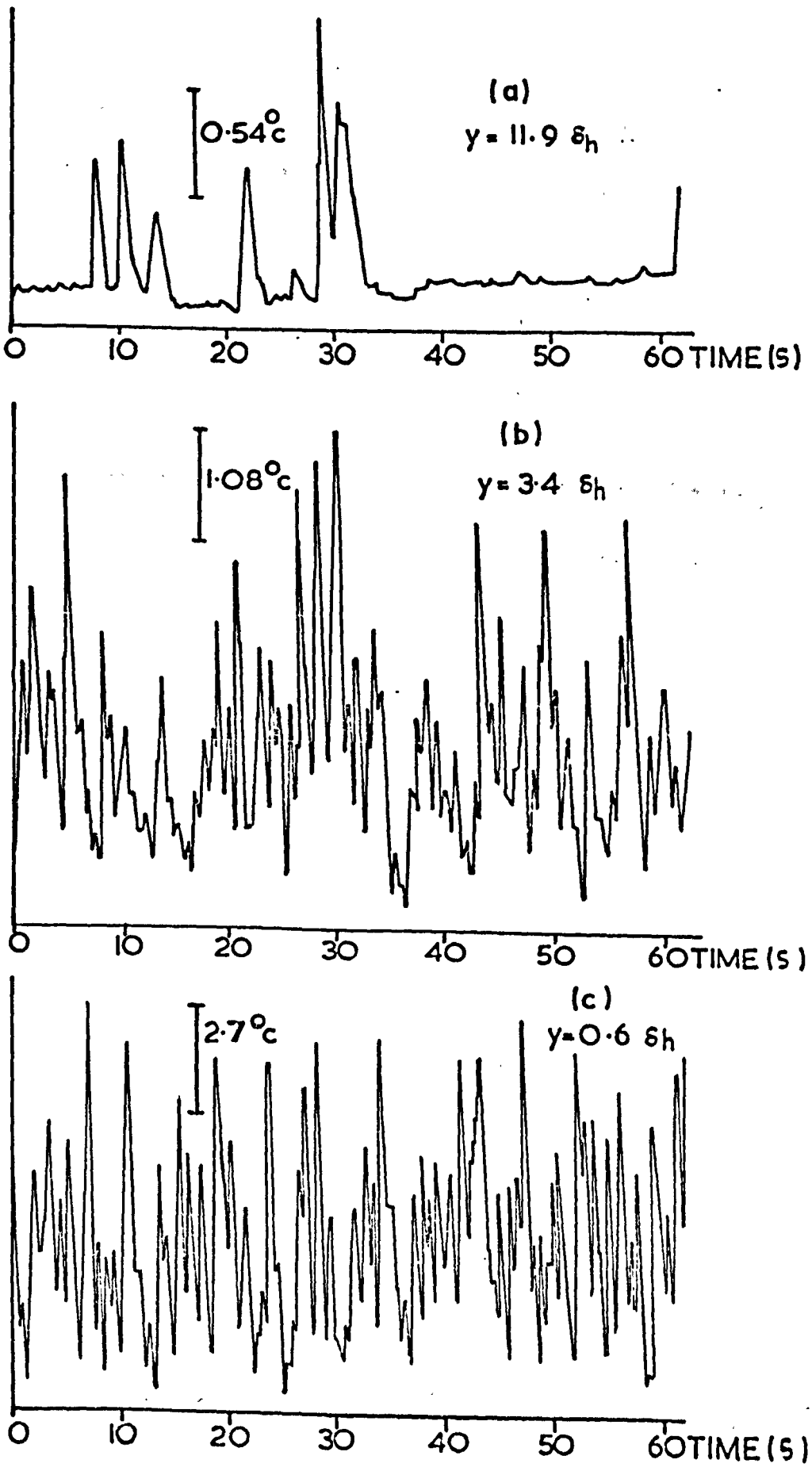

FIGURE 7·20

TEMPERATURE FLUCTUATIONS IN THE BOUNDARY LAYER

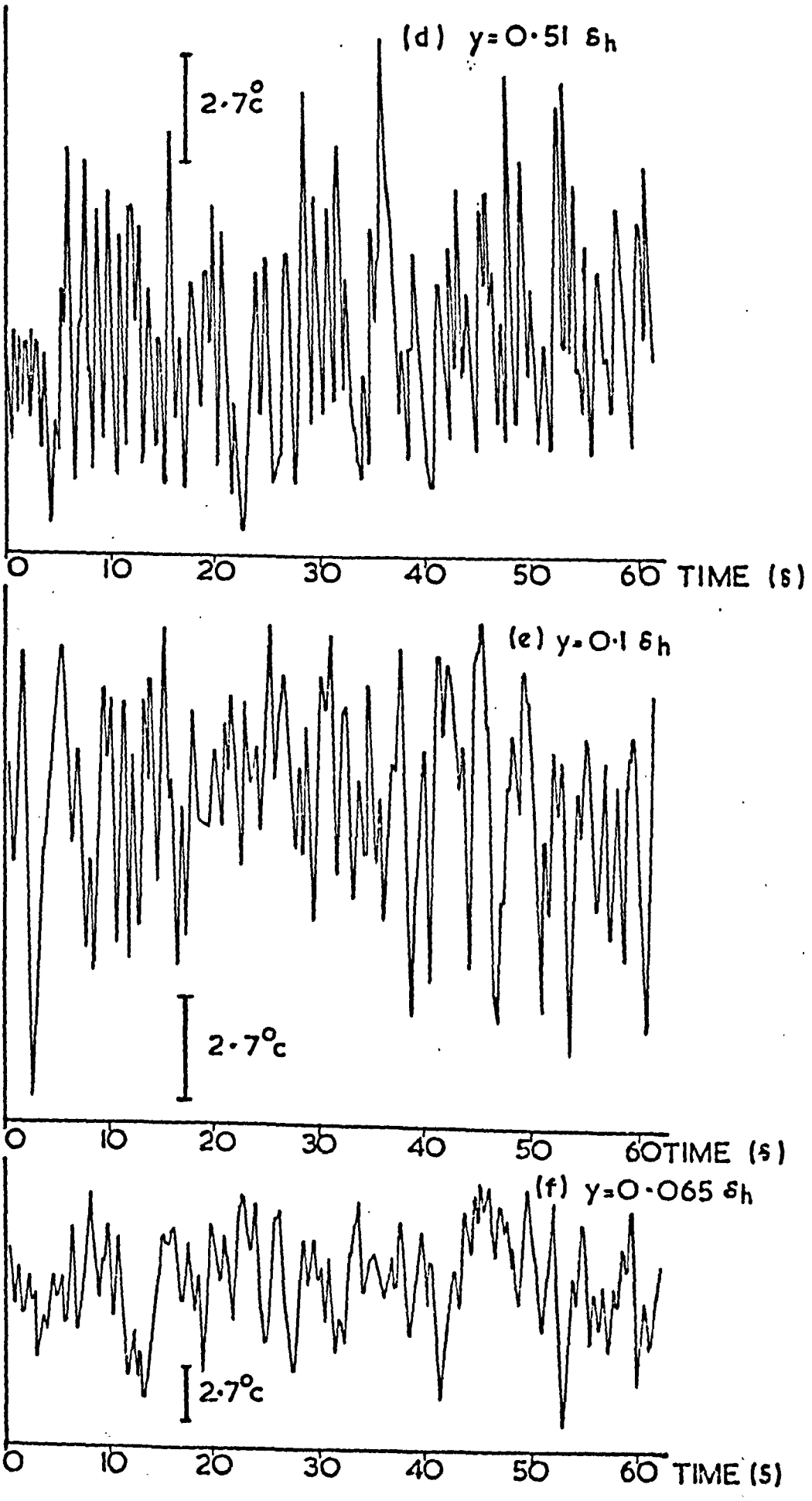

FIGURE 7·20

TEMPERATURE FLUCTUATIONS IN THE BOUNDARY LAYER

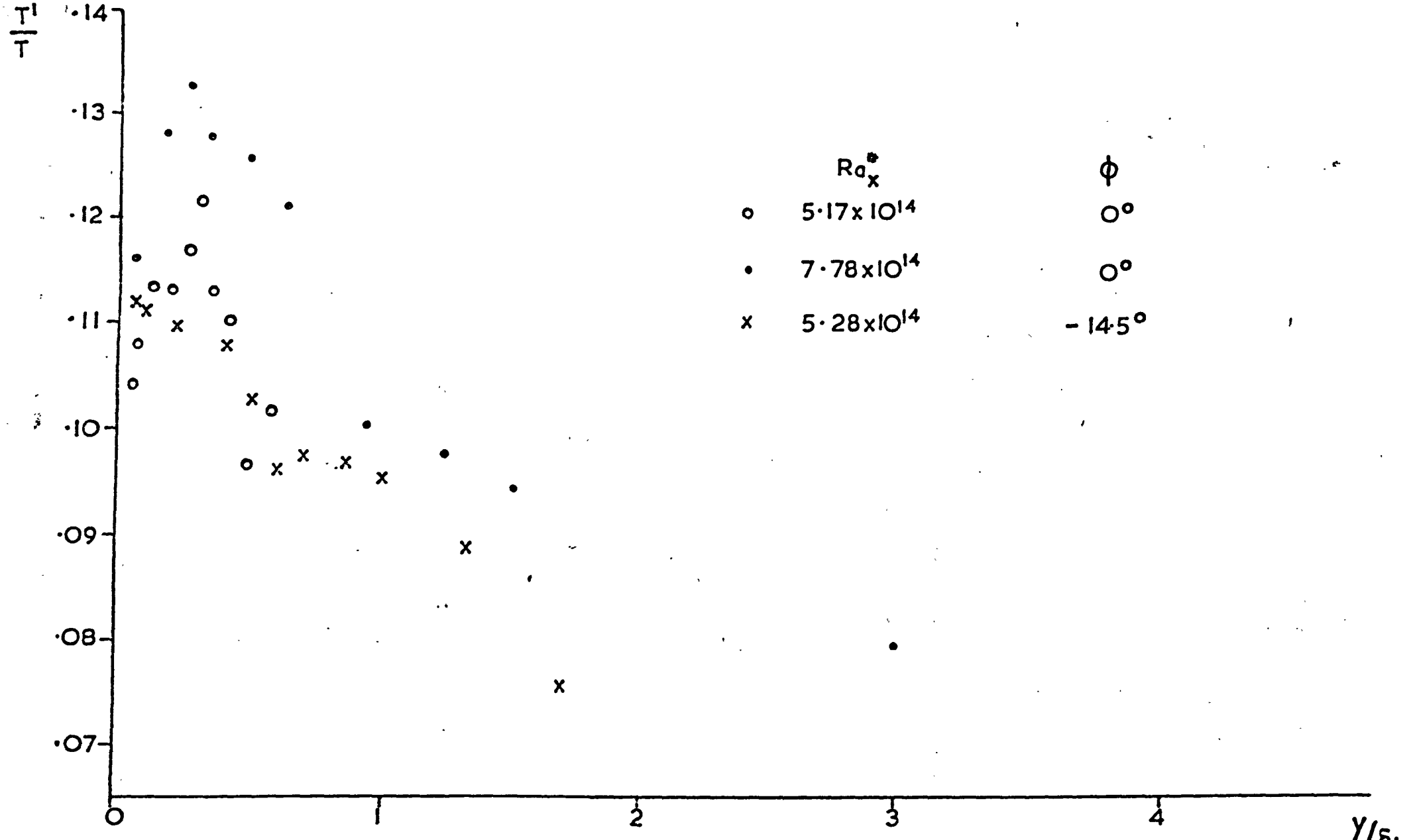

FIGURE 7·21
GRAPH OF T'/T AGAINST y/δ_h

7.3.3 Laminar Boundary Layer Velocity Profile

The programme of work on velocity profiles was continuously plagued with problems. During the probe calibration three hot-fibre probes were broken, one due to a mistake in setting up the calibration equipment and two due to bad electrical connections in the equipment. In the process of taking velocity profiles, the temperature-compensating element developed a fault which was irrepairable. Within the timescale of the project it was not possible to replace the temperature-compensating element due to a long delivery time. For this reason, only one velocity profile was obtained in the laminar flow region for an angle of -83.67°. The profile is shown in Figure 7.22 together with the theoretical velocity profile deduced from the work of Chang, Akins, Burris and Bankoff (1964). The temperature profile is also shown.

The experimental maximum velocity was about 23% below the theoretical maximum but in general the theoretical and experimental profile shapes were similar. One reason for the 23% discrepancy in the theoretical and experimental curves could be that the temperature-compensating element was not in exactly the same plane as the hot-fibre probe. For $y > 12$ mm the temperature of the fluid was approximately constant and the velocity results were in reasonable agreement with the theory. For values of $y < 12$ mm the fluid temperature began increasing and at this point the velocity profile began moving away from the theoretical curve. At this higher temperature the overheat ratio would decrease, causing a reduction in the anemometer output. Dring and Gebhart (1969) also found that for a vertical constant-heat-flux plate in silicone, the velocity maxima differed by 22%, but as the temperature of their fluid only changed by 0.3°C this

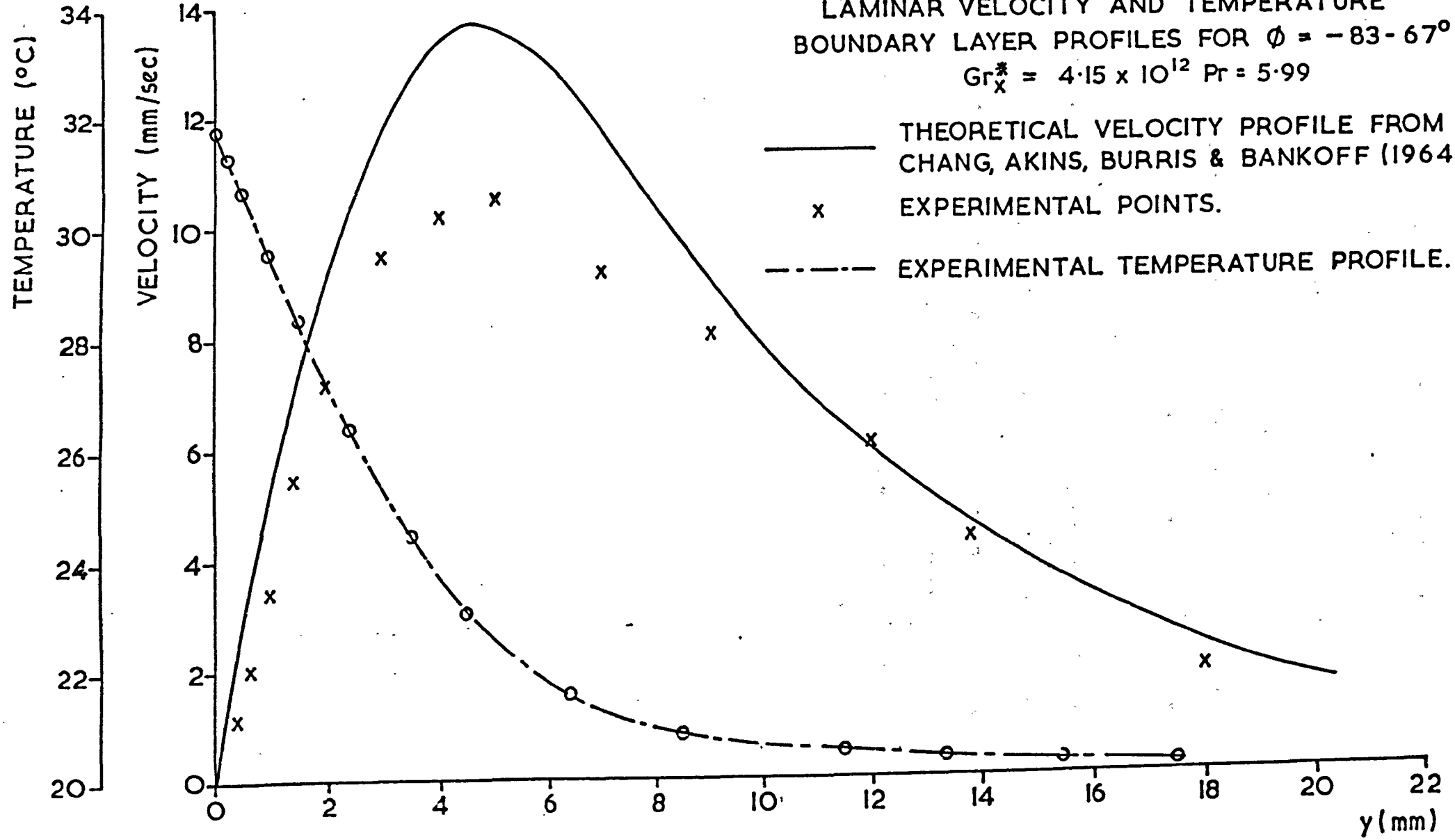

FIGURE 7·22

LAMINAR VELOCITY AND TEMPERATURE BOUNDARY LAYER PROFILES FOR $\phi = -83 \cdot 67°$

$Gr_x^* = 4 \cdot 15 \times 10^{12}$ $Pr = 5 \cdot 99$

THEORETICAL VELOCITY PROFILE FROM CHANG, AKINS, BURRIS & BANKOFF (1964)

x EXPERIMENTAL POINTS.

EXPERIMENTAL TEMPERATURE PROFILE.

would not account for the discrepancy in their results (see Figure 7.23).

7.4 FLOW VISUALIZATION RESULTS

The main objective of the flow visualization programme was to ensure that no re-circulating flows were present in the main bulk of the fluid. Details of this work were given earlier in Section 5.3.4.

Plate 7.1 shows a typical streak photograph for the upper half of the vertical plate for $Ra_L^* = 10^{15}$. The photograph was taken at f 5.6 with an exposure time of 5 seconds. Using a shorter focal length lens, Plate 7.2 shows a more detailed photograph of the turbulent region at a similar Rayleigh Number. In the outer edge of the boundary layer, large eddies, similar to those described by Vliet and Liu (1969) were observed.

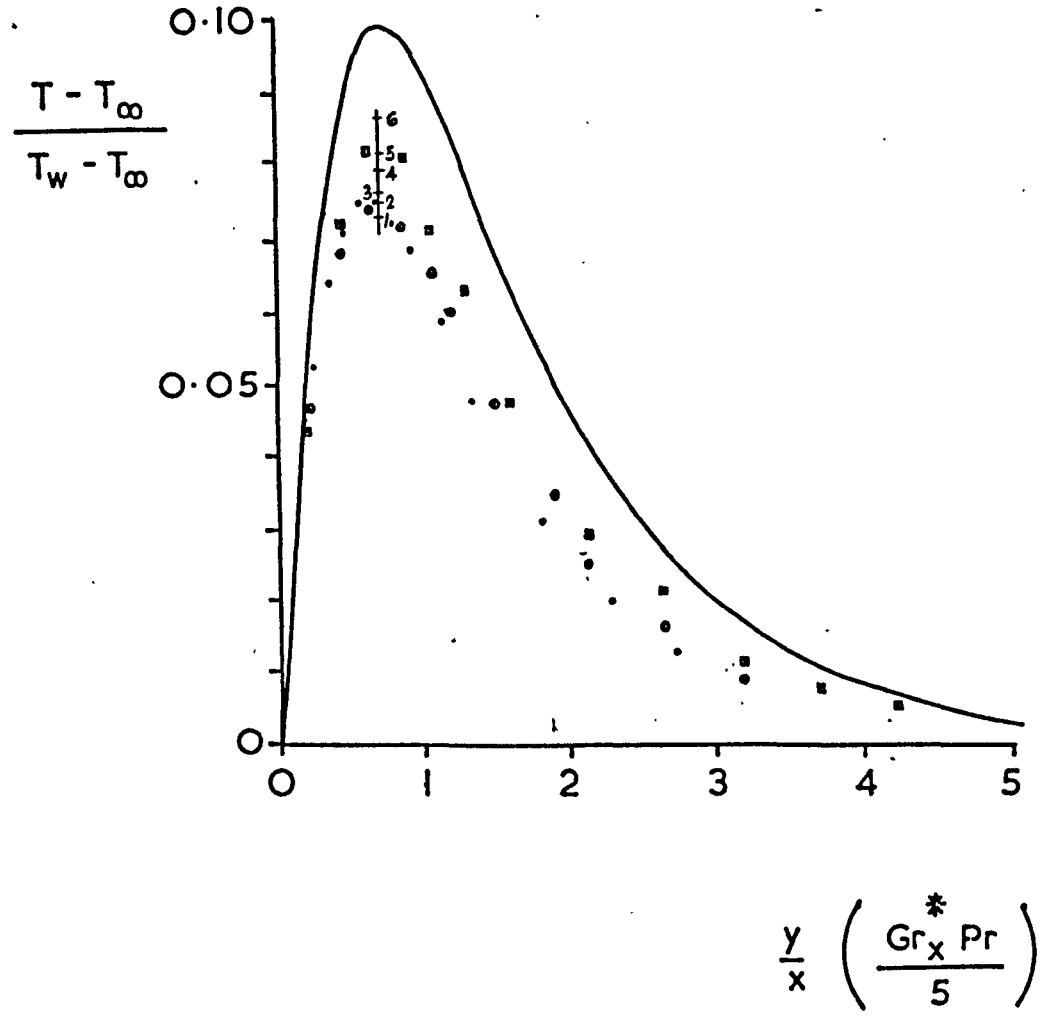

FIGURE 7·23

LAMINAR BOUNDARY LAYER VELOCITY PROFILE FOR A VERTICAL PLATE FROM DRING & GEBHART (1969)

PLATE 7·1

PLATE 7·2

FLOW PATTERNS OF THE TURBULENCE FOR $\phi = 0°$

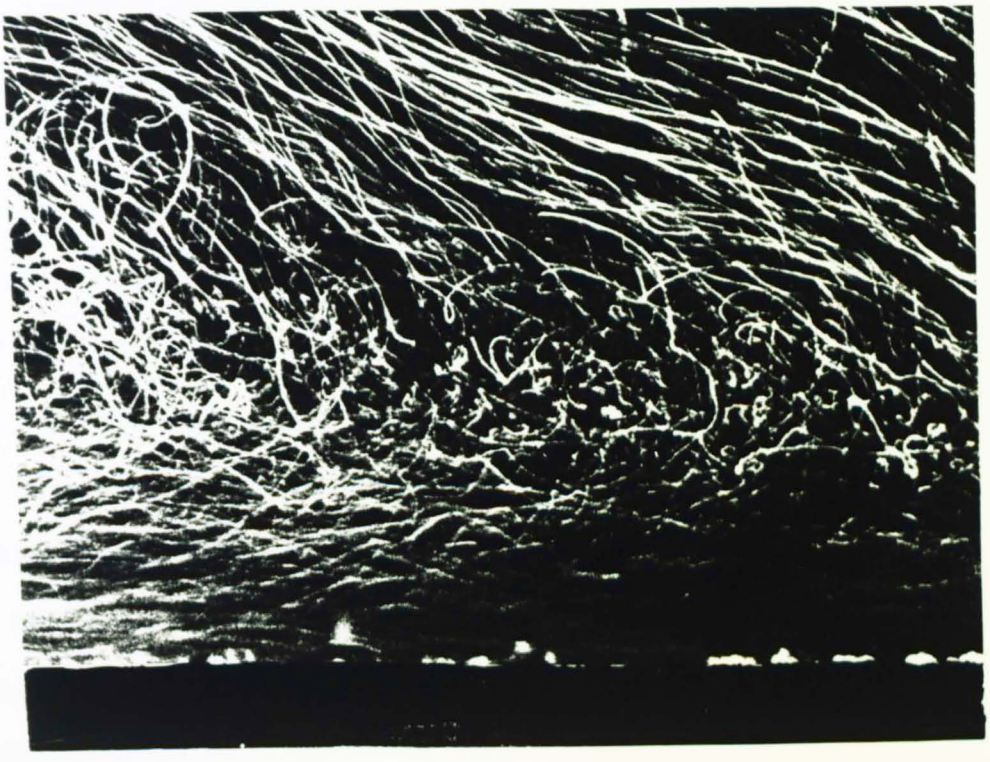

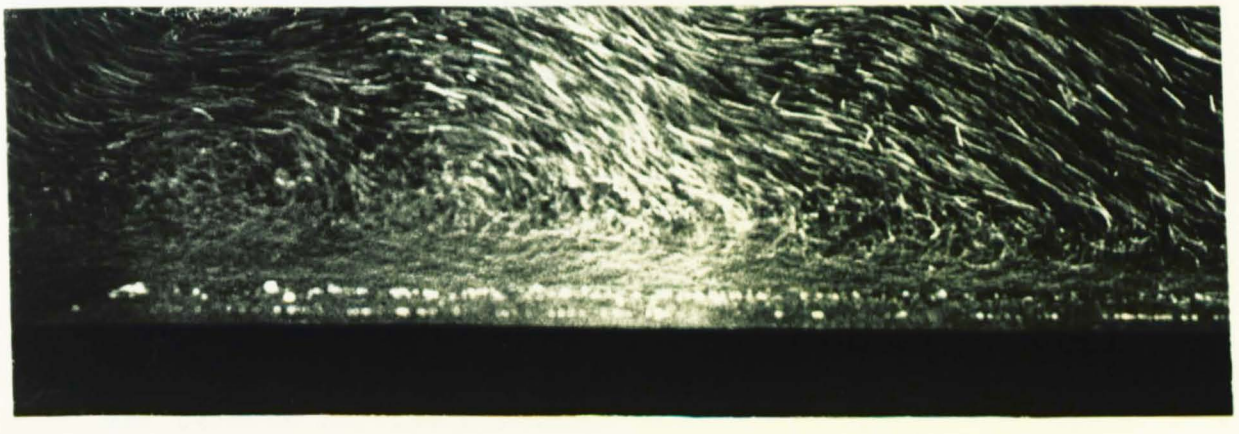

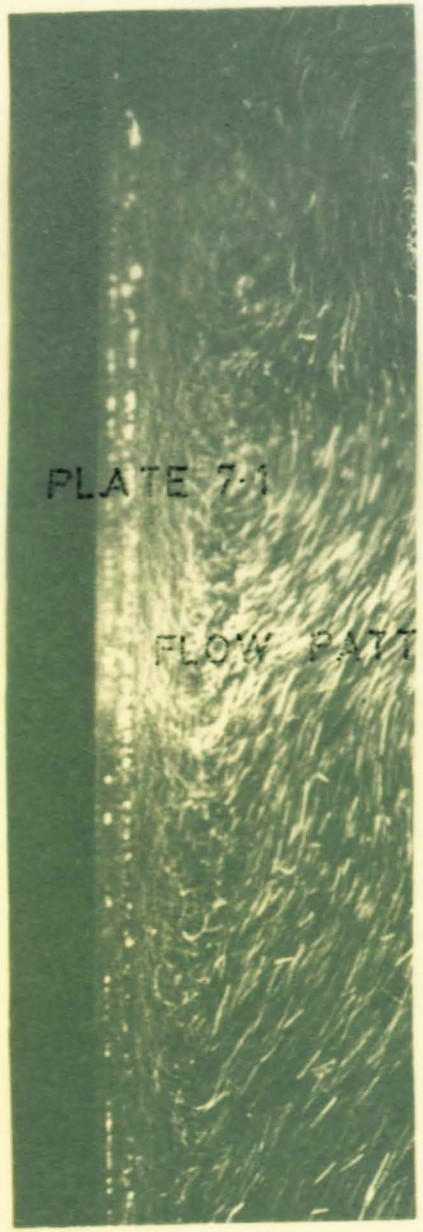

PLATE 7·1

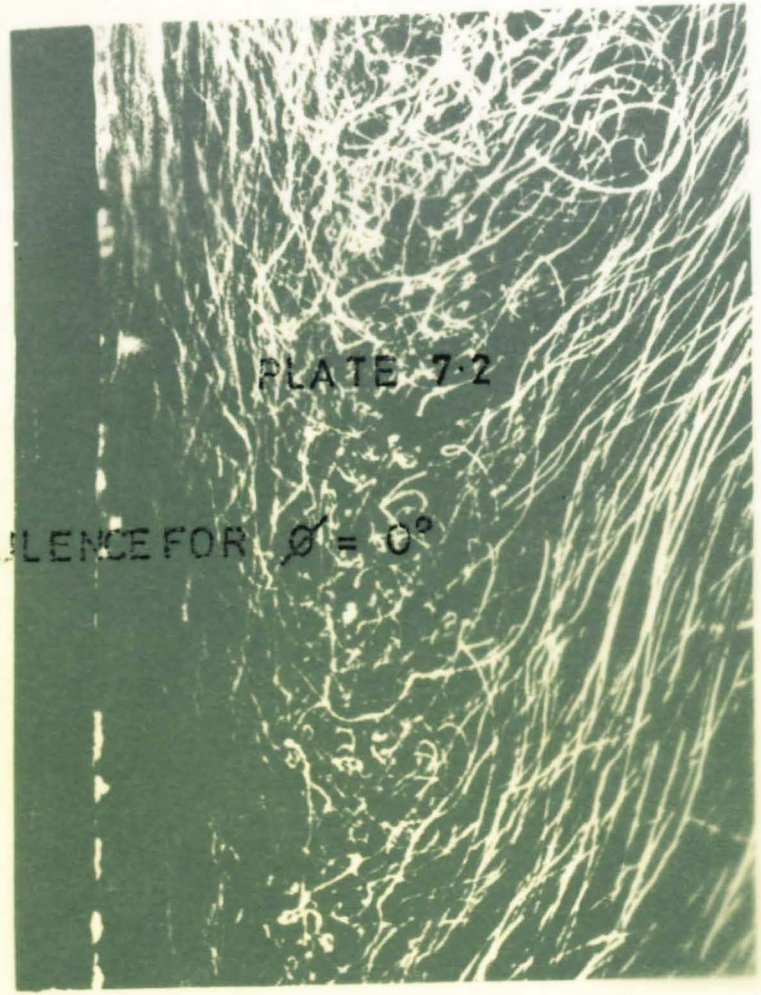

PLATE 7·2

FLOW PATTERNS OF THE TURBULENCE FOR $\phi = 0°$

CHAPTER 8

DISCUSSION

8.1 COMPARISON OF THE HEAT TRANSFER RESULTS

In Chapter 3, three methods were presented for solving approximately the integrated laminar boundary layer equations for an inclined plate. In the first method, the pressure gradient in the direction normal to the plate was assumed to be zero; the second method assumed that the pressure gradient in the direction normal to the plate could be represented by a horizontal plate solution and the final method involved calculating the sin ϕ term in equation (3.13) from the first approximate solution. These solutions are summarised in Table 8.1 together with the experimental results from the small and large rigs. Equation (6.4) was evaluated at Pr = 5.

The theoretical result for equation (6.1) is 2.4% higher than the vertical plate theory obtained by Sparrow and Gregg (1956) using a numerical analysis technique. For a Prandtl Number of 5 they found

$$Nu_x = 0.584\ (Gr_x^* Pr)^{\frac{1}{5}} \qquad \ldots (8.1)$$

Comparing the heat transfer results for the small and large rigs (equations (6.6) and (7.1)) with equation (8.1) shows that the correlations are 6.5% low and 1.37% high respectively but both equations agree within the errors of the experiment. The larger error in equation (6.6) is probably due to the varying heat flux along the plate surface which produced a larger standard deviation for the small rig results.

The results for the differing data are presented in Figure 8.1 as a function of $Nu_x/(Gr_x^* Pr)^{\frac{1}{5}}$ normalised to the vertical plate data against plate angle of inclination. The solid black

$$Nu_x = K_1 \, (Gr_x^* \, Pr \cos \phi)^{\frac{1}{5}} \qquad \ldots (6.1)$$

$$Nu_x = K_2 \, (Gr_x^* \, Pr \cos \phi)^{K_3} \qquad \ldots (6.2)$$

$$Nu_x = K_4 \, \left(\frac{1 + \cos \phi}{2}\right) (Gr_x^* \, Pr)^{\frac{1}{5}} \qquad \ldots (6.3)$$

$$Nu_x = K_5 \, Pr^{\frac{2}{5}} (0.8 + Pr - K_6 \, Pr \sin \phi)^{-\frac{1}{5}} \, (Gr_x^* \cos \phi)^{\frac{1}{5}} \qquad \ldots (6.4)$$

$$Nu_x = K_7 \, Pr^{\frac{2}{5}} \, (0.8 + Pr)^{-\frac{1}{5}} \, (1 + K_8 \, f \, (Pr, Gr_x^*, \phi) \tan \phi)^{\frac{1}{5}} \, (Gr_x^* \cos \phi)^{\frac{1}{5}} \ldots (6.5)$$

where $f \, (Pr, Gr_x^*, \phi) = Pr^{-\frac{2}{5}} \, (0.8 + Pr)^{\frac{1}{5}} \, (Gr_x^* \cos \phi)^{-\frac{1}{5}}$

	Equation (6.1)	Equation (6.2)		Equation (6.3)	Equation (6.4)		Equation (6.5)	
	K_1	K_2	K_3	K_4	K_5	K_6	K_7	K_8
Theoretical Results	0.600	0.600	0.200	0.600	0.616	1.3	0.616	0.487
Small Rig Results	0.546	0.455	0.208	0.602	0.609	0.938	-	-
Large Rig Results	0.592	0.535	0.204	0.668	0.630	0.15	0.619	0.798

TABLE 8.1

COMPARISON OF THE LAMINAR HEAT TRANSFER CORRELATIONS

$$\left.\frac{\frac{Nu_x}{(Gr_x^* Pr)^{1/5}}}{\frac{Nu_x}{(Gr_x^* Pr)^{1/5}}}\right|_{\phi = 0}$$

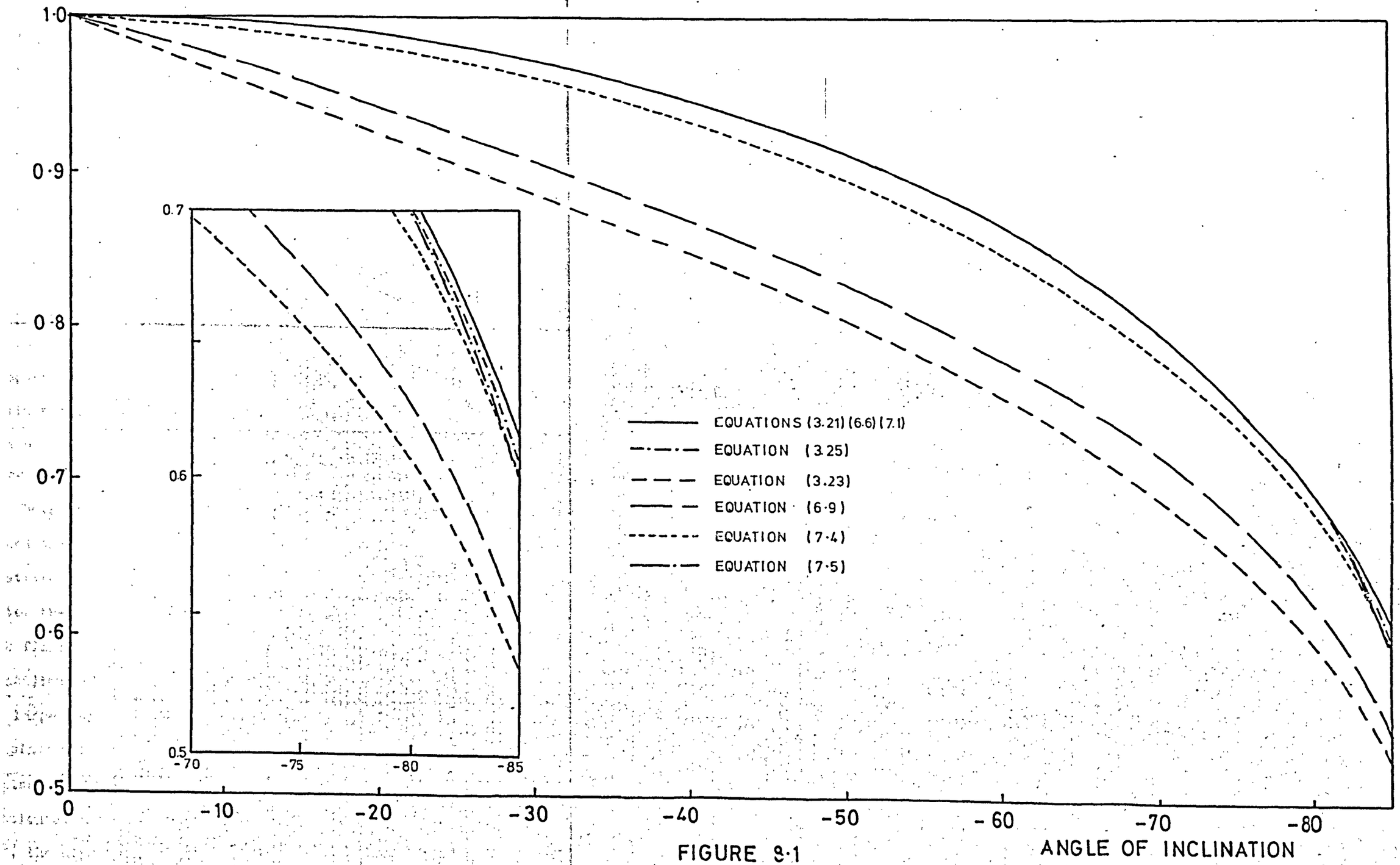

FIGURE 8·1

COMPARISON OF THE HEAT TRANSFER CORRELATIONS

line represents equations (3.24), (6.6) and (7.1). All equations were evaluated at Pr = 5. Figure (8.1) shows the difference in shape of the theoretical curves produced by the second approximate solution (equation (6.4)) and the other two (equations (6.1) and (6.5)). The second approximation gives the correct value when the heated plate is vertical but begins to diverge from the other two solutions when the plate is inclined until near the horizontal when the curve takes the same shape as the other two. The experimental results show that the theoretical constant, K_6, was too large, it being reduced to 0.938 and 0.15 for the small and large rigs respectively.

There is a discrepancy in the trends between the small and large rig heat transfer results. A larger correction was required for the small rig, so much so that the additional correction factor in equation (6.5) was not sufficient to allow for the effect of inclination. This is believed to be due to stratification in the main bulk of the fluid, causing a change in the heat transfer coefficient.

Both Cheesewright (1967) and Jaluria and Gebhart (1974) showed that the heat transfer coefficient increased as the stratification increased. They suggested that at any point up the plate, the temperature difference between the heated plate and the bulk fluid ($T_w - T_\infty$) was less than one would expect. Now the stratification in the small rig ($\sim 5^\circ C/m$) was much larger than in the large rig ($\sim 1^\circ C/m$), hence the heat transfer coefficient on the plate was greater than would be expected. As the angle of inclination approached the horizontal, the stratification as a function of distance up the plate was effectively smaller (at $\phi = -85^\circ$, the stratification up the plate was only 0.09 of that when

$\phi = 0^{o}$) giving a larger temperature drop between the plate and fluid and a smaller heat transfer coefficient. This would then explain why such a large correction factor was required for the small rig compared with the large rig.

The numerical solution for an upward-facing inclined flat plate (Section 3.2.4) showed that the constant K_3 in equation (6.2) varied from 0.2 for the vertical plate to 0.167 for the horizontal plate facing up, the most significant changes occurring at high angles of inclination. For the downward-facing horizontal plate, it has also been found experimentally that $K_3 = 0.167$, therefore it is very probable that K_3 changes in a similar manner for the downward-facing inclined plate as for the upward-facing plate. The results in Tables 6.1 and 7.1 show no consistent changes in K_3.

The results for the horizontal plate were rather confusing and the scatter on the heat transfer correlation was greater than that for the vertical plate. Figure (6.7) showed the variation of $Nu_x/(Gr_x^* Pr)^{\frac{1}{6}}$ against x/l. There was no observable consistency in the scatter and a similar plot by Birkebak and Abdulkadir (1970) showed a similar amount of scatter. This could indicate that this is not a suitable method of correlating the data and that boundary layer theory is not applicable, as suggested by Rotem (1970).

The discrepancy between the transition data for the isothermal data and the constant-heat-flux data may be due to the effect of stratification. Jaluria and Gebhart (1974) showed both theoretically and experimentally that stratification initially stabilises the flow but further downstream the amplification rates become larger than for unstratified flows. For stratification of

$1^{o}C/m$, the transition Rayleigh Number is increased by about two orders of magnitude which would bring the two sets of data into agreement.

Figure 8.2 gives a comparison of the local heat transfer correlations for the small and large rigs in the laminar, transition and turbulent regimes, and shows the increase in heat transfer coefficient in going from laminar to turbulent flow.

The laminar boundary layer temperature profiles showed good agreement between theory and experiment for the vertical plate but began to deviate from the theory at angles near the horizontal. One interesting fact which was not reported earlier was the laminar boundary layer temperature profile in a stratified media. This profile, shown in Figure 8.3, was obtained on the small heated plate at $Ra_x^* = 9.4 \times 10^{10}$ and $\phi = 0^{o}$. The problem was not pursued further due to lack of time but it should be noted that Cheesewright (1967) and Jaluria and Gebhart (1974) obtained similar profiles theoretically when the temperature in a part of the boundary layer was less than that outside the boundary layer.

The flow visualization programme showed how careful one should be when studying natural convection in finite vessels. Most theoretical analyses have assumed that the heated plate was immersed in a fluid of infinite extent and of uniform or known temperature. In reality, experiments are confined to a small finite volume where, if care is not taken, the experimental results may be misleading. This was the case for the small heated plate where initial results had to be discarded when the flow visualization results showed the boundary layer flow was being broken up by recirculating flows. An excellent description of the effects of stratification has been given by Schwind and

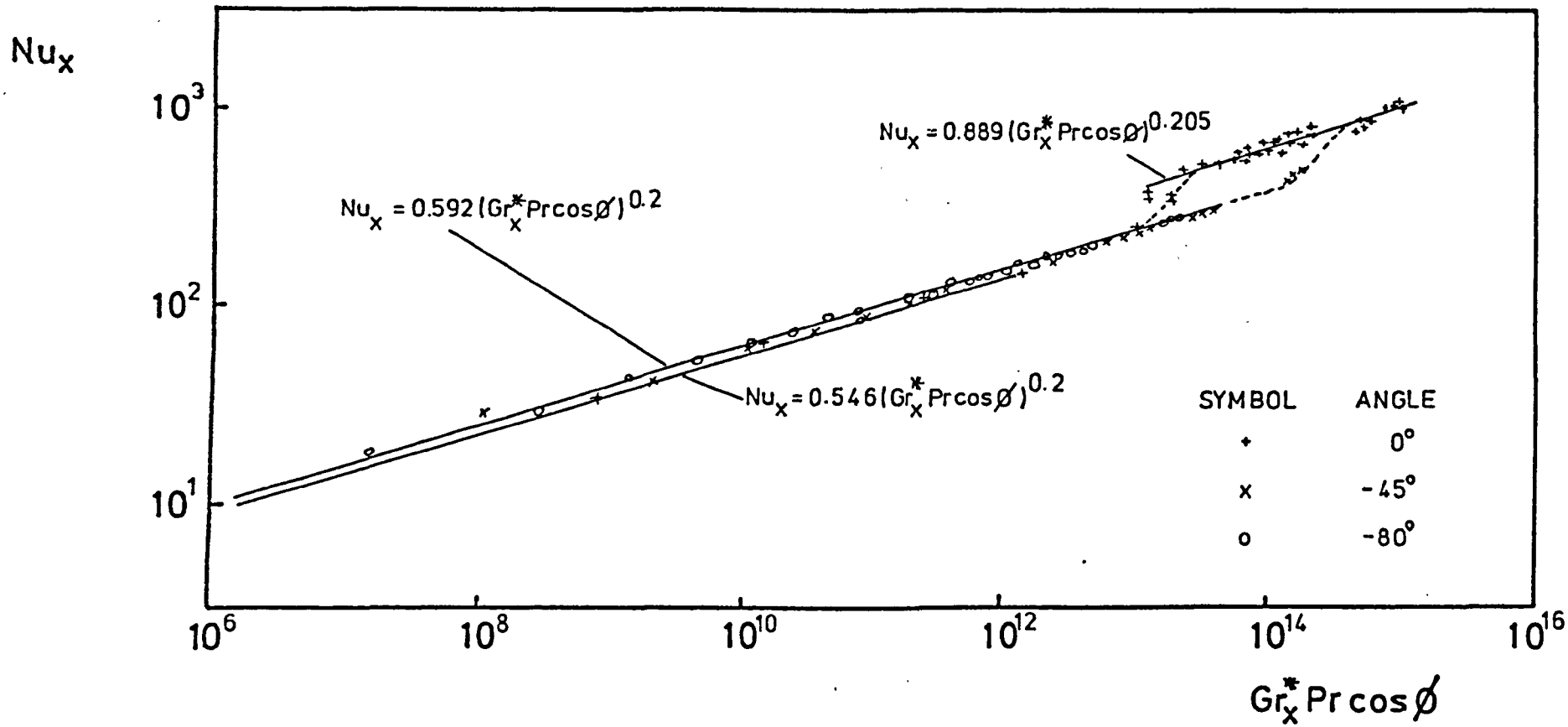

FIGURE 8·2

LAMINAR AND TURBULENT HEAT TRANSFER CORRELATIONS

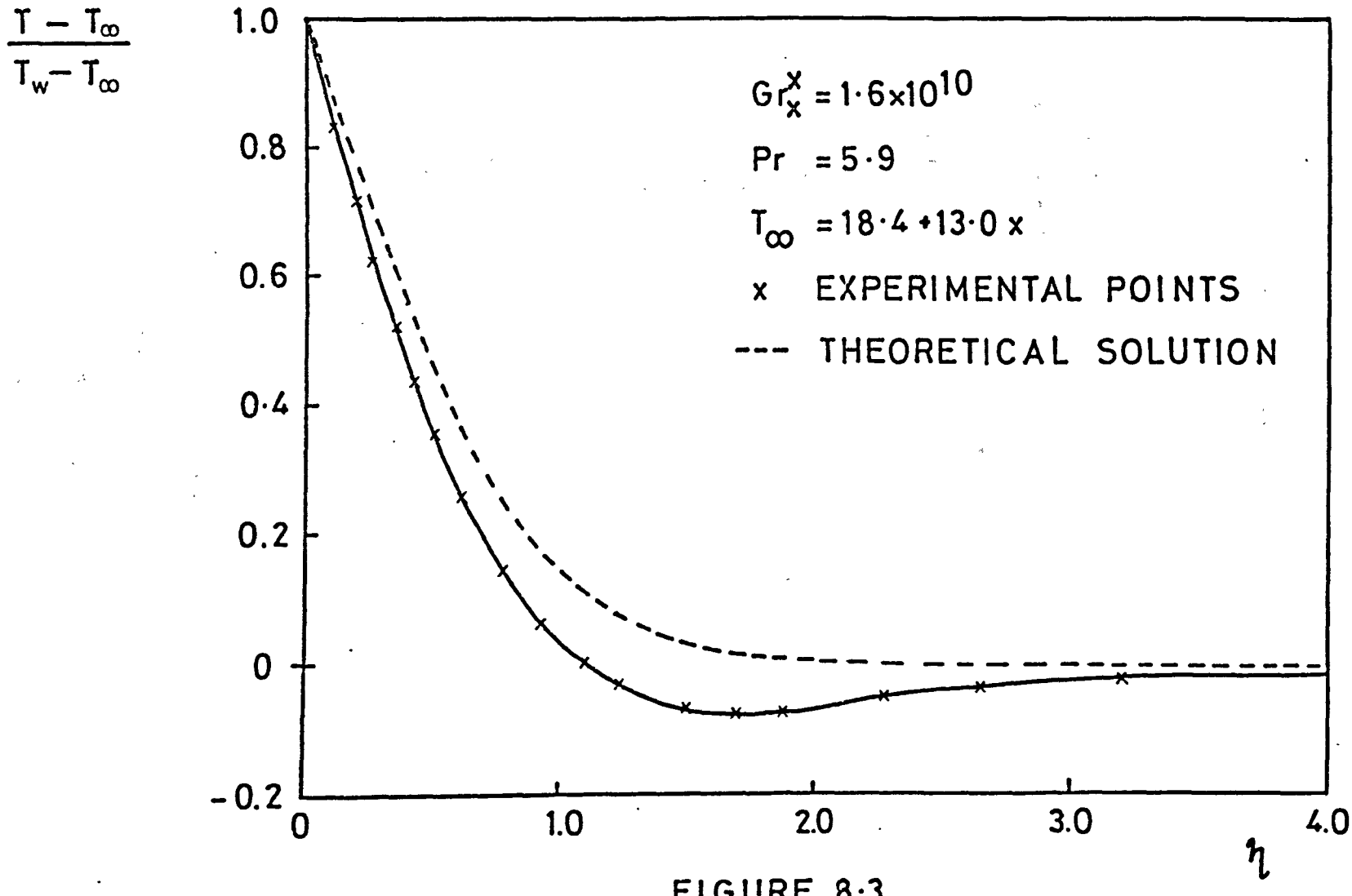

FIGURE 8·3

LAMINAR BOUNDARY LAYER TEMPERATURE PROFILE IN A STRATIFIED MEDIUM

Vliet (1964). In their study of natural convection and stratification phenomena of fluids in a vessel (6 in. x 6 in. x 10 in.) they found four stages in the development of the stratification:

(a) Initial transients

(b) First appearance of 'Quasi-steady state' stratification

(c) Intermediate stratification

(d) Extended time stratification

For the small rig, their results suggest that the heat transfer data were obtained in an 'intermediate stratification' stage where the plume of hot water leaving the plate wall is beginning to penetrate the unstratified region.

8.2 APPLICATION OF THE RESULTS TO THE DESIGN OF A CORE CATCHER

Having dealt with the experimental and theoretical results in detail, we now return to the problem of the core catcher. The work of Hunt and Moore (1970), referred to in Chapter 1, employed a number of assumptions when calculating the temperature difference between the core catcher and the liquid sodium. These were:

(a) The core catcher could be represented by a 1.3 m long plate inclined at 15° to the horizontal with a surface heat flux of 10^6 W/m^2.

(b) that the heat transfer correlations in air and water were applicable to liquid metals with low Prandtl Numbers.

(c) that the criterion for transition in air and water on a vertical plate may be used for liquid metals and was not affected by inclination.

(d) that the flow was turbulent.

(e) that the effect of inclination could be accounted for by using the gravitational component parallel to the plate surface in the Grashof Number.

The results presented here may be used to clarify some of the problems encountered by Hunt and Moore (1970).

The extrapolation of heat transfer data from water or air to low Prandtl Number fluids is very questionable. Because of the differing thermal and velocity boundary layers and the longitudinal heat conduction in the boundary layer in liquid metals, the theoretical solutions underestimate the heat transfer coefficients. Very little experimental work is available on natural convection in liquid metals. A recent paper by White, Welty and Hart (1973) concerned with vertical plate natural convection in mercury (Pr = 0.0237) gave the heat transfer correlation

$$Nu_x = 0.240\ Gr_x^{*0.190}$$

At a modified Grashof Number of 10^8 this equation is 30% higher than the integral solution (equation (3.17)), the difference decreasing the larger the Grashof Number. No data are available for liquid sodium which has a Prandtl Number one order of magnitude lower than mercury.

The assumption that the flow on the core catcher will be turbulent is believed to be incorrect. Our results have shown that as the plate is inclined, the point of transition moves further up the plate and at an inclination of -75° the transition Rayleigh Number, Ra_x^*, was found to be 1.25×10^{15}. The theoretical results of Sparrow, Tsou and Kurtz (1965) showed that over a range of Prandtl Number from 7 to 0.7, the critical Grashof Number for the onset of instability decreased as the Prandtl Number decreased. A speculative extrapolation of this data to liquid metals (Pr ~ 0.01) gives a transition Grashof Number four orders of magnitude lower than in water. This would give a

transition Grashof Number of 2.5×10^{10} for a liquid metal. The theoretical work of Hieber and Gebhart (1971) using linear stability theory showed that the neutral stability curves are only weakly dependent on the Prandtl Number over the range 0.1 to 0.01. There has been no broad study of transition in liquid metals but Collwell (1973) found transition occurred at $Gr_x^* = 5 \times 10^9$ on a vertical plate in mercury. Our transition results may be expressed as

$$Gr_x^* = Gr_{x_{VERTICAL}}^* \; e^{-0.0705\phi}$$

Using Collwell's value for Gr_x^* gives a transition Grashof Number of 9.89×10^{11} at an angle of -75°. The Grashof Number for the plate described by Hunt and Moore (1970) would be 9.7×10^{14}. Even though the Grashof Number of the core catcher is larger than the value predicted for transition, it is very unlikely that the flow will be turbulent because the transition region continues over a considerable range of x at angles of inclination near the horizontal.

The experimental results from this project have shown that for an inclined plate at angles of inclination near the horizontal, the heat transfer coefficient is lower than that predicted using the gravitational component parallel to the plate surface by a factor given by

$$(1 + K_8 \, Pr^{-\frac{2}{5}} \, (0.8 + Pr)^{\frac{1}{5}} \, (Gr_x^* \cos \phi)^{-\frac{1}{5}} \tan \phi)^{\frac{1}{5}}$$

where K_8 lies in the range 0.49 to 0.8. Hunt and Moore (1970) had calculated that the temperature difference between the core catcher and the sodium would be $87^\circ C$ for a plate inclined at 15° to the horizontal. Assuming that the flow is laminar up the plate then the temperature difference increases to $256^\circ C$ using equation (3.21) or $257^\circ C$ using equation (3.25). At these high

Grashof Numbers, the correction factor is very small but at angles of inclination nearer the horizontal and for lower Grashof Numbers the correction factor may be as large as 10%. It should be appreciated that these temperatures have been extrapolated from data for water and it is most likely that the temperature differences will be lower in liquid sodium.

To reduce the temperature difference between the core catcher and the sodium, Peckover (1973) has suggested the use of a multiple array of core catchers. These could be in a staggered layer, as shown in Figure 8.4, or in staggered and alternate layers as shown in Figure 8.5. With either of these methods, careful attention would have to be given to ensuring that there was not too much interference between the trays from either a plume of hot sodium rising from a lower tray to a higher tray or from the interference of the boundary layers (which are of the order 40 mm thick) on two adjacent trays.

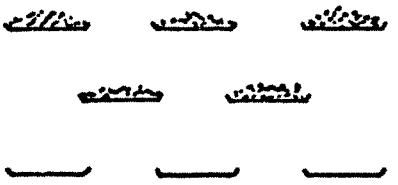

FIGURE 8·4

THREE STAGGERED LAYERS OF CATCHERS

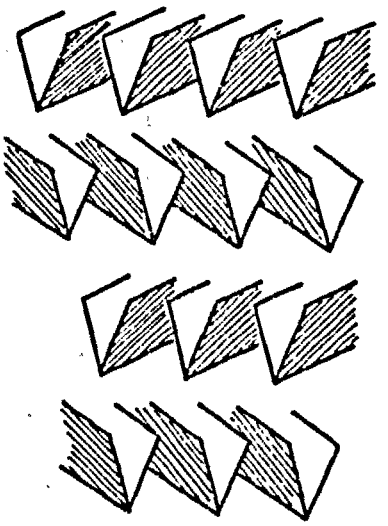

FIGURE 8·5

FOUR LAYERS OF V-SHAPED TROUGH CATCHERS STAGGERED AND ALTERNATED

CHAPTER 9

SUMMARY OF CONCLUSIONS

a. The theoretical investigation comprised an analysis of the integrated boundary layer equations for steady two-dimensional laminar and turbulent flow. Approximate analytical solutions have been presented for a heated plate inclined at any angle of inclination. The results showed that up to $|70^{\circ}|$ from the vertical, the vertical plate theory is perfectly adequate in predicting the heat transfer coefficients provided the gravitational component parallel to the plate surface is used. Above $|70^{\circ}|$, a small correction factor is required due to the pressure gradient normal to the plate surface. A numerical solution of the integrated boundary layer equations was also presented for laminar natural convection from an upward-facing inclined plate. This showed above 70° from the vertical, the index of the Grashof Number changed slowly from 0.2 to 0.167 as the plate approached the horizontal. The solution for the turbulent region showed that the vertical plate theory was adequate provided the gravity component parallel to the plate surface is used.

b. The experimental results for the two rigs covered a range of modified Grashof Number from 10^{6} to 10^{15} and plate angle of inclination from the vertical to the horizontal facing down. The local laminar heat transfer data agreed well with the theory and the results of other workers. To a first approximation, the data may be correlated using the vertical plate theory modified to include the gravitational component parallel to the plate surface. Above angles of 70° from the vertical facing down, the data began to deviate from the first approximation. To take

into account this deviation, the data were correlated to the equations derived in the theoretical analysis and the following two correlations are proposed:

$$Nu_x = K_5 \, Pr^{\frac{2}{5}} \, (0.8+Pr-K_6 \, Pr \sin \phi)^{-\frac{1}{5}} \, (Gr_x^* \cos \phi)^{\frac{1}{5}}$$

$$Nu_x = K_7 \, Pr^{\frac{2}{5}} \, (0.8+Pr)^{-\frac{1}{5}} \, (1+K_8 f(Pr,Gr_x^*,\phi) \tan \phi)^{\frac{1}{5}} \, (Gr_x^* \cos \phi)^{\frac{1}{5}}$$

where

$$f\,(Pr,Gr_x^*,\phi) = Pr^{-\frac{2}{5}} \, (0.8 + Pr)^{\frac{1}{5}} \, (Gr_x^* \cos \phi)^{-\frac{1}{5}}$$

For the large rig, the constants have been determined as:

$K_5 = 0.630$ $\qquad$ $K_7 = 0.619$
$K_6 = 0.150$ $\qquad$ $K_8 = 0.798$

In stratified media, the constants K_6 and K_8 begin to increase.

c. Transition was found to begin at $Ra_x^* = 6.31 \times 10^{12}$ and was found to vary with angle as

$$Ra_x^* = 6.31 \times 10^{12} \, e^{-0.0705\phi}$$

up to an angle of -75° from the vertical. As the angle of inclination decreased the transition length was found to increase in length but no quantitative results can be given as the plate did not go to high enough Rayleigh Numbers.

d. In the turbulent regime, the local heat transfer coefficient may be expressed as

$$Nu_x = 0.889 \, (Gr_x^* \, Pr \cos \phi)^{0.205}$$

over the range $0 < \phi < -31^\circ$. Agreement between the theoretical and experimental results was poor.

e. Boundary layer temperature profiles were obtained over a wide range of Rayleigh Number and plate angle of inclination. For angles greater than -80°, the profiles agreed well with the vertical plate laminar boundary layer temperature profiles where

the gravity component was taken parallel to the plate surface. At angles less than -80°, the data began to deviate from the theoretical profile. Boundary layer temperature profiles were also presented for the turbulent regimes and good agreement was found with other workers.

f. A hot-fibre anemometer was successfully calibrated to measure velocities less than 100 mm/s and was used to obtain a velocity profile at -83.67° from the vertical. The data gave lower velocities than predicted by theory.

g. An extensive flow visualization programme was undertaken to ensure that no unwanted flows were present in the main bulk of the fluid away from the plate. Two types of tracer were used, aluminium particles and neutral density polystyrene particles. The aluminium particles were found to be more amenable for natural convection work where changes in the density of the fluid caused the drift velocity of the polystyrene particles to alter. A baffle system was developed for the large rig to isolate the unwanted flows. Near the boundary layer, the flow was found to move in horizontally towards the plate rather than perpendicularly as assumed in the theoretical work of Kierkus (1968).

CHAPTER 10

RECOMMENDATIONS FOR FUTURE WORK

The application of the experimental data in water to liquid sodium has been shown to be uncertain and experiments are now being undertaken at the U.K.A.E.A. to obtain heat transfer coefficients on an inclined flat plate in liquid sodium. These experiments will cover a range of angles from the vertical to the horizontal facing down in a fluid with Prandtl Number less than mercury. From the present work, it is recommended that:

a. attention is focused on angles of inclination near the horizontal where changes in gradient of the $Nu_x - Ra_x^*$ graph are expected to occur.

b. the interference of the boundary layers on two adjacent core catchers should be studied by placing an isothermal wall near the trailing edge of the plate, and

c. the interference between the core catchers from a plume of hot sodium rising from a lower tray to a higher tray should be studied by placing a sodium jet beneath the leading edge of the plate and observing the effects on the plate heat transfer coefficients.

Regarding the general field of inclined plate natural convection, it is felt that there is still considerable scope for further work and several suggestions are given below:

a. On the theoretical side, it is felt that a numerical solution of the governing differential equations would be of great value. In the laminar flow regime, this should be relatively easy and the effects of stratification, free surfaces and finite volumes of fluid on the boundary layer

growth could also be incorporated. In the turbulent regime, Mason and Seban (1974) have obtained numerical solutions for turbulent natural convection on a vertical surface using a programme of the Patankar-Spalding type (1970). These results showed reasonable agreement with the available experimental results and it would be most interesting to modify this programme to study the effects of inclination on the heat transfer coefficient, particularly the difference between an upward- and downward-facing plate.

b. There are numerous experimental projects which need to be undertaken both from a practical point of view and to aid the numerical solutions. At angles near the horizontal, much greater information is required on the change in heat transfer coefficient. This would be best supplemented by detailed velocity measurements where it is recommended that a laser Doppler anemometer, such as the one described briefly in Chapter 4, be used. A more detailed investigation of stratification would be very useful as most flows of engineering importance are never in a motionless fluid of uniform temperature. This could also include the effects of overall flow patterns in the experimental vessel.

REFERENCES

AIHARA T., YAMADA Y. and ENDŌ S. (1972). "Free convection along the downward-facing surface of a heated horizontal plate", Int. J. Heat Mass Transfer, 15, 2535-2549.

AMOS P. G. (1973). Private communication.

BAKER D. J. (1966). "A technique for the precise measurement of small fluid velocities", J. Fluid Mech., 26, 573-575.

BAYLEY F. J. (1955). "An analysis of turbulent free-convection heat-transfer", Proc. I. Mech. E., London, 169, 361-370.

BIRKEBAK R. C. and ABDULKADIR A. (1970). "Heat transfer by natural convection from the lower side of finite horizontal, heated surface", Paper NC2.2, Proc. 4th Int. Heat Transfer Conf., Paris.

BRADSHAW P. (1971). An Introduction to Turbulence and its Measurement, Pergamon Press, Oxford.

BRODOWICZ K. and KIERKUS W. T. (1965). "Determination of streamlines and velocity components in free convection", Archiwum Budowy Maszyn, 12, 473-486.

C.E.G.B.(1970). Steam Tables in S.I. Units.

CHANG K. S., AKINS R. G., BURRIS L. and BANKOFF S. G. (1964). "Free convection of a low Prandtl Number fluid in contact with a uniformly heated vertical plate", Argonne National Laboratory, Report Number ANL 6835.

CHEESEWRIGHT R. (1967). "Natural convection from a plane, vertical surface in non-isothermal surroundings", Int. J. Heat Mass Transfer, 10, 1847-1859.

CHEESEWRIGHT R. (1968). "Turbulent natural convection from a vertical plane surface", J. Heat Transfer, 90, 1-8.

COLLIS D. C. and WILLIAMS M. J. (1959). "Two-dimensional convection from heated wires at low Reynolds Numbers", J. Fluid Mech., 6, 357-384.

COLWELL R. (1973). "Experimental investigation of natural convection in mercury in an open, uniformly heated, vertical channel", Ph.D. Thesis, Oregon State University, Corvallis, Ore., U.S.A. Cited in Wiles L. E. and Welty J. R. "An experimental investigation of natural convection with vertical cylinders in mercury", J. Heat Transfer, 96, 455-458, 1974.

COOPER D. (1974). Unpublished work.

COUTANCEAU J. (1969). "Convection naturelle turbulente sur une plaque verticale isotherme, transition, échange de chaleur et frottement pariétal, lois de répartition de vitesse et de température", Int. J. Heat Mass Transfer, 12, 753-769.

COX M. G. and HAYES J. G. (1973). "Curve fitting: A guide and suite of algorithms for the non-specialist user", National Physical Laboratory, Report Number NAC 26.

DRING R. P. and GEBHART B. (1969). "Hot-wire anemometer calibration for measurements at very low velocity", J. Heat Transfer, 91, 241-244.

ECKERT E. R. G. and CARLSON W. O. (1961). "Natural convection in an air layer enclosed between two vertical plates with different temperatures", Int. J. Heat Mass Transfer, 2, 106-120.

ECKERT E. R. G. and JACKSON T. W. (1955). "Analysis of turbulent free-convection boundary layer on a flat plate", NASA Tech. Note 1015.

EDE A. J. (1956). "Natural convection on free vertical surfaces", Mech. Eng. Research Laboratory Report, Heat 141, Glasgow.

EDE A. J. (1967). "Advances in free convection" in Advances in Heat Transfer, 4, 1-64, edited by H. J. P. Hartnett and T. F. Irvine, Academic Press, Inc., New York.

EICHHORN R. (1961). "Flow visualization and velocity measurement in natural convection with the tellurium dye method", J. Heat Transfer, 83, 379-381.

ENIKEEV M. P. (1958). "Free convection heat transfer from a plane surface inclined at different angles", Proc. Kazan M. Gorki Agricultural Institute, 37-50.

FARMER F. R. (1970). Foreword in U.K.A.E.A. (1970).

FUJII T. (1959). "Experimental studies of free convection heat transfer", Bull. J.S.M.E. 2, 555.

FUJII T., HONDA H. and MORIOKA I. (1973). "A theoretical study of natural convection heat transfer from downward-facing horizontal surfaces with uniform heat flux", Int. J. Heat Mass Transfer, 16, 611-627.

FUJII T. and IMURA H. (1972). "Natural-convection heat transfer from a plate with arbitrary inclination", Int. J. Heat Mass Transfer, 15, 755-767.

FUJII T., TAKEUCHI M., FUJII M., SUZAKI K. and UEHARA H. (1970). "Experiments on natural-convection heat transfer from the outer surface of a vertical cylinder to liquids", Int. J. Heat Mass Transfer, 13, 753-787.

GASTER M. (1964). "A new technique for the measurement of low fluid velocities", J. Fluid Mech., 20, 183-192.

GEBHART B. (1962). "Effects of viscous dissipation in natural convection", J. Fluid Mech., 14, 225-232.

GEBHART B. (1969). "Natural convection flow, instability, and transition", J. Heat Transfer, 91, 293-309.

GEBHART B. (1973a). "Natural convection flows and stability" in Advances in Heat Transfer, 9, 273-348, edited by T. F. Irvine and J. P. Hartnett, Academic Press, Inc., New York.

GEBHART B. (1973b). "Instability, transition and turbulence in buoyancy-induced flows", in Annual Review of Fluid Mechanics, 5, 213-246, edited by M. van Dyke, W. G. Vincenti and J. V. Wehausen, Annual Review Inc., California, U.S.A.

GODAUX F. and GEBHART B. (1974). "An experimental study of the transition of a natural convection flow adjacent to a vertical surface", Int. J. Heat Mass Transfer, 17, 93-107.

GREGORY C. V. and LORD D. J. (1974). "The study of local blockages in fast reactor sub-assemblies", J. Brit. Nucl. Energy Soc., 13, 251-260.

HAALAND S. E. and SPARROW E. M. (1973a). "Vortex instability of natural convection flow on inclined surfaces", Int. J. Heat Mass Transfer, 16, 2355-2367.

HAALAND S. E. and SPARROW E. M. (1973b). "Wave instability of natural convection on inclined surfaces accounting for non-parallelism of the basic flow", J. Heat Transfer, 95, 405-407.

HASSAN K. E. and MOHAMED S. A. (1970). "Natural convection from isothermal flat surfaces", Int. J. Heat Mass Transfer, 13, 1873-1886.

HEAD M. R. (1972). "Weighing pressures - a simple micromanometer", Aeronautical Journal, 76, 615-616.

HIEBER C. A. and GEBHART B. (1971). "Stability of vertical natural convection boundary layers: some numerical solutions", J. Fluid Mech., 48, 625-646.

HOLLASCH K. and GEBHART B. (1972). "Calibration of constant-temperature hot-wire anemometers at low velocities in water with variable fluid temperature", J. Heat Transfer, 94, 17-22.

HOLMAN J. P. (1971). Experimental Methods for Engineers, McGraw Hill, U.S.A., 2nd edition.

HUNT D. L. and MOORE J. G. (1970). "Problems associated with molten fuel", in U.K.A.E.A. (1970).

INGER G. R. (1955). "Interferometric studies of natural convection heat transfer from inclined heated flat plates in air", M.Sc. Thesis, Department of Aeronautical Engineering, Wayne University.

IYER P. A. and KELLY R. E. (1974). "The stability of the laminar free convection flow induced by a heated inclined plate", Int. J. Heat Mass Transfer, 17, 517-525.

JALURIA Y. and GEBHART B. (1974). "Stability and transition of buoyancy-induced flows in a stratified medium", J. Fluid Mech., 66, 593-612.

KAHAWITA R. A. and MERONEY R. N. (1974). "The vortex mode of instability in natural convection flow along inclined plates", Int. J. Heat Mass Transfer, 17, 541-548.

von KÄRMÄN T. (1921). "Über laminare und turbulente reibung", ZAMM, 1, 233-252.

KATO H., NISHIWAKI N. and HIRATA M. (1968). "On the turbulent heat transfer by free convection from a vertical plate", Int. J. Heat Mass Transfer, 11, 1117-1125.

KIERKUS W. T. (1968). "An analysis of laminar free convection flow and heat transfer about an inclined isothermal plate", Int. J. Heat Mass Transfer, 11, 241-253.

KUTATELADZE S. S., KIRDYASHKIN A. G. and IVAKIN V. P. (1972). "Turbulent natural convection on a vertical plate and in a vertical layer", Int. J. Heat Mass Transfer, 15, 193-202.

LEE J. B. and LOCK G. S. H. (1972). "Instability in boundary-layer free convection", Paper 28, Proc. of 4th Western Canadian Heat Transfer Conf., University of Manitoba.

LEVY S. (1955). "Integral methods in natural-convection flow", J. Applied Mech., 22, 515-522.

LLOYD J. R. and SPARROW E. M. (1970). "On the instability of natural convection flow on inclined plates", J. Fluid Mech., 42, 465-470.

LLOYD J. R., SPARROW E. M. and ECKERT E. R. G. (1972a). "Laminar, transition and turbulent natural convection adjacent to inclined and vertical surfaces", Int. J. Heat Mass Transfer, 15, 457-473.

LLOYD J. R., SPARROW E. M. and ECKERT E. R. G. (1972b). "Local natural convection mass transfer measurements", J. Electro. Chem. Soc., 119, 702-707.

LOCK G. S. H., GORT C. and POND G. R. (1967). "A study of instability in free convection from an inclined plate", Appl. Sci. Res., 18, 171-182.

LOCK G. S. H. and TROTTER F. J. de B. (1968). "Observations on the structure of a turbulent free convection boundary layer", Int. J. Heat Mass Transfer, 11, 1225-1232.

MASON H. B. and SEBAN R. A. (1974). "Numerical predictions for turbulent free convection from vertical surfaces", Int. J. Heat Mass Transfer, 17, 1329-1336.

MAYERS D. F. (1962). "Methods of Runge-Kutta type", in Numerical Solution of Ordinary and Partial Differential Equations, edited by L. Fox, 16-27, Pergamon Press, Oxford.

MERK H. J. and PRINS J. A. (1954). "Thermal convection in laminar boundary layers", Parts I, II and III, Appl. Sci. Res., 4, 11-24, 195-206, 207-221.

MICHIYOSHI I. (1964). "Heat transfer from an inclined thin flat plate by natural convection", Bull. J.S.M.E., 7, 745-750.

MORRISON G. L. and TRAN V. Q. (1974). "Low velocity limits of a laser Doppler anemometer", School of Mechanical and Industrial Engineering, University of New South Wales, Australia, Report No. 1974/FMT/5.

N.A.G. LIBRARY MANUAL (1974). Cripps Computing Centre, University of Nottingham.

OSTRACH S. (1952). "An analysis of laminar free-convection flow and heat transfer about a flat plate parallel to the direction of the generating body force", NACA, Tech. Note 2635.

OSTRACH S. (1964) in "High Speed Aerodynamics and Jet Propulsion", IV, 528-718, Theory of Laminar Flows, edited by F. K. Moore, Section F, Oxford University Press.

PAFEC 70+ (1972), edited by R. D. Henshall, Department of Mechanical Engineering, University of Nottingham.

PATANKAR S. V. and SPALDING D. B. (1970). Heat and Mass Transfer in Boundary Layers, 2nd edition, Intertext Books, London.

PECKOVER R. S. (1973). "The use of core catchers in fast reactors", Paper 13. Proc. International Meeting on Reactor Heat Transfer, Karlsruhe, October 9-11.

PERA L. and GEBHART B. (1973a). "Natural convection boundary layer flow over horizontal and slightly inclined surfaces", Int. J. Heat Mass Transfer, 16, 1131-1146.

PERA L. and GEBHART B. (1973b). "On the stability of natural convection boundary layer flow over horizontal and slightly inclined surfaces", Int. J. Heat Mass Transfer, 16, 1147-1163.

PLAPP J. E. (1957). "The analytic study of laminar boundary-layer stability in free convection", J. Aero. Sciences, 24, 318-319.

POHLHAUSEN K. (1921). "Zur näherungsweisen integration der differentialgleichung der laminaren reibungsschicht", ZAMM, 1, 252-268.

POPOVICH A. T. and HUMMEL R. L. (1967). "A new method for non-disturbing turbulent flow measurements very close to a wall", Chem. Eng. Sci., 22, 21-25.

RESTREPO F. and GLICKSMAN L. R. (1974). "The effect of edge conditions on natural convection from a horizontal plate", Int. J. Heat Mass Transfer, 17, 135-142.

RICH B. R. (1953). "An investigation of heat transfer from an inclined flat plate in free convection", Trans ASME, 75, 489-499.

ROGERS G. F. C. and MAYHEW Y. R. (1967). Engineering Thermodynamics Work and Heat Transfer, 2nd edition, Longmans, Bath.

ROTEM Z. (1970). "Free convection from heated, horizontal downward-facing plates, ZAMP, 21, 472-475.

SCHMIDT E. (1932). "Schlieren pictures of the temperature field in the neighbourhood of bodies with heat removal", Forsch. Geb. Ingen., 3, 181.

SCHMIDT E. and BECKMANN W. (1930). "Temperature and velocity distribution around a heated vertical plate by natural convection", Tech. Mech. Therm., 1, 341 and 391.

SCHUH H. (1948). "Boundary layers of temperature", Sect. B.6, Brit. Min. of Supply, Ger. Doc. Cent., Ref. 3220T, Reports and Translations No. 1007.

SCHWIND R. G. and VLIET G. C. (1964). "Observations and interpretations of natural convection and stratification in vessels", Paper 5, Proc. 1964 Heat Transfer and Fluid Mechanics Institute, California, edited by W. H. Giedt and S. Levy, Stanford University Press.

SIEGEL R. (1954). "Analysis of laminar and turbulent free convection from a smooth vertical plate with uniform heat dissipation per unit surface area", General Electric, U.S.A., Report No. R54 GL89.

SING S. N., BIRKEBAK R. C. and DRAKE R. M. (1969). "Laminar free convection heat transfer from downward-facing horizontal surfaces of finite dimensions", in Progress in Heat and Mass Transfer, 2, 87-98, edited by T. F. Irvine, W. E. Ibele, J. P. Hartnett and R. I. Goldstein, Pergamon Press, Oxford.

SMITH R. R. (1972). "Characteristics of turbulence in free convection flow past a vertical plate", Ph.D. Thesis, Faculty of Engineering, Queen Mary College, London.

SPARROW E. M. (1955). "Laminar free convection on a vertical plate with prescribed nonuniform wall heat flux or prescribed nonuniform wall temperature", NACA, Technical Note 3508.

SPARROW E. M. and GREGG J. L. (1956). "Laminar free convection from a vertical plate with uniform surface heat flux", Trans. ASME, 78, 435-440.

SPARROW E. M. and GREGG J. L. (1958). "The variable fluid-property problem in free convection", Trans. ASME, 80, 879-886.

SPARROW E. M. and HUSAR R. B. (1969). "Longitudinal vortices in natural convection flow on inclined plates", J. Fluid Mech., 37, 251-255.

SPARROW E. M., TSOU F. K. and KURTZ E. F. (1965). Phys. Fluids, 8, 1559 cited in EDE (1967).

SQUIRE H. B. (1938) in Modern Developments in Fluid Mechanics, edited by S. Goldstein, Oxford.

TAFT M. (1971). "Natural convection below an inclined constant-heat-flux plate", Final Year Honours Project, Department of Mechanical Engineering, University of Nottingham.

TAUTZ H. (1943). "Wärmeübergang durch freie konvektion an einer quadratischen platte verschiedener neigung", Diplom-Arbeit aus der, Institut der Universität, Leipzig.

TIMOSHENKO S. (1956). Strength of Materials, Part II, Advanced Theory and Problems, van Nostrand, New York. 3rd edition.

TOULOUKIAN Y. S. and MAKITA T. (Editors) (1970). Thermophysical Properties of Matter, 6, IFI/PLENUM, New York.

TOULOUKIAN Y. S., LILEY P. E. and SAXENA S. C. (Editors) (1970). Thermophysical Properties of Matter, 3, IFI/PLENUM, New York.

TRITTON D. J. (1963a). "Turbulent free convection above a heated plate inclined at a small angle to the horizontal", J. Fluid Mech., 16, 282-312.

TRITTON D. J. (1963b). "Transition to turbulence in the free convection boundary layers on an inclined heated plate", J. Fluid Mech., 16, 417-435.

TRITTON D. J. (1963c). "The use of a fibre anemometer in turbulent flows", J. Fluid Mech., 16, 269-281.

U.K.A.E.A. (1970). "An appreciation of Fast Reactor Safety", H.M.S.O.

VLIET G. C. (1969). "Natural convection local heat transfer on constant-heat-flux inclined surfaces", J. Heat Transfer, 91, 511-516.

VLIET G. C. and LIU C. K. (1969). "An experimental study of turbulent natural convection boundary layers", J. Heat Transfer, 91, 517-531.

WARNEFORD I. P. and FUSSEY D. E. (1974). "Natural convection from a constant-heat-flux inclined flat plate", Paper No. NC 1.7, Proc. of 5th Int. Heat Transfer Conf., Tokyo.

WARNER C. Y. and ARPACI V. S. (1968). "An experimental investigation of turbulent natural convection in air at low pressure along a vertical heated flat plate", Int. J. Heat Mass Transfer, 11, 397-406.

WHITE D. H., WELTY J. R. and HURT J. C. (1973). "Experimental study of natural convection heat transfer from vertical flat plates in mercury", in Progress in Heat and Mass Transfer, 7, 485-501, edited by O. E. Dwyder, Pergamon Press, Oxford.

YANG K. T. and JERGER E. W. (1964). "First-order perturbations of laminar free-convection boundary layers on a vertical plate", J. Heat Transfer, 86, 107-115.

YUNG S. C. (1965). "Free-convection heat transfer from an inclined heated flat plate in air", M.Sc. Thesis, Department of Mechanical Engineering, University of Missouri, cited in Yung and Oetting (1969).

YUNG S. C. and OETTING R. B. (1969). "Free-convection heat transfer from an inclined heated flat plate in air", J. Heat Transfer, 91, 192-194.

APPENDIX A

TEMPERATURE-COMPENSATION OF FILM PROBES USING CORRECTING NETWORK

This section gives details of the derivation of the matching network resistance values together with the assumptions involved and has been taken from Amos (1973). The temperature-compensating network is shown in Figure A 1.

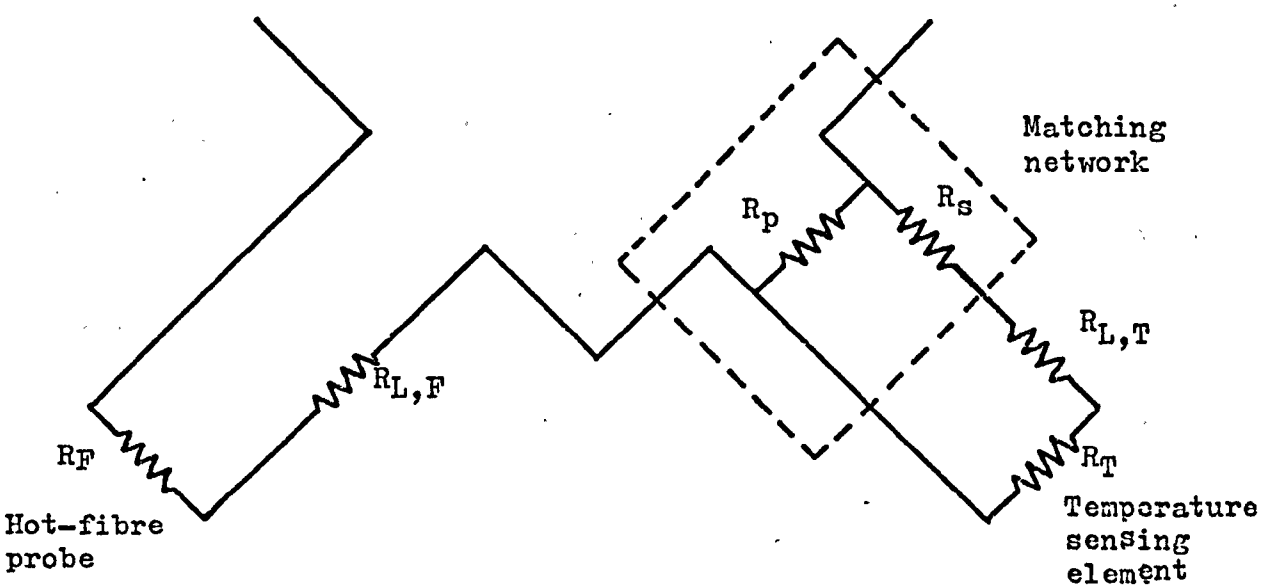

FIGURE A 1 TEMPERATURE-COMPENSATING NETWORK

The total resistance of the compensating unit R_c is determined by the overheat ratio b as follows:

$$R_c = (1 + b) R_F + R_{L,F} \quad \ldots (A\ 1)$$

The requirement for constant overheating ratio at varying temperatures is filled when:

$$\frac{dR_c}{dT} = (1 + b) \frac{dR_F}{dT} + \frac{dR_{L,F}}{dT} \quad \ldots (A\ 2)$$

Calculation of R_s and R_p

$$R_c = \frac{R_p (R_s + R_{L,T} + R_T)}{R_p + R_s + R_{L,T} + R_T} \quad \ldots (A\ 3)$$

where R_p is a non-inductive resistor with $\alpha \simeq 0$

R_s is a non-inductive resistor with $\alpha \simeq 0$

$$R_T = R_{T_o} (1 + \alpha_{T_o} (T - T_o))$$

$$R_{L,T} = R_{L,T_o} (1 + \alpha_{L,T_o} (T - T_o))$$

$$R_c = \frac{R_p [R_s + R_{L,T_o} (1+\alpha_{L,T_o} (T-T_o)) + R_{T_o} (1+\alpha_{T_o} (T-T_o))]}{R_p+R_s+R_{L,T_o} (1+\alpha_{L,T_o} (T-T_o))+R_{T_o} (1+\alpha_{T_o} (T-T_o))}$$

$$\left.\frac{dR_c}{dT}\right|_{T=T_o} = \frac{R_p^2 (R_{T_o} \alpha_{T_o} + R_{L,T_o} \alpha_{L,T_o})}{(R_p+R_s+R_{L,T_o}+R_{T_o})^2} \qquad \ldots (A\ 4)$$

From (A 3) we have for R_p:

$$R_p = \frac{(R_s+R_{L,T_o}+R_{T_o})\ R_{c_o}}{(R_s+R_{L,T_o}+R_{T_o}) - R_{c_o}} \qquad \ldots (A\ 5)$$

Inserting (A 5) into (A 4) we have:

$$\left.\frac{dR_c}{dT}\right|_{T=T_o} \quad \frac{R_{c_o}^2 (R_{T_o} \alpha_{T_o} + R_{L,T_o} \alpha_{L,T_o})}{(R_s+R_{T_o}+R_{L,T_o})^2} \qquad \ldots (A\ 6)$$

$$R_F = R_{F_o} (1 + \alpha_{F_o} (T-T_o))$$

$$R_{L,F} = R_{L,F_o} (1+\alpha_{L,F_o} (T-T_o))$$

$$(1+b) \left.\frac{dR_F}{dT}\right|_{T=T_o} + \left.\frac{dR_{L,F}}{dT}\right|_{T=T_o} = (1+b)\ R_{F_o}\alpha_{F_o}+R_{L,F_o}\alpha_{L,F_o} \qquad \ldots (A\ 7)$$

Inserting (A 6) and (A 7) into (A 2) we have:

$$\frac{R_{c_o}^2 (R_{T_o}\alpha_{T_o}+R_{L,T_o}\alpha_{L,T_o})}{(R_s+R_{T_o}+R_{L,T_o})^2} = (1+b)\ R_{F_o}\alpha_{F_o}+R_{L,T_o}\alpha_{L,F_o} \qquad \ldots (A\ 8)$$

Separating R_s we get

$$R_s = R_{c_o}\sqrt{\frac{R_{T_o}\alpha_{T_o} + R_{L,T_o}\alpha_{LT_o}}{(1+b)R_{F_o}\alpha_{F_o}+R_{L,F_o}\alpha_{L,F_o}}} - (R_{T_o} + R_{L,T_o}) \qquad \ldots (A\ 9)$$

Normally $R_{L,T_o}\alpha_{L,T_o}$ and $R_{L,F_o}\alpha_{L,F_o}$ are small compared to $R_{T_o}\alpha_{T_o}$ and $R_{F_o}\alpha_{F_o}$, i.e. (A 9) may be written as:

$$R_s = R_{c_o} \sqrt{\frac{R_{T_o}\ \alpha_{T_o}}{(1+b)\ R_{F_o}\ \alpha_{F_o}}} - (R_{T_o} + R_{L,T_o})$$

Or, when introducing the overheat ratio:

$$R_s = [(1+b)R_{F_o} + R_{L,F_o}] \sqrt{\frac{R_{T_o}\ \alpha_{T_o}}{(1+b)\ R_{F_o}\ \alpha_{F_o}}} - (R_{T_o} + R_{L,T_o})$$

$$R_p = \frac{(R_s+R_{L,T_o}+R_{T_o})\ ((1+b)\ R_{F_o}+R_{L,F_o})}{(R_s+R_{L,T_o}+R_{T_o}) - ((1+b)\ R_{F_o}+R_{L,F_o})}$$

APPENDIX B

CURVE FITTING ROUTINES

The coefficients in equation (6.2) were calculated using the curve fitting routine E02ABF and those in equations (6.4) and (6.5) using the minimisation routine E04FAF from the University of Nottingham N.A.G. library. Below a brief description of the routines is presented, the description being taken from the N.A.G. Library Manual (1974).

The subroutine E02ABF calculated a weighted least squares polynomial approximation to a set of data points by Forsythe's method using orthogonal polynomials. The procedure computed the coefficients of the polynomial p(x) and minimised the expression

$$\sum_{i=1}^{n} w_i \, (p(x_i) - f_i)^2$$

over the set of polynomials, where n is the number of points (x_i, f_i). The polynomial was set to a degree of 1.

The subroutine E04FAF found the minimum of the sum of squares of m non-linear functions, as residuals, each of n variables

$$S(\underline{x}) = \underline{f}^T\underline{f} = \sum_{i=1}^{m} f_i \, (x_1, x_2, \ldots, x_n)^2 \quad (m \geq n)$$

The method was essentially Gauss-Newton in that the functions $\underline{f}\,(\underline{x})$ were approximated at the point $\underline{x}$ by a linear form $\underline{f} = \underline{h} + J\underline{x}$ where $\underline{h}$ is a constant vector and J is the Jacobian matrix $J_{ij} = (\partial f_i/\partial x_j)_{\underline{x}}$. Thus, an estimate of the minimum of the sum of squares was given by $\underline{y}$ where

$$J^T J\underline{y} = -J^T\underline{h} \qquad \ldots \text{(B 1)}$$

From an initial estimate of the minimum point, a set of at least (n + 1) points, x^i, was generated, and the corresponding function values $\underline{f}^i$ were calculated. Formulae estimating the

coefficients of the linear approximation (i.e. J and $\underline{h}$) were obtained in terms of $\underline{f}^i$ and $\underline{x}$ by considering minimising the weighted sum of squares, over this point set, of the difference between the linear approximation and the actual function values. The weights were chosen to give more emphasis to function values near the minimum. These formulae were used in equation (B 1) to give a set of equations for $\underline{y}$, in terms of the known quantities x^i and f^i, which were then solved using orthogonal transformations. One iteration consisted of replacing that point of the current point set which had the largest sum of squares by the estimated solution of the previous iteration, and solving the set of equations derived from this new set to obtain a new estimate of the solution. If at any time the point set did not span the whole space, then a new point was generated using a random number generator.

One of the problems associated with minimising routines is to ensure that the minimum is the global minimum and not a local one. This may only be found by trying several starting conditions and observing whether the routine gives the same solution.

APPENDIX C

DESIGN OF THE LARGE WATER TANK

As there were no design standards for large water tanks with no internal tie bars, thin plate bending theory was used to calculate the stresses and deflections of the walls and glass windows. Timoshenko (1956, p.115) gives several formulae for calculating the maximum stresses in plates built in at the edges. For glass, the maximum stress is 6.89 MN/m^2, giving a minimum glass thickness of 20 mm for a window 1.22 m x 0.61 m. At this thickness, the deflection of the window was calculated to be 0.1 mm.

Figure C 1 gives a detailed sketch of the water tank. The two glass windows were fitted into a rigid angle iron window frame and sealed with a polysulphide rubber/resin. The sealant provided a firm but slightly plastic seal which accommodated the movement in the glass panels when the tank was filled or emptied. The rigidity of the tank was increased by welding angle section around the top and middle of the tank.

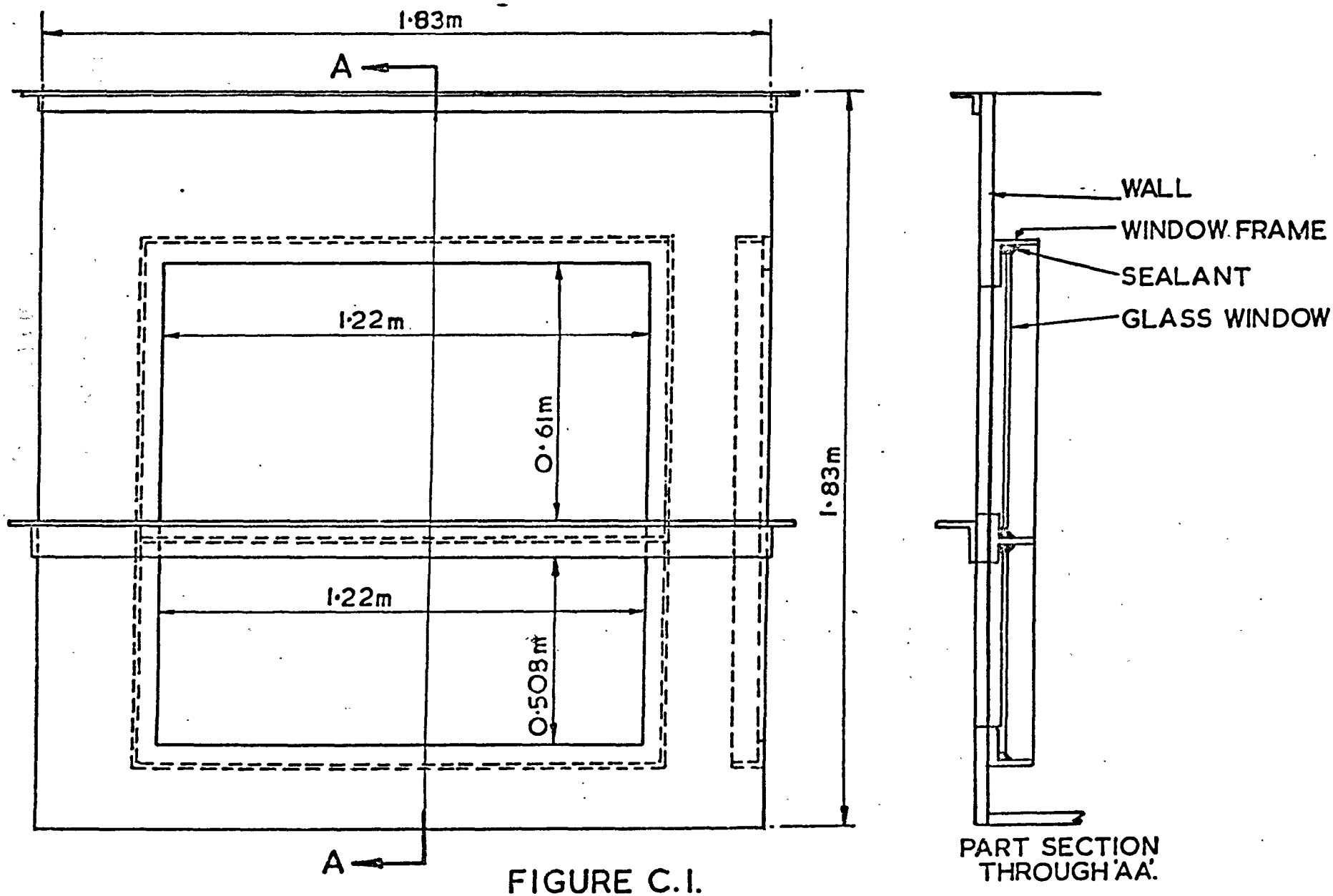

FIGURE C.I.

LARGE WATER TANK (NOT TO SCALE)

APPENDIX D

CORRELATIONS FOR THE PHYSICAL PROPERTIES OF WATER

The physical properties of water in the form of polynomial equations were taken from various sources and are given below:

Specific Heat (C_p), Touloukian and Makita (1970)

$$C_p(J/kgK) = 4186.8\,[2.13974 - 9.68137 \times 10^{-3}\,(T_{ref} + 273.16) + 2.68536 \times 10^{-5}\,(T_{ref} + 273.16)^2 - 2.42139 \times 10^{-8}\,(T_{ref} + 273.16)^3]$$

Thermal Conductivity (k), Touloukian, Liley and Saxena (1970)

$$k(W/mK) = 418.68 \times 10^{-6}\,[-1390.53 + 15.1937\,(T_{ref} + 273.16) - 0.0190398\,(T_{ref} + 273.16)^2]$$

Density (ρ), CEGB (1970)

$$\rho(kg/m^3) = 999.8 + 9.2863 \times 10^{-2}\,T_{ref} - 1.0561 \times 10^{-2}\,T_{ref}^2 + 1.3676 \times 10^{-4}\,T_{ref}^3 - 1.5930 \times 10^{-6}\,T_{ref}^4 + 1.0698 \times 10^{-8}\,T_{ref}^5 - 2.9775 \times 10^{-11}\,T_{ref}^6$$

Kinematic Viscosity (ν), Fujii, Takeuchi, Fujii, Suzaki and Uehara (1970)

$$\nu\,(m^2/s) = 10^{-6}\,[1.792 - 6.205 \times 10^{-2}\,T_{ref} + 16.009 \times 10^{-4}\,T_{ref}^2 - 29.780 \times 10^{-6}\,T_{ref}^3 + 35.314 \times 10^{-8}\,T_{ref}^4 - 23.075 \times 10^{-10}\,T_{ref}^5 + 6.240 \times 10^{-12}\,T_{ref}^6]$$

Volumetric thermal expansion coefficient (β)

This was evaluated from the density using the following formula taken from Rogers and Mayhew (1967, p.87)

$$\beta\,(K^{-1}) = \rho \left| \frac{\partial}{\partial T} \frac{1}{\rho} \right|_p$$